Dynamic Structural Analysis of Beams

Wasseem Jabboor

Submitted for the degree of Doctor of Philosophy

Heriot-Watt University

School of the Built Environment

October 2011

Abstract

The research reviews the various methods, accurate and approximate, analytical and numerical, used for the analysis of beams that are subjected to dynamic loads. A review of previous research is presented. A detailed description of one of the methods, the Simplified Elastic Plastic Method (the SEP Method), a well-developed approximate method, is given. A finite element model, built with the aid of the computer software ABAQUS, is described. Results of 20 experiments made by others are provided and used as a benchmark for the finite element analysis.

The methodology used for the validation of the ABAQUS Model and the SEP Method is to do, for various study cases, a comparison between the experimental results, those computed using the ABAQUS Model and those predicted using the SEP Method. Having validated the ABAQUS Model, it has been used as a benchmark with which to check the SEP Method. Therefore, additional cases have been analysed using the ABAQUS Model in order to cover a more comprehensive range of variables.

A good agreement has been found between the results. The accuracy of the ABAQUS model and the conservatism of the SEP Method are shown. A design procedure using the SEP Method has been developed. Calibration factors are also proposed in order to reduce the conservatism in the SEP Method.

The results and recommendations of the research can be employed in the defence industry, civil and structural engineering.

To

my father Ghassan

my mother Amal

my sister Emeline

my brother Adonis and his daughter Elissar

Acknowledgements

Acknowledgements are due to Prof. Ian May for his excellent supervision of the Thesis, his valuable guidance and his generous concern.

Many thanks to Gillian Rae, Prof. Ghassan Mahmoud, Dr. Amin Abdulmajid, Dr. Christopher Lang and Dr. Chaham Alalouch.

Table of Contents

Chapter 1 – Introduction

1.1 Introduction 2
1.2 Objectives and Contribution of the Research 5
1.3 Justification for the Research and Applicability of its Outcomes 6
1.4 Layout of Thesis 6

Chapter 2 – Methods of Dynamic Analysis and Review of Previous Research

2.1 Introduction 10
2.2 Structures Modelled as a Single Degree of Freedom System 11
2.2.1 Introduction 11
2.2.2 Degrees of Freedom in Structural Dynamic Modelling 12
2.2.3 Modelling Structures as a Single Degree of Freedom System 13
2.2.4 General Governing Equation of Motion 14
2.2.5 Governing Equation of Free Motion and its Solution 15
2.2.6 Natural Period of Vibration 16
2.2.7 Dynamic Load Factor (DLF) 17
2.2.8 Dynamic Response to Suddenly Applied Rectangular Load 18
2.2.9 Dynamic Response to Suddenly Applied Triangular Load 18

2.3 Accurate Analytical Method of Dynamic Analysis of Beams (Distributed Properties) 19
2.3.1 Introduction 19
2.3.2 General Governing Equation of Motion of Beams 20
2.3.3 Governing Equation of Free Motion of Beams 21
2.3.4 Equation of Motion Including the Axial Force Effect (Geometric Nonlinearity) 22
2.3.5 Equation of Motion Including the Effect of Shear and Rotatory Inertia (Timoshenko Equation) 23

2.4 Method of Approximate Dynamic Analysis of Beams (Discrete Properties) 25
2.4.1 Introduction 25
2.4.2 Displacement Vector 25
2.4.3 Shape Functions 26
2.4.4 Stiffness Matrix 27
2.4.5 Geometric Stiffness Matrix (Effect of Axial Forces) 27
2.4.6 Combined Stiffness Matrix 28
2.4.7 Mass Matrix 29
2.4.8 Dynamic Load Vector 30
2.4.9 Governing Equation of Motion 31
2.4.10 Nodal Element Forces 32

2.5 Strain Rate Sensitivity of Materials in Dynamic Problems 33
2.5.1 Introduction 33
2.5.2 Constitutive Law for Modelling Materials with Strain Rate Sensitivity 33

2.6 Review of Previous Research 35
2.7 Conclusions 56

Chapter 3 – Impulsive Loads

3.1 Introduction 63
3.2 Explosions as Source of Dynamic Loading 63
3.2.1 Introduction 63
3.2.2 Types of Explosions 64
3.2.3 Examples of Explosion Incidents in the Past 64

3.3 Explosive Loads in Structural Design 65
3.3.1 Principle of Design 65
3.3.2 Occurrence vs. Loss Cost and Importance of Including Explosions in Design 66
3.3.3 Design Criteria and Requirements 66
3.3.4 Explosion Hazards 67

3.4 Surface Pressure of Blast 67
3.4.1 Introduction 67
3.4.2 Time History and Spatial Distribution of Blast Surface Pressure 68

3.5 Simplification of Spatial Distribution and Time History of Blast Pressure 70
3.5.1 Simplification of Spatial Distribution 70
3.5.2 Simplification of Time History 71

3.6 The Initial Velocity and the Pulse Theorem 73
3.7 Blast Loading of Beams 74
3.8 Conclusion 75

Chapter 4 – The SEP Method

4.1 Introduction 84
4.2 Main Assumptions 84
4.3 Analytical Techniques 86
4.3.1 Introduction 86
4.3.2 Determination of a_{20} and $\dot{a}_{20}$ 88
4.3.3 The Δ_0 Minimum Device 89
4.3.4 Summary 90

4.4 Steps and Procedures of the SEP Method 90
4.4.1 Introduction 90
4.4.2 Stage I – Fully Elastic 91
4.4.3 Stage II – Fully Plastic Pure Bending 95
4.4.4 Stage III – Fully Plastic Pure Axial Tension 97
4.4.5 Stage IV – Elastic Recovery 99

4.5 Conclusion 100

Chapter 5 – Finite Element Modelling and Numerical Analysis

5.1 Introduction 105
5.2 Numerical Methods of Dynamic Analysis 106
5.2.1 Introduction 106
5.2.2 Numerical Integration of the Differential Equation of Motion 107

5.3 Nonlinearity in Structural Dynamics 112
5.3.1 Introduction 112
5.3.2 Nonlinear Modelling 112
5.3.3 Numerical Evaluation of Nonlinear Solutions 115
5.3.4 Constant Acceleration Step-by-Step Integration Technique 116
5.3.5 Linear Acceleration Step-by-Step Integration Technique 119
5.3.6 Accuracy of the Recurrence Formulae and Selection of the Time Step 123

5.4 Finite Element Method and Time Stepping Schemes 124
5.4.1 Introduction 124
5.4.2 Governing Equation of Motion in Nonlinear Finite Element Analysis 125
5.4.3 Wilson-θ Time Stepping Scheme 125
5.4.4 Newmark-β Time Stepping Scheme 126
5.4.5 Explicit Integration Schemes 128
5.4.6 Implicit Integration Schemes 129

5.5 Finite Element Modelling and Analysis of Beams Using ABAQUS 130
5.5.1 Introduction 130
5.5.2 Description of the Model Geometry 131
5.5.3 Strain Rate Sensitivity and Modelling of the Material 131
5.5.4 Boundary Conditions 132
5.5.5 Modelling of Dynamic Loads 132
5.5.6 The Numerical Integration Scheme Used in the Nonlinear Analysis 132
5.5.7 The Time Step Chosen for the Analysis 133
5.5.8 Effect of Axial Forces and Geometric Nonlinearity 133
5.5.9 Type of Finite Elements and Meshing Techniques 133

5.6 Conclusions 134

Chapter 6 – Symonds and Jones' Experiments

6.1 Introduction 138
6.2 Test Rig 138
6.2.1 Ballistic Pendulum 138
6.2.2 Experimental Instrumentation 139
6.2.3 Imparted Explosive Momentum 139

6.3 Experimental Specimens 140
6.3.1 Introduction 140
6.3.2 Details of Specimens and Head of the Ballistic Pendulum 140
6.3.3 Mechanical Properties of Specimen Material 141
6.3.4 Sheet Explosives 142

6.4 The Experiments 142
6.5 Conclusion 143

Chapter 7 – Analysis, Results and Discussion

7.1 Introduction 149
7.2 Methodology 152
7.2.1 Introduction 152
7.2.2 Percentage Difference of Permanent Displacement 152
7.2.3 Validation of the ABAQUS Model 154
7.2.4 Validation of the SEP Method 155

7.3 Data and Study Cases 156
7.3.1 Introduction 156
7.3.2 General Description 156
7.3.3 Geometry and Dimensions of Beam 156
7.3.4 Mechanical Properties of Beam Material 157
7.3.5 Intensities of Impulsive Load 157
7.3.6 Summary 158

7.4 Results 159
7.4.1 Overview 159
7.4.2 The Permanent Displacement a_p 159
7.4.3 The Permanent Displacement Percentage Difference Δa_p % 160

7.5 Validation of the ABAQUS Model 161
7.5.1 Introduction 161
7.5.2 Comparison of Results and Discussion 161
7.5.3 Discussion on the Percentage Difference 164

7.6 Validation of the SEP Method 166
7.6.1 Introduction 166
7.6.2 Comparison of Results and Discussion 166
7.6.3 Calibration Factors 168

7.7 Some Comments on the Permanent Displacement of the Beams 173
7.7.1 The Permanent Displacement as Predicted by the ABAQUS Model 173
7.7.2 The Permanent Displacement as Predicted by the SEP Method 175
7.7.3 The Permanent Displacement Measured Experimentally 177

7.8 Practical Use of the SEP Method and its Engineering Significance 179
7.9 Summary 184

Chapter 8 – Conclusions

8.1 The Literature 209
8.2 The Theory 209
8.3 Finite Element Modelling and Time Stepping 210
8.4 The ABAQUS Model 210
8.5 The SEP Method 211
8.6 The Design Procedure 212
8.7 Recommendations for Future Research 213

References

Chapter 1 – Introduction

1.1 Introduction

Dynamic Loads are time-dependent forces. These forces are imposed on structures by either natural phenomena such as earthquakes and hurricanes or human activities such as explosions and machine vibrations. Structures affected by dynamic forces can be as simple as a beam or a plate, or as complex as a high rise building or a power station. In the analysis and design of these structures, the time-dependent inertial forces should be considered. During its response to dynamic loads, a structure shows resistance to these loads in the form of internal forces some of which are related proportionally to the displacements (spring forces) and some to the velocities (damping forces). These resistance forces are also time-dependent and should also be considered in the analysis.

For many reasons, there has been a growing interest in the field of the dynamic analysis of structures in recent years. The most important reasons are the observed failure of structures due to dynamic loads, such as earthquakes and explosions, and the increased awareness of the importance of designing structures that are more resistant to these kinds of loads. Other reasons are the growth of knowledge in the fields of structural engineering, structural dynamics, strength of materials and stability, the increase in the use of high-strength materials and the development of numerical methods and of powerful computers which can apply these methods quickly and efficiently. Also, these have led to the possibility of more accurate design and therefore to the development of structures that are larger, taller, more slender, less rigid, less material-consuming and hence more susceptive to dynamic loads as these structures generally tend to be more flexible and having longer natural periods. These developments have highlighted the necessity of designing structures to bear the various dynamic effects.

Even though a lot of structures under dynamic loading can properly be designed as if the loading was static, there are many important exceptions and it is very necessary that the structural engineer is able to decide which/when loads should be considered static and which/when they should be considered dynamic.

Actually, with the obvious exception of dead loads, all loads are dynamic in reality as they have to be applied to the structure in some way, and this would impose a time variation to these loads. Nevertheless, if the load is applied in a manner in which its value increases slowly, it will have no dynamic effect and could be considered as static.

However, the term "slowly" is not definite, and obviously the decision of whether to consider the load as static or dynamic is taken based on subjective standards. It has been found that the natural period of the structure could be assumed to be the most important deciding factor. When the loading is applied during a long period of time compared to this natural period, it could be treated as if it was a static loading. The natural period, defined in loose terms, is the time taken by the structure to go through one cycle of free vibration.

Examples of problems in which dynamic analysis should be executed are structures which vibrate due to earthquakes, structures affected by dynamic loads due to vibrating machines, structures subjected to impulsive forces from nearby explosions or tornadoes, and structures that carry moving loads like bridges.

It is important to note that the dynamic analysis of structures consists mainly of the determination of the time history of displacements, from which other structural variables such as velocities, accelerations, internal stresses and support reactions could be calculated using directly applicable expressions. Therefore, all governing equations of motion in the dynamic analysis are found in terms of the displacements, and the displacements are in their turns found from these equations.

The governing equations of motion of the dynamic response of a structure are generally nonlinear partial differential equations that are very difficult to solve by mathematical methods. However, recent developments in the area of the dynamic analysis and design of structures have enabled such analysis and design to be executed in a quick and practical manner. Examples of these are the employment of simplifying assumptions and easy dynamic models, and of modern numerical and computational techniques.

The focus of this research work is on the dynamic response of structural members, in particular, beams. These members are the basic components of larger more complex structures. Therefore, it is very important to study their dynamic behaviour in the first instance in order to better clarify the dynamic characteristics of more complex structures.

The dynamic response of a structure is nonlinear when the restoring forces are not proportional to the displacements. This Thesis describes two kinds of nonlinearity which were included in the dynamic analysis.

The first kind is geometric nonlinearity and that is when displacements are too large to ignore. For example, if the transverse displacements of a beam are large then the axial internal force is large and the interaction between both is also significant. Thus, the nonlinearity caused by this interaction is significant and should be considered in the analysis.

The second kind is material nonlinearity and that is when the mechanical properties of the material change during the response, for example, when the stress is not proportional to the strain and thus Young's modulus of elasticity E is not constant. Also, materials sensitive to strain rates, such as steel, are nonlinear as their mechanical properties, especially the yield stress, increase as the strain rate increases.

The effect of plasticity the material would experience if subjected to dynamic loading which leads to stresses greater than the elastic limit has been included together with the effect of elasticity. This is shown to be very important in the analysis and design of structural members because the maximum energy that the material can absorb by having plastic deformation is much greater than the maximum energy that can be absorbed if the material remains completely elastic. This indicates that it is usually more expensive to design a structural member to act within its elastic capacity.

1.2 Objectives and Contribution of the Research

One of the objectives of the research is to review the various methods used for the dynamic analysis of beams. The methods investigated include both accurate and approximate methods. In the more accurate methods, the beam is dealt with as a structure which has an infinite or very large number of degrees of freedom. The governing equation of motion is a partial differential equation that can be solved either analytically or numerically. In numerical methods, such as the finite element method, the structure is meshed and the time divided into intervals then finite summations and iterations are carried out to get the solution. In approximate methods on the other hand, the beam is considered to have a finite small number of degrees of freedom and various simplifying assumptions are introduced. The governing equation of motion thus becomes a matrix or single differential equation with its unknown(s) being function(s) of time only and which can be easily solved analytically or numerically.

A further contribution of the research is to build a finite element model for beams which are subjected to dynamic loads, and then to validate the employment of this model in the dynamic analysis of beams so that it can also be used as an 'accurate' benchmark to compare with and validate other methods of dynamic analysis. This numerical model has been built using the nonlinear finite element computer software ABAQUS provided by SIMULIA, Dassault Systèmes. The validation process is carried out by making comparisons between the experimental results and those computed by ABAQUS.

Also, the research aims to give a detailed description of one of the most well developed approximate methods of the dynamic analysis of beams, the Simplified Elastic Plastic Method (the SEP Method), and to validate the use of this method for the dynamic analysis of beams. The validation process is conducted by making comparisons

between the experimental results, those computed by ABAQUS and the results calculated using the SEP Method.

1.3 Justification for the Research and Applicability of its Outcomes

The results, conclusions and recommendations of the research can be employed for the dynamic analysis of beams in structures in the following situations:

a- Structures subjected to impulsive loads due to, for example, blasts

b- Shields of military/civil tanks and vehicles against explosions

c- Structures subjected to dynamic loads due to human activities such as those due to vibrating working machines or those caused by moving vehicles, on bridges for example

d- Structures subjected to dynamic loads due to natural phenomena such as wind, earthquakes, tornados, hurricanes or tsunami tidal waves

1.4 Layout of Thesis

In Chapter 2, a comprehensive literature review of current knowledge is provided. It discusses the main theoretical principles of the dynamic analysis of structures from point masses to elementary members such as beams. An explanation is given, with the governing equations of motion, of the different methods and techniques of analysing beams subjected to dynamic loads. This includes a description of the analytical accurate method. Also, a review of approximate methods is given. An insight of the

phenomenon of strain rate sensitivity of certain materials as their mechanical properties are altered by dynamic, especially rapid, loading is also presented.

Chapter 2 also provides a review of previous research that has been carried out with the relevant findings and conclusions. It consists of a review of the numerous studies which include useful empirical formulae suggested for the fast dynamic analysis of beams, various approximate methods, both analytical and numerical, and the numerous finite element analyses carried out.

In Chapter 3, an introduction to the nature of impulsive loads is presented. In particular, one kind of this loading, the air blast of an explosion, is discussed. The importance of including explosive loads in the dynamic analysis and design of structures is revealed. The computational equations used for simulating the blast wave pressure applied to the exposed surface of a structure are detailed. Also, the principles of dynamic analysis and design of structures subjected to impulsive loads together with the various simplification techniques used in the simulation of these loads such as the pulse theorem are explained.

Chapter 4 contains a detailed description of the Simplified Elastic Plastic Method (the SEP Method), an approximate method for the dynamic analysis of beams, the validation of which will be carried out in the Thesis. It includes an introduction to the approximation assumptions made and an illustration of the analytical techniques used. All the steps and the procedures for the SEP Method with the various equations and relationships are given.

Numerical methods, such as the Finite Element Method (FEM), are powerful methods which have shown to be accurate and efficient when used for structural analysis and design especially in the most difficult and complex situations in civil engineering. The methods came to existence many decades ago and have been developed quite thoroughly over the years. They have arisen due to the need to find the response of structures in particular cases, like dynamic loading, nonlinear behaviour and material

becoming plastic, which would prove to be extremely difficult if the classical methods were to be used, and due to the massive revolution in computer technology in recent years. Chapter 5 provides a brief review of numerical methods including an overview of integration techniques and iteration formulae, a discussion of nonlinearity and an explanation of the finite element method with the various time-stepping schemes. These are followed by a detailed description of the ABAQUS finite element model built for the beams in the research and the validation of which was carried out and described later in the Thesis. It includes information about the modelling of the material, dynamic loads, boundary conditions, details of the meshing, type and number of elements used, geometry, time step chosen for the analysis and numerical integration scheme employed.

In Chapter 6, a detailed description of the experimental work carried out by Symonds and Jones (1972) is given. This includes the test rig and instrumentation, the beam specimens tested and the explosive load applied to the beam in each experiment.

Chapter 7 explains the methodology adopted to validate the analytical models described in the preceding Chapters. Detailed information for the study cases considered, which consisted of beams loaded impulsively, is provided in this Chapter, this includes data for the geometry and dimensions of beams, the mechanical properties of the beam material and the different intensities of impulsive load applied to the beam.

Chapter 7 also presents the values of the permanent lateral displacements of the beams of the study cases. These include the results from the experiments, those computed using the ABAQUS Model and the results predicted using the SEP Method. The results are discussed and compared in order to validate the ABAQUS Model and the SEP Method. An important part of the comparison process presented is the calculated percentage difference between the two compared results. Also, a design procedure developed for the SEP Method is described.

Finally, in Chapter 8, conclusions from this investigation are drawn.

Chapter 2 – Methods of Dynamic Analysis and Review of Previous Research

2.1 Introduction

The subject of dynamic analysis has not been yet studied to the extent where analytical accurate methods for solving complex structural problems, especially nonlinear, have been developed. Instead, the provision of such methods has been limited to simple cases of linear structural dynamics. The paramount reason behind this is the great analytical difficulty encountered in the development of such methods. This has led to the substitution, adopted by many structural engineers, of the accurate dynamic analysis by an approximate dynamic, or even equivalent static, analysis. However, the interest in this area of knowledge has considerably increased in recent years due to the rapid development of powerful computers and the continuous development of modern reliable experimental instrumentation which have provided invaluable help in the process of understanding such complex structural dynamic problems.

This Chapter provides a broad overview of the dynamic analysis of beams. It includes the main assumptions, the different methods of analysis and the governing equations of motion which will be used later in the Thesis. Also, an insight into the phenomenon of strain rate sensitivity for certain materials when their mechanical properties are altered by dynamic, especially rapid, loading is presented.

The methods used for the dynamic analysis can be placed into one of the following categories and which are presented in detail in the following text:

1- Analytical accurate methods
2- Approximate methods
3- Numerical methods

A summary of the relevant research that has been carried out is given in this Chapter together with the findings and the conclusions drawn from them. This includes various investigations that cover one or more of the following issues:

1- The empirical formulae that have been developed and could be used for the dynamic analysis of beams
2- The various approximate methods, both analytical and numerical
3- Finite element analysis

2.2 Structures Modelled as a Single Degree of Freedom System

2.2.1 Introduction

Under dynamic conditions, finding the accurate analytical description of the behaviour of a structure has often proven to be a very difficult task, Paz (1991). Only a few simple problems can be solved rigorously in closed form expressions. In the case of complicated situations of structural dynamics, such as those involving complex dynamic loading, material properties or boundary conditions, many simplifications and assumptions might need to be made in order to substitute the structure by a much simpler approximate model which is easy to solve analytically but at the same time is still able to simulate the dynamic behaviour of this structure accurately enough to meet the requirements of both safety and economy. This model represents the connection between the approximate results produced and the real structural situation by a symbolic idealization that satisfies all the assumptions suggested for this particular situation.

The assumptions introduced to simplify complex dynamic problems can be placed into one of the following categories, Paz and Leigh (2004):

1- Geometric assumptions some of which include

- modelling beams, frames and trusses as structures that consist of one dimensional elements.

- assuming plates, slabs and shells as two-dimensional elements of relatively small thicknesses.
- idealizing continuous systems by discrete models that are divided using different nodes assigned coordinate systems to measure their displacements.

2- Material assumptions: these deal with the properties of the materials of construction like isotropy or homogeneity, and those properties that describe the material behaviours such as linearity, elasticity, nonlinearity, plasticity, etc.

3- Loading assumptions examples of which are

- assuming concentrated forces to be applied at geometric points.
- considering forces to be applied instantaneously.
- simulating forces by constant, trigonometric or periodic time-history functions.

The dynamics of the single degree of freedom model is reported widely in the literature, for example Biggs (1964), Warburton (1964), Major (1980), Vertes (1985), Clough and Penzien (1993) and Paz and Leigh (2004).

2.2.2 Degrees of Freedom in Structural Dynamic Modelling

A degree of freedom of a structure is defined as the ability of a point of the structure to change its position (to displace). Thus, the total number of degrees of freedom of a structure is equal to the number of independent displacements possible in the structure, Biggs (1964). These independent coordinates are necessary and sufficient to completely determine the position and shape (the displacements of all geometric points) of the whole structure at any time, Biggs (1964), Paz (1991) and Warburton (1964).

2.2.3 Modelling Structures as a Single Degree of Freedom System

By definition, the number of degrees of freedom of a continuous system is infinite though they still need to be identified and this can sometimes be a very difficult task. However, analytical simulation usually limits them to a finite number and sometimes to a single degree of freedom only (the system of this case is called the simple mass-spring model) from which the infinite degrees of freedom of the continuous structure can be computed using direct relations or expressions derived from assumed shapes. This reduction in the number of degrees of freedom is often adopted in order to accomplish that difficult task a lot easier and without actually too much reduction in the accuracy of the solution. Examples of this are shown in figure 2.1 where structures having an infinite number of degrees of freedom have each been considered in simulation as a single degree of freedom system. Figure 2.1a shows a plane frame, subjected to a dynamic horizontal concentrated force F(t), which has been modelled as having one degree of freedom which is the horizontal linear displacement x(t) of the top level of the frame. A cantilever with a dynamic vertical concentrated force F(t) applied at its free end is presented in figure 2.1b where it has been simulated as a system of a single degree of freedom which is the vertical linear displacement y(t) of the free end of this cantilever. Similarly, figure 2.1c shows a simply supported beam subjected to a dynamic vertical distributed pressure p(t). The vertical linear displacement y(t) of the middle node of this beam is the single degree of freedom chosen in modelling.

The single degree of freedom model described above is illustrated in figure 2.2a. As shown, this model consists of the following components:

1- The mass m of the model measured in kg in this Thesis and which represents the inertial effect. This mass has one degree of freedom y, measured in metres, which is a function of time t measured in seconds.
2- The spring attaching the mass of the model to its support, which has the stiffness value k measured in Newton/metre and representing the linearly elastic restoring forces of the structure simulated by this model.

3- The excitation dynamic force F(t) applied on the mass of the model in the same direction as the single degree of freedom y of this model and which is a function of time, t. This force is measured in Newtons.
4- The support of the model and which holds the mass by the spring.
5- The one dimensional reference frame of the model and which consists of the single axis o-y. This y-axis has the same direction of the single degree of freedom y, stated above, of this model.

2.2.4 General Governing Equation of Motion

Figure 2.2b shows the free body diagram of the mass after being displaced by y at time t. The forces acting upon the mass are F(t) the excitation force, ky the restoring force imposed by the spring assuming it is linearly elastic, and m $\ddot{y}$ the inertial force of the mass where $\ddot{y}$ is the second derivative of the displacement y with respect to time t representing the acceleration of the mass.

By applying Newton's second law of motion to the model shown in figure 2.2b, the following equation results:

$$m\ddot{y} + ky = F(t) \tag{2.1}$$

This equation is the general governing equation of motion of the single degree of freedom model. It is obvious that this equation is a linear differential equation of second order and by solving it with the initial conditions for this model, which are the displacement y_0 and the velocity $\dot{y}_0 = (dy / dt)_{t=0}$ of the mass at the initial time t = 0, the unknown, which is the single degree of freedom displacement function y(t), can be found.

2.2.5 Governing Equation of Free Motion and its Solution

When there is no excitation force applied to a vibrating structure, the motion is described as a free motion. Thus, since F(t) = 0, the previous equation becomes:

$$m\ddot{y} + ky = 0 \tag{2.2}$$

This is the governing equation of free motion for the single degree of freedom model; a homogeneous second order linear differential equation the solution of which is given by the harmonic function:

$$y = y_0 \cos \omega t + \frac{\dot{y}_0}{\omega} \sin \omega t \tag{2.3}$$

where y_0 and $\dot{y}_0$ are the model initial conditions mentioned above and ω is the natural frequency of free vibration of the model measured in radians/second. It represents one of the most important dynamic characteristics of the structure being modelled and is given by:

$$\omega = \sqrt{\frac{k}{m}} \tag{2.4}$$

Equation (2.3) fully describes the free vibration of the single degree of freedom model.

2.2.6 Natural Period of Vibration

Equation (2.3) clearly indicates that the free vibration of the previous model is harmonic which means by definition that it is also periodic. The period of this free vibration is called the natural period of the structure represented by this model. It is a constant value and is measured in seconds. The natural period represents another one of the most important dynamic characteristics of the structure being modelled and can be computed from the natural frequency ω defined previously using the following equation:

$$T = \frac{2\pi}{\omega} \tag{2.5}$$

The natural period of a structure is a very useful and widely-used parameter in structural dynamic analysis and design. Irvine (1986) has shown that the kinds of structures that can be simulated by a single degree of freedom model have natural periods that typically lie in the range 0.1 to 10 seconds. The lower limit of this range would correspond for example to low-rise buildings, while the upper limit would correspond to some types of footbridges, slender high-rise buildings or long-span bridges (for example the famous Golden Gate Suspension Bridge has a fundamental natural period of about 8.5 seconds). Nevertheless, the dynamic criteria of static serviceability and comfort of users or pedestrians and which govern live-load deflections require the natural period of structures to be reasonably low. This implies that the structural stiffness should be high and the mass associated with the dead weight of the structure should be low. However, without special care being taken, these dual conditions can be mutually exclusive.

Clough and Penzien (1993) and Jones (1989) have shown that the ratio between the excitation period of periodic dynamic forces or the duration of limited-time dynamic loading and the natural period of a structure plays a fundamental role in determining the dynamic behaviour of this structure from response spectra, in deciding whether or not to consider the finite-duration dynamic loading as impulsive as well as choosing the most suitable simulation for impulsive loading, and in deciding the most efficient method

(elasto-plastic, purely plastic …etc) to be employed in the dynamic analysis and design of the structure.

2.2.7 Dynamic Load Factor (DLF)

The Dynamic Load Factor (DLF) is defined as the number of times the static displacement y_{st} the dynamic displacement (response) y is, where the former is the displacement of the structure under a static load equal to F_m, the maximum value of the dynamic load applied. Hence:

$$DLF = \frac{y}{y_{st}} \tag{2.6}$$

where

$$y_{st} = \frac{F_m}{k} \tag{2.7}$$

If the dynamic load factor DLF is known, the response y can then be determined by:

$$y = DLF . y_{st} \tag{2.8}$$

Therefore, the dynamic load factor multiplied by the static displacement actually represents the response of the structure.

2.2.8 Dynamic Response to Suddenly Applied Rectangular Load

Figure 2.3a shows a suddenly applied dynamic load which is constant during its duration t_d. This load is defined by:

$$F(t) = F_m , \qquad 0 \le t \le t_d$$
$$F(t) = 0 \quad , \qquad t > t_d \tag{2.9}$$

The constant value F_m is also the maximum value of the load. For a structure initially at rest and in dimensionless terms, the dynamic response is given by:

$$DLF = 1 - \cos 2\pi \frac{t}{T} \qquad , \qquad 0 \le t \le t_d$$
$$DLF = \cos 2\pi\left(\frac{t}{T} - \frac{t_d}{T}\right) - \cos 2\pi \frac{t}{T} \ , \qquad t \ge t_d \tag{2.10}$$

2.2.9 Dynamic Response to Suddenly Applied Triangular Load

A linear applied dynamic load of a maximum value F_m initially which then decays with time until vanishing after a time t_d, the duration of the load, is presented in figure 2.3b. This load is defined by:

$$F(t) = F_m\left(1 - \frac{t}{t_d}\right) , \qquad 0 \le t \le t_d$$
$$F(t) = 0 \qquad , \qquad t \ge t_d \tag{2.11}$$

For a structure initially at rest and in dimensionless terms, the dynamic response is given by:

$$DLF = 1 - \cos 2\pi \frac{t}{T} + \frac{\sin 2\pi \frac{t}{T}}{2\pi \frac{t_d}{T}} - \frac{t}{t_d} \qquad , \quad 0 \le t \le t_d$$

$$DLF = \frac{\sin 2\pi \frac{t}{T} - \sin 2\pi\left(\frac{t}{T} - \frac{t_d}{T}\right)}{2\pi \frac{t_d}{T}} - \cos 2\pi \frac{t}{T} \ , \qquad t \ge t_d \tag{2.12}$$

2.3 Accurate Analytical Method of Dynamic Analysis of Beams (Distributed Properties)

2.3.1 Introduction

The accurate analytical methodology in structural dynamics has been presented in the previous section for single degree of freedom systems along with the governing differential equations of motion and their possible solutions. This section provides a detailed explanation of this accurate method when used for the dynamic analysis of more complex structural systems, beams. Beams are structural members that have, relatively, one long dimension (the length) and two short dimensions (the width and the height or the thickness). They are important members that are often used as elementary parts of whole structures such as buildings and bridges.

In fact, beams are continuous structural systems with distributed properties and which, consequently, have an infinite number of degrees of freedom. This description of

beams is considered in the procedures for the accurate dynamic analysis of members. Therefore, the results obtained from this method provide an accurate description of the response of beams when subjected to dynamic loads. A more detailed investigation of this methodology can be found in Timoshenko and Young (1955), Den Hartog (1956), Biggs (1964), Thomson (1966 and 1993), Clough and Penzien (1993), Paz and Leigh (2004) and Rao (2004).

This section considers the dynamic theory of beams having distributed mass and stiffness for which the governing equations of motion are partial differential equations. The integration of these equations is generally more complicated than the solution of ordinary differential equations governing the dynamic response of single degree of freedom systems. Due to this analytical complexity, the dynamic analysis of structures as systems of distributed properties has had limited use in practice. However, the analysis, as continuous models, of some simple structures gives, without great effort, solutions which are very essential in assessing approximate methods based on discrete multiple or even single degree of freedom systems.

2.3.2 General Governing Equation of Motion of Beams

The treatment of beam flexure developed herein is based on the simple bending theory as it is commonly used for engineering purposes. The method of analysis is known as the Bernoulli-Euler theory which assumes that a plane cross section of a beam remains plane during flexure.

Figure 2.4 shows a beam of a uniform cross section, made from a homogeneous material and subjected to a general lateral distributed dynamic load p(x,t) per beam unit length. ρ and E are respectively the mass density and the elasticity modulus of the beam material, while A and I are respectively the area and the second area moment of the beam cross section. The dynamic response of the beam is represented by the lateral

displacement y(x,t), a function found from solving the governing equation of motion of the beam:

$$\rho A \frac{\partial^2 y}{\partial t^2} + EI \frac{\partial^4 y}{\partial x^4} = p(x,t) \tag{2.13}$$

This equation is the Euler-Bernoulli beam equation, a partial differential equation of the fourth order applicable as long as the beam remains elastic. It models the dynamic behaviour of the beam reasonably accurately. However, solving this equation is difficult even though it is for a member which remains elastic. If plasticity exists in the beam, it has not been possible to derive the governing equation.

In the previous equation, only the flexural deflections are considered while the shear deflections and the rotatory inertia of the cross section are neglected. The inclusion of both these effects in the differential equation of motion renders it more accurate but considerably increases its complexity. Such an equation is known as the Timoshenko beam equation, first introduced by Timoshenko (1921). Also, the Euler-Bernoulli equation does not include the effect of the axial force on the behaviour of the beam. The more accurate equation which includes such an effect and the Timoshenko equation are presented later.

2.3.3 Governing Equation of Free Motion of Beams

For free vibration, when p(x,t) = 0, the governing equation of Euler-Bernoulli becomes homogeneous:

$$\rho A \frac{\partial^2 y}{\partial t^2} + EI \frac{\partial^4 y}{\partial x^4} = 0 \tag{2.14}$$

Solving this equation, which is also difficult, while considering the boundary conditions, gives the natural frequencies and the shape functions of the normal modes of vibration of the beam.

For a fully fixed uniform beam of span 2l and rectangular cross section of width b and thickness h, the fundamental natural frequency of free vibration is given by:

$$\omega = 1.615 \frac{h}{l^2} \sqrt{\frac{E}{\rho}} \tag{2.15}$$

and thus the fundamental natural period of this beam, equation (2.5), is given by:

$$T = 3.891 \frac{l^2}{h} \sqrt{\frac{\rho}{E}} \tag{2.16}$$

2.3.4 Equation of Motion Including the Axial Force Effect (Geometric Nonlinearity)

When a beam has an axial force, the governing equation of its motion is affected by the presence of this force. Including the axial force effect in the dynamic analysis of beams increases its accuracy. Figure 2.5 shows a beam under a general dynamic load p(x,t) and having an axial force N. The general governing equation of motion which takes into account the effect of this force is:

$$\rho A \frac{\partial^2 y}{\partial t^2} + N \frac{\partial^2 y}{\partial x^2} + EI \frac{\partial^4 y}{\partial x^4} = p(x,t) \tag{2.17}$$

and the relevant governing equation of free motion is:

$$\rho A \frac{\partial^2 y}{\partial t^2} + N \frac{\partial^2 y}{\partial x^2} + EI \frac{\partial^4 y}{\partial x^4} = 0 \qquad (2.18)$$

2.3.5 Equation of Motion Including the Effect of Shear and Rotatory Inertia (Timoshenko Equation)

The applicability of the previous equations of motion is limited to structural dynamic problems where only flexure and translatory inertia are of dominant effect. Therefore, it must be recognized that these equations do not provide a completely accurate description of beams behaviour under dynamic loading. The reason is that these equations still do not consider the effect of wave travel which is the propagation of disturbance from the points of the dynamic load application along the length of the beam. Instead, these equations imply effect of wave components with short wavelengths travelling along the beam with infinite velocities.

Hughes and Speirs (1982) have shown that a disturbance wave starting from the application point of dynamic loading will in fact take a finite time to travel out to the beam supports and more time to return to the loading point. Thus, the beam does not 'know' its boundary conditions until sometime after application of the loading. It follows that all beams, irrespective of boundary conditions, respond in the same manner until they 'know' their boundary conditions. Therefore, if the dynamic loading is of relatively short duration, the behaviour of the beam during this short duration will be independent of its boundary conditions.

A more accurate description of beam vibration was presented by Timoshenko (1921). This differential equation of motion allows additionally for the effect of shear and rotatory inertia:

$$\rho A \frac{\partial^2 y}{\partial t^2} + EI \frac{\partial^4 y}{\partial x^4} - \rho I \left(1 + \frac{E}{sG} \right) \frac{\partial^4 y}{\partial x^2 \partial t^2} + \frac{\rho^2 I}{sG} \frac{\partial^4 y}{\partial t^4} = 0 \qquad (2.19)$$

in which s is a factor which accounts for the non uniform shear distribution across the cross section and depends on the shape of the cross section, and G is the shear modulus of elasticity. Goldsmith (1960) has presented some of the many values of s which are 0.667 and 0.750 for rectangular and circular cross sections, respectively.

Equation (2.19) is very accurate and gives a more realistic description of wave travel. Goldsmith (1960) and Hughes and Speirs (1982) have shown using this equation that an impulsive disturbance involving both shear and moment will result in two wave trains: a shear wave train of velocity $\sqrt{sG/\rho}$ and a moment wave train of velocity $\sqrt{E/\rho}$. Furthermore, reflections of these waves at the beam supports will result in more wave trains, when the situation becomes more complicated.

Both the Euler-Bernoulli equation (2.14) and the Timoshenko equation (2.19) can be solved for particular dynamic problems and the results compared to examine the effect of shear and rotatory inertia on response. Hughes and Speirs (1982) proved that these effects become more significant as the number of vibration modes excited during the response increases. Weaver et al. (1990) also reached to the same conclusion for natural frequencies of vibration. They found that the contribution of the effect of shear and rotatory inertia on the natural frequency becomes more important as the order of the natural frequency (the vibration mode order) increases. It was shown that the effect of shear on the frequency is 3.2 times larger than the effect of rotatory inertia, and they also estimated the maximum total contribution of both these effects on the frequency at about 1.7%.

2.4 Method of Approximate Dynamic Analysis of Beams (Discrete Properties)

2.4.1 Introduction

In the previous section, the theory for the accurate analysis of beams considering the stiffness and inertial properties as distributed has been presented. This section describes the approximate analysis which assumes that the beam has discrete properties, that is, a multi degree of freedom system. In this system, the properties are assigned to the nodes consistent with the static deflections of the beam. The equations given herein will be used later in the Thesis. More details of the approximate method can be found in Biggs (1964), Clough and Penzien (1993) and Paz and Leigh (2004).

2.4.2 Displacement Vector

Figure 2.6 shows a beam element of cross sectional second moment of area I and area A, length L and material modulus of elasticity E and mass density ρ. The linear and angular nodal displacements δ_1, δ_2, δ_3 and δ_4 at both ends of the beam element are also shown. The local displacement vector of the beam element can be written as:

$$\{\delta\} = \begin{bmatrix} \delta_1 \\ \delta_2 \\ \delta_3 \\ \delta_4 \end{bmatrix} \tag{2.20}$$

The global displacement vector of the entire structure is referred to as {y} where each value y of this vector represents a nodal linear or rotational displacement (degree of freedom) of the structure.

2.4.3 Shape Functions

The shape function $N_i(x)$ of a beam element represents the variation of its lateral displacement due to a nodal displacement δ_i of its end equal to one unit while all other nodal displacements are maintained at zero. From this definition, the shape functions of the beam element shown in figure 2.6 are given by the following equations:

$$N_1(x) = 1 - 3\left(\frac{x}{L}\right)^2 + 2\left(\frac{x}{L}\right)^3$$

$$N_2(x) = x\left(1 - \frac{x}{L}\right)^2$$

$$N_3(x) = 3\left(\frac{x}{L}\right)^2 - 2\left(\frac{x}{L}\right)^3 \qquad (2.21)$$

$$N_4(x) = \frac{x^2}{L}\left(\frac{x}{L} - 1\right)$$

The total lateral displacement y(x) of the beam element due to arbitrary nodal displacements δ_1, δ_2, δ_3 and δ_4 at both its ends can then be found using the previous shape functions and a superposition to give:

$$y(x) = N_1(x)\delta_1 + N_2(x)\delta_2 + N_3(x)\delta_3 + N_4(x)\delta_4 \qquad (2.22)$$

2.4.4 Stiffness Matrix

The stiffness coefficient k_{ij} of a beam element is the nodal force at and in the direction of the nodal displacement δ_i due to a unit nodal displacement δ_j while all other nodal displacements are maintained at zero. From this definition, the stiffness coefficient k_{ij} can be determined using the relevant shape functions as follows:

$$k_{ij} = \int_0^L EI\left(\frac{d^2 N_i(x)}{dx^2}\right)\left(\frac{d^2 N_j(x)}{dx^2}\right)dx \tag{2.23}$$

Using this equation, the local stiffness matrix of the beam element is:

$$[k] = \begin{bmatrix} k_{11} & k_{12} & k_{13} & k_{14} \\ k_{21} & k_{22} & k_{23} & k_{24} \\ k_{31} & k_{32} & k_{33} & k_{34} \\ k_{41} & k_{42} & k_{43} & k_{44} \end{bmatrix} = \frac{EI}{L^3}\begin{bmatrix} 12 & 6L & -12 & 6L \\ 6L & 4L^2 & -6L & 2L^2 \\ -12 & -6L & 12 & -6L \\ 6L & 2L^2 & -6L & 4L^2 \end{bmatrix} \tag{2.24}$$

The global stiffness matrix of the entire structure is referred to as [K] and is assembled from the local stiffness matrices of the elements that form the structure.

2.4.5 Geometric Stiffness Matrix (Effect of Axial Forces)

When axial forces in the beam are considered in addition to the flexural forces, the stiffness coefficients will be modified. The modification to the stiffness coefficient k_{ij} is known as the geometric stiffness coefficient of the beam k_{Gij} which is defined as the nodal force, resulting from the axial forces in the beam, at and in the direction of the nodal displacement δ_i due to a unit nodal displacement δ_j while all other nodal

displacements are maintained at zero. From this definition, the geometric stiffness coefficient k_{Gij} is given by:

$$k_{Gij} = \int_0^L N(x)\left(\frac{dN_i(x)}{dx}\right)\left(\frac{dN_j(x)}{dx}\right)dx \tag{2.25}$$

where N(x) is the axial force at position x of the beam and $N_i(x)$ and $N_j(x)$ are the relevant shape functions of the beam. The axial force is assumed to be positive when compressive.

This coefficient represents the effect of geometric nonlinearity in the structure and from the previous equation the local geometric stiffness matrix of the beam element is:

$$[k_G] = \begin{bmatrix} k_{G11} & k_{G12} & k_{G13} & k_{G14} \\ k_{G21} & k_{G22} & k_{G23} & k_{G24} \\ k_{G31} & k_{G32} & k_{G33} & k_{G34} \\ k_{G41} & k_{G42} & k_{G43} & k_{G44} \end{bmatrix} = \frac{N}{30L}\begin{bmatrix} 36 & 3L & -36 & 3L \\ 3L & 4L^2 & -3L & -L^2 \\ -36 & -3L & 36 & -3L \\ 3L & -L^2 & -3L & 4L^2 \end{bmatrix} \tag{2.26}$$

The global geometric stiffness matrix of the entire structure is referred to as $[K_G]$.

2.4.6 Combined Stiffness Matrix

The total stiffness of a beam is represented by the local and global combined stiffness matrices, $[k_c]$ and $[K_c]$ respectively, which are given by:

$$[k_c] = [k] - [k_G] \tag{2.27}$$

$$[K_c] = [K] - [K_G] \tag{2.28}$$

2.4.7 Mass Matrix

It is possible to evaluate the coefficients in the mass matrix corresponding to the nodal displacements of a beam element by a procedure similar to the determination of element stiffness coefficients. In this manner, the mass coefficient m_{ij} of a beam element is defined as the nodal force in direction i (direction of the displacement δ_i) at one end of this beam due to a nodal acceleration in direction j ($\ddot{\delta}_j$) equal to one unit while all other nodal accelerations are maintained at zero. From this definition, the mass coefficient m_{ij} is given by:

$$m_{ij} = \int_0^L \rho A N_i(x) N_j(x) dx \tag{2.29}$$

where $N_i(x)$ and $N_j(x)$ are the relevant shape functions of the beam.

From the previous equation, the local mass matrix of the beam element is:

$$[m] = \begin{bmatrix} m_{11} & m_{12} & m_{13} & m_{14} \\ m_{21} & m_{22} & m_{23} & m_{24} \\ m_{31} & m_{32} & m_{33} & m_{34} \\ m_{41} & m_{42} & m_{43} & m_{44} \end{bmatrix} = \frac{\rho AL}{420} \begin{bmatrix} 156 & 22L & 54 & -13L \\ 22L & 4L^2 & 13L & -3L^2 \\ 54 & 13L & 156 & -22L \\ -13L & -3L^2 & -22L & 4L^2 \end{bmatrix} \tag{2.30}$$

The global mass matrix of the entire structure is referred to as [M].

2.4.8 Dynamic Load Vector

Figure 2.6 shows the forces and moments $r_1(t)$, $r_2(t)$, $r_3(t)$ and $r_4(t)$ at the ends of the beam element (nodal element forces). The local nodal force vector of the beam element can be written as:

$$\{r(t)\} = \begin{Bmatrix} r_1(t) \\ r_2(t) \\ r_3(t) \\ r_4(t) \end{Bmatrix} \tag{2.31}$$

When dynamic loads consist of only concentrated forces and moments applied to the nodes of discretization of the structure, the load vector can be written directly. In general, however, loads can be applied to other points. Loads may include distributed forces such as p(x,t) shown in figure 2.7. In this case, resulting forces at the ends of the beam element are called the equivalent nodal element forces, $r_{e1}(t)$, $r_{e2}(t)$, $r_{e3}(t)$ and $r_{e4}(t)$ in figure 2.7, and form the local equivalent dynamic load vector of the beam element as follows:

$$\{r_e(t)\} = \begin{Bmatrix} r_{e1}(t) \\ r_{e2}(t) \\ r_{e3}(t) \\ r_{e4}(t) \end{Bmatrix} \tag{2.32}$$

The global equivalent dynamic load vector of the entire structure is referred to as $\{F_e(t)\}$.

The equivalent nodal element force is given by:

$$r_{ei}(t) = \int_0^L p(x,t) N_i(x) dx \tag{2.33}$$

where $N_i(x)$ is the relevant shape function of the beam element.

The other dynamic loads concentrated at the nodes of discretization of the entire structure form the global concentrated dynamic load vector $\{F_{co}(t)\}$ which together with $\{F_e(t)\}$, the global dynamic load vector $\{F(t)\}$ of the entire structure can be determined as follows:

$$\{F(t)\} = \{F_{co}(t)\} - \{F_e(t)\} \tag{2.34}$$

2.4.9 Governing Equation of Motion

As shown above, the distributed properties of the beam and its load in the approximate method of analysis are expressed in terms of discrete quantities at defined nodes. The governing equations of motion as functions of these quantities are then established by imposing the conditions of dynamic equilibrium between the forces at the nodes. In simulations where the effect of axial forces is neglected due to it being small, the differential matrix equation of motion is:

$$[M]\{\ddot{y}\} + [K]\{y\} = \{F(t)\} \tag{2.35}$$

If the effect of axial forces is included, the equation of motion becomes:

$$[M]\{\ddot{y}\} + [K_c]\{y\} = \{F(t)\} \tag{2.36}$$

For free vibrations, the governing equation excluding the axial forces effect is:

$$[M]\{\ddot{y}\} + [K]\{y\} = \{0\} \tag{2.37}$$

and including the axial forces effect is:

$$[M]\{\ddot{y}\}+[K_c]\{y\}=\{0\} \tag{2.38}$$

By solving the equation of motion, the global displacement vector {y}, from which the local displacement vector {δ} of each single element of the model can be known, is determined. In practice, the solution can be accomplished easily by standard methods of analysis such as modal analysis with the assistance of computer software.

2.4.10 Nodal Element Forces

Once the nodal displacements {δ} are found, the dynamic equilibrium condition for each element can be applied in order to calculate the local vector {r(t)} of nodal element forces as follows if the effect of axial forces is neglected:

$$\{r(t)\}=[m]\{\ddot{\delta}\}+[k]\{\delta\}+\{r_e(t)\} \tag{2.39}$$

and as follows when including the effect of axial forces:

$$\{r(t)\}=[m]\{\ddot{\delta}\}+[k_c]\{\delta\}+\{r_e(t)\} \tag{2.40}$$

2.5 Strain Rate Sensitivity of Materials in Dynamic Problems

2.5.1 Introduction

Some dynamic loads, especially impulsive ones such as shock and impact, can cause high strain rates in the materials they act upon, where the strain rate is defined as the rate of change of strain with time. Most metals, especially steel, tend to exhibit enhanced mechanical properties at high rates of strain, due to dynamic loads, compared to their properties under static and quasi-static loading. The stress strain curve is elevated as the strain rate increases such that the mechanical properties, such as the yield stress and the elasticity modulus, increase. In such cases, the metal is described as a strain rate sensitive material.

The phenomenon of strain rate sensitivity in materials has been investigated by many researchers including Cowper and Symonds (1957), Buchar, Bilek and Dusek (1986), Tinkler (1986) and Al-Hassani and Reid (1992). It has been found that the behaviour of strain rate sensitive metals is very complex. Therefore, several empirical formulae have been suggested in order to describe such behaviour as accurately as possible.

2.5.2 Constitutive Law for Modelling Materials with Strain Rate Sensitivity

Among the many formulae that represent strain rate sensitivity, the power law, which was experimentally derived by Cowper and Symonds (1957), is important and is one of the most widely used constitutive equations for modelling strain rate sensitive metals. This law assumes an increase in the yield stress and no change in the elasticity modulus and relates the dynamic yield stress σ_{yd}, the strength of the material under dynamic loading, to the strain rate $\dot{\varepsilon}$ as follows:

$$\dot{\varepsilon} = D\left(\frac{\sigma_{yd}}{\sigma_{ys}} - 1\right)^{q} \tag{2.41}$$

where

σ_{ys} is the static yield stress, the strength of the material under static loading
D is the multiplier of strain rate sensitivity of the material
q is the exponent of strain rate sensitivity of the material

D and q are constants, which are determined experimentally, for a particular material. For mild steel, these constants have been found to be approximately equal to 40 and 5 respectively.

The previous equation can be recast to give the dynamic yield stress directly as follows:

$$\sigma_{yd} = \sigma_{ys}\left[1 + \left(\frac{\dot{\varepsilon}}{D}\right)^{\frac{1}{q}}\right] \tag{2.42}$$

It can be seen that the yield stress is always greater under dynamic loading than static loading.

2.6 Review of Previous Research

In the following, a survey of what has been done so far in the field of dynamic analysis of beams is presented. This includes the studies made for the development of various methods, both analytical and numerical, to determine dynamic response of beams and their potential applications, shortcomings and limitations. Also, several finite element models are discussed with the results of analysis. Empirical formulae for beam dynamics derived from observations are given as well. The literature review is presented in chronological order.

It was recognized by the early researchers in the problem of a transversely vibrating beam that the bending effect was the single most important factor. The Euler-Bernoulli beam model, named after Leonhard Euler, and Daniel and Jacob Bernoulli and which dates back to the 18th century, took this effect into account and was therefore the first 'accurate' model to be introduced and the most widely used for dynamic analysis of beams. However, the Euler-Bernoulli model had a deficiency in that it tended to slightly overestimate the natural frequencies of the vibrations of the beam. This overestimation was exacerbated for the natural frequencies of the higher normal modes of vibration. This frequency problem was shown by Strutt (1877), Timoshenko (1953), Timoshenko and Young (1955), Hughes and Speirs (1982) and Weaver et al. (1990).

Strutt (1877) improved the Euler-Bernoulli model by including the effect of rotatory inertia of the beam. This improvement partially corrected the overestimation of natural frequencies. However, Strutt (1877) and some subsequent researchers, for example Davies (1937), found that the frequencies were still overestimated even when the rotatory inertia effect was included.

However, a further improvement to the beam model made by Timoshenko (1921 and 1922) did actually address the problem of frequency overestimation. He proposed and discussed a beam model which added the effect of shear distortion as well as the effect of rotatory inertia to Euler-Bernoulli model. This improved model, the Timoshenko

beam model, considerably increased the accuracy of the estimation of the natural frequencies and was therefore a major breakthrough in the analysis of high-frequency dynamic problems where the shear and rotatory effects could not be neglected.

Den Hartog (1928) derived formulae for estimating the first and second natural frequencies of vibration of a part of a circular arc clamped at both its ends using the Rayleigh-Ritz approximate method and including the limiting case when the arc had a very small central angle and thus was considered as a straight beam. It was found that the type of vibration, in which extension of the axial length occurred, under certain conditions had a lower natural frequency than any non-extensional type of vibration.

Shanley (1947) adopted and clarified a greatly simplified statics model originally suggested by Ryder of the American Civil Aeronautics Authority, to analyse inelastic columns acting in bending with axial forces, and which was later successfully used to represent nonlinear elastic plastic beams including axial force effects, whether in statics or dynamics. This model, the Ryder-Shanley Model, consisted of two infinitely rigid half beams connected with a hinge, which was a cell of negligible dimension compared to the beam length. The hinge was formed from two elastic plastic flanges which carried axial load only. Thus, the model had only one degree of freedom, the displacement of the hinge at the middle of the beam, eliminating the computational work of integration over the length of the beam. Moreover, as the cross section at the hinge consisted of two axial flanges only, integration over the cross section of the beam was also eliminated. Thus, it was found that the Ryder-Shanley model significantly simplified the complex problem of a beam, but represented the behaviour reasonably well and included most structural effects.

Symonds (1953) studied the dynamic characteristics of plastic, simply supported uniform beams of rectangular cross sections undergoing large plastic deformations in bending due to high transverse middle-concentrated impulsive loads. The approximations of the rigid plastic method, with two rigid halves of the beam and a plastic hinge in the middle, were adopted. The governing equation of motion was

integrated numerically and the results were used to derive the following empirical formula for the permanent middle rotation θ_p of the beam:

$$\theta_p = \frac{0.37}{\rho\sigma_y^{\frac{5}{3}} b^{\frac{5}{3}} h^{\frac{10}{3}} l^{\frac{1}{3}}} F_m^{\frac{2}{3}} I_F^{\,2} \qquad (2.43)$$

where ρ, σ_y, b, h, l, F_m and I_F are respectively the mass density, yield stress of the material, width, thickness of the cross section, half span of the beam, maximum value and impulse of the load.

Seiler, Cotter and Symonds (1956) analysed a uniform beam, made of a ductile material, subjected to impulsive loading. The elastic and elastic-plastic motions were analysed under the assumption that plastic flow was confined to the critical cross-sections, and the final maximum deformations were compared with those computed from an analysis which neglected all elastic deformations, that was a rigid-plastic analysis. The purpose was to provide further information which might help in estimating the range of validity of rigid-plastic analysis. Whilst the elastic-plastic solution was more accurate, the rigid-plastic analysis could be expected to give good results for intense dynamic loading where the energy absorbed by the beam in plastic deformations significantly exceeded the elastic strain energy of the beam. For other cases, the elastic behaviour of the beam should not be ignored.

Martin and Symonds (1966) examined the use of the elementary rigid-plastic method in the dynamic analysis of beams subjected to short duration high intensity loads (impulsive loads). The method required that a suitable mode shape for beam vibrations be chosen first. Thereafter, the deceleration was determined from the governing equation of motion and the initial mode velocity followed without further assumptions. The load range, over which the method is valid, was found to be upper bounded by the requirement that the deformations should not be so large that the geometry change effects became significant, and to be lower bounded by the requirement that the energy of disturbance dissipated should be very large compared to the maximum energy which could be absorbed elastically by the beam in order to justify neglecting the elastic behaviour in the analysis. The importance of the elementary rigid-plastic method was

the ability to provide an estimation of major deformations caused by large dynamic loads simply and quickly, and the possibility to include effects normally neglected such as the finite deflections when necessary.

Martin and Lee (1968) described a unified method of approximating the dynamic response of beams subjected to impulsive loading which included the elastic behaviour in addition to the plastic behaviour. The rigid-plastic method was also discussed. The methods were based on the solution uniqueness proved by Martin (1966) for such kinds of dynamic problems. It was found that the elastic-plastic method successfully approximated the behaviour of an impulsively loaded beam more accurately than the rigid-plastic method.

Kaneko (1975) investigated Timoshenko's correction for shear in vibrating beams and a review of the studies of the shear coefficient in Timoshenko's differential equation for flexural vibrations of beams was first provided. Expressions of this coefficient previously proposed for circular and rectangular cross sections were tabulated, together with expressions previously overlooked and unknown, and compared with one another. It was pointed out that the expressions for the shear coefficient for both the circular and rectangular cross section which were previously proposed by Timoshenko (1922) were the best estimates at this stage of the relevant theories and experiments.

An attempt to follow on the work of Timoshenko (1921) but for the plastic state was made by Jones and Gomes de Oliveira (1979) who included rotatory inertia and transverse shear in the dynamic analysis of beams undergoing plastic deformations rather than the elastic deformations considered by Timoshenko. They presented a theoretical procedure to examine the influence of retaining the transverse shear force in the yield criterion and rotatory inertia on the dynamic plastic response of beams. An exact rigid-plastic solution was derived for an impulsively loaded beam. It transpired that rotatory inertia played a small, but not negligible, role on the dynamic behaviour of the beam. Also, results from this investigation indicated that the greatest departure from an analysis which neglected rotatory inertia but retained the effect of bending moment

and transverse shear force in the yield condition was approximately 11% for the particular range of parameters considered.

Lepik and Just (1983) developed a FORTRAN programme, DINOPT, which employed the method of mode form motion, for the automatic calculation of permanent deflections of rigid-plastic beams of rectangular cross-section under rectangular impulsive pressure loads. The fitness and effectiveness of the programme was demonstrated by solving several examples. It was also shown that the mode form solution, with nonmoving plastic hinges formed at the critical sections only, using this programme was cheaper computationally than and could be used to obtain reasonably accurate results instead of the complicated, but more accurate solution, with multiple travelling plastic hinges.

An important investigation carried out by Symonds and Yu (1985) examined in detail the particular problem of short pulse loading on a pin-ended beam. The elastic-plastic dynamic response was predicted by ABAQUS and a number of other well-known computer programmes including ANSYS, DYCAST, MARC, MENTOR, REPSIL, WHAMS and WRECKER. The results for the time history of the displacement were plotted and compared. The permanent displacement predicted by ABAQUS and some of the other programmes was found to be in the direction opposite to that of the load, which was seen as counterintuitive. Analysis of a Shanley-type model of the same problem for a broader range of input values for the pulse, which included the above loading, was carried out and cases of this surprising behaviour were found. In these cases, which occurred for a small number of very narrow ranges of pulses, the permanent displacement produced was opposite to the pulse direction. An explanation was given that this might be due to plastic irreversibility and geometric nonlinearity.

Also, the results showed vast discrepancies in the responses predicted by the different softwares, or even by the same software analysing slightly different models of the same problem, except for the first peak displacement, which represented the design range, where all predictions were found to be in an excellent agreement. These discrepancies

indicated a strong sensitivity of the problem to both the physical modelling and computational procedures.

Vaziri, Olson and Anderson (1987) presented the analysis of a rigid perfectly plastic rectangular beam with axially constrained ends subjected to a rectangular pressure pulse of finite duration, a blast load. Closed form expressions were obtained for the maximum permanent deflection for both simply supported and clamped boundary conditions. These expressions were valid for the full dynamic range from a pseudo-static step load to high pressure impulsive loading. The results indicated that the dynamic response was strongly influenced by geometry changes even for small deflections. Finally, the response expressions were combined to form isoresponse relationships which when plotted formed isoresponse curves for direct engineering use.

Jones (1989) presented a detailed explanation, with equations, of the rigid-plastic method for the dynamic analysis of beams, especially fully clamped homogenous slender beams of uniform rectangular cross sections and subjected to impulsive loads such as explosions. He included extensive research done on the subject by him and other researchers. It was found that for small displacements, bending dominated the dynamic behaviour of the beam where fully plastic bending hinges formed at the beam critical sections, the middle and end sections, while the beam segments between these hinges moved as rigid bodies. The influence of finite, large displacements, geometric nonlinearity, was investigated also. It was shown that axial tension became more significant in the beam as displacements increased while bending became less dominant as the fully plastic hinges went into pure axial tension plasticity with no bending and the beam transformed into a string. The interaction between tension and bending at the fully plastic cross section for the hinges during the transitional stage was illustrated. The relation that represented this interaction in a rectangular cross section and its graphic depiction, the yield curve of the cross section, were presented.

Benamar, Bennouna and White (1991) presented a method for calculating the nonlinear mode shapes and natural frequencies of fully clamped beams at large vibration amplitudes and compared their results with those of previous studies and of

experimental measurements. First, the transverse displacement was assumed to be harmonic and was expanded in the form of a finite series of functions. Then, the nonlinear deformation energy was expressed by taking into account the nonlinear terms due to the axial strain induced by large deflections. A set of nonlinear algebraic equations, which reduced to the classical linear eigenvalue problem when nonlinear terms were neglected, was determined through Hamilton's principle. It was also shown that unless a condition was imposed on the contribution of one mode, the solution of this set led to the linear case. Consequently, in order to obtain a numerical solution for the nonlinear problem in the neighbourhood of a given mode, the contribution of this mode was chosen and those of other modes were calculated. In this work, the method was also applied to obtain the first three nonlinear mode shapes of clamped-clamped and simply supported beams. The results obtained corresponding to the fundamental nonlinear mode shape were in good agreement with those of a previous theoretical and experimental study. In particular, high values of beam curvatures were noticed near the clamps causing a highly nonlinear increase in bending strains with increasing deflections.

Abhyankar, Hall II and Hanagud (1993) examined the utility of direct numerical solution procedures, such as finite difference or finite element methods, for partial differential equations in chaotic dynamics of beams. They noted that in the past, procedures for solving such equations to detect chaos in beam behaviours had utilised Galerkin approximations which reduced the partial differential equations to a set of truncated nonlinear ordinary differential equations. They demonstrated that a finite difference solution instead was actually equivalent to a Galerkin solution and that the finite difference method was more powerful in that it might be applied to problems for which the Galerkin approximations would be difficult, if not impossible to use. In particular, a nonlinear partial differential equation which modelled a slender Euler-Bernoulli beam in compression was solved to investigate chaotic motions under periodic transverse forcing. The equation, cast as a system of first-order partial differential equations, was directly solved by an explicit finite difference scheme. The numerical solutions were shown to be the same as the solutions of an ordinary differential equation approximating the first mode vibration of the buckled beam. Then, rigid stops of a finite length, with which the beam collided during the motion, were incorporated into the model to demonstrate a problem in which the Galerkin procedure

was not applicable. It was shown that the finite difference method could however be used to study this stop problem with prescribed restrictions over a selected subdomain of the beam. Results obtained were briefly discussed. The conclusion was that a more general solution technique applicable to problems in chaotic dynamics of beams had been introduced.

Lepik (1994) discussed the problem of elastic-plastic dynamic response of fully clamped uniform beams and flat arches under transverse impulsive loading. The equations of motion were integrated by Galerkin's method with two degrees of freedom for deflections. The possibility of chaotic behaviour exhibited by beams and arches impulsively loaded was investigated. For this purpose, displacement time histories, phase portraits and power spectrum diagrams for different values of the initial velocity imposed by the impulsive loading were computed and put together for comparisons. It was noticed that weak chaotic effects existed especially in the initial phase as to the long-term motion it usually changes to periodic vibrations of smaller amplitude. Also, it was shown that for pulse loading of short duration the permanent deflection of the beam might be on the opposite direction of the acting load. This phenomenon which was previously observed by other researchers such as Symonds and others was called the counterintuitive or anomalous behaviour. In fact, the computations carried out in this work for uniform beams led to the same results previously found by Symonds and others using Shanley-type models for beams.

Lewandowski (1994) presented a computational method for determining the backbone curves (the amplitude-frequency relations) of freely vibrating slender beams. The beam response was expanded into a truncated Fourier series with respect to time. The resulting non-linear eigenvalue problem was formulated using the variational approach and the finite element method and solved by the continuation method to obtain the non-linear frequencies and modes of vibration. Numerical results for various beams were obtained and compared with other published results, both exact and numerical, to demonstrate the accuracy and applicability of the method. Also, some bifurcation points were found to exist on some beams backbone curves and were reported accordingly for the first time.

Houmat (1995) introduced a four-node Timoshenko beam finite element with variable degrees of freedom. The element transverse displacement and rotation of the beam cross-section were each described by a cubic polynomial plus a variable number of trigonometric sine terms. The polynomial terms were used to describe the transverse displacements and rotations of the beam cross-section at the element's four nodes while the sine terms were used to provide additional freedom to the interior of the element. The four nodal transverse displacements and rotations of the beam cross-section and the amplitudes of the trigonometric sine terms were used as generalized coordinates. Inter-element compatibility was achieved by matching the generalized coordinates at the element end nodes. Numerical results of frequency calculations were given for slender beams with two different slenderness ratios. Comparisons were made with exact Timoshenko beam solutions and with finite element solutions for the degenerate case with no trigonometric terms to represent an only-polynomial finite element. It was found that using one or two variable order Timoshenko beam finite elements with a few trigonometric terms yielded a better accuracy with obviously fewer degrees of freedom for the entire model than using many only-polynomial Timoshenko beam finite elements.

Lepik (1995) discussed the non-linear vibrations of a buckled beam under harmonic excitation. The material of the beam was elastic-plastic with linear strain-hardening. The equations of motion were integrated by Galerkin's method. Also, in the elastic case, the Melnikov method was used for estimating the threshold transverse load at which chaotic motion could take place. Chaotic motion of the beam was discussed as well in the range of elastic-plastic vibrations. By carrying out computations for several values of the beam, material and load parameters, it was concluded that chaotic vibrations in the case of harmonic excitation were more common than for beams under pulse loading.

Shi and Mei (1996) presented a finite element modal formulation in the time domain for the large amplitude free vibration of beams. The non-linear modal equations of motion were derived using a simple and general procedure and accurate frequency-maximum deflection relations were obtained for the fundamental and higher non-linear modes.

The number of modes to be included in the analysis for accurate frequency results was determined depending on the percentage of participation from each mode. Numerical examples on beams were given and results were compared with classical continuum analytical solutions of Galerkin's method where a good agreement was found.

Corn, Bouhaddi and Piranda (1997) proposed a new method for simply and systematically constructing finite Timoshenko beam elements. The continuous model, which took into account both rotary inertia and transverse shear deformation, was presented as a tutorial review. This model allowed certain vibratory phenomena characteristic of relatively short beams to be demonstrated. The proposed method involved constructing a two-node finite element based on Guyan condensation that led to the results of classical formulations, but in a simple and systematic manner. This element was verified with numerical and experimental tests. The method was then generalized in order to obtain new improved three-node finite elements. In addition to the fact that the technique proposed for constructing the finite elements had the advantage of being simple and systematic, the finite elements in this method themselves were found to yield results which were in good agreement with the continuous model, especially in the case of relatively short beams. Moreover, it was shown that, for the two-node element, all choices of polynomial interpolations of order three or higher led necessarily to the same stiffness and mass element matrices. However, for the three-node element, the generalization of this method to higher order interpolations allowed elements which performed better to be obtained, provided that Guyan condensation was still employed.

For the dynamic analysis of the problem of an elastic-plastic beam, Xu and Hasebe (1997) suggested a continuous fourth-order ordinary differential equation Shanley-type model. A co-dimension three bifurcation problem and its simplified case, an incomplete co-dimension two bifurcation of a pair of pure imaginary eigenvalues and a simple zero eigenvalue were presented and analyzed, and the normal form analysis and the unfoldings of 2-jet and 4-jet cases of the incomplete normal forms were provided. Since elastic-plastic beam dynamics were of great non-linear complexity and the vector fields were multiple degeneracies, small differences of physical parameters caused dramatic essential changes of behaviour of the motion. Through these results the rich

dynamical behaviours of the elastic-plastic beam, including the counterintuitive behaviour and its sensitivity to small parameters of this problem, were illustrated. It was found that the continuous Shanley-type model was very suitable for analyzing the complicated dynamic behaviours of the problem of elastic-plastic beams and although the incomplete normal form which well described this beam dynamics problem had no separate singular point, its unfoldings still presented rich bifurcation phenomena and could be used to explain the interesting behaviours of the beam in this problem. Also, it was emphasized that the dynamics of elastic-plastic systems and their strong nonlinearities of both materials and geometries were still a necessary research field.

Han and Lu (1999) proposed an unconventional finite element technique for the elastoplastic dynamic analysis of beams called the space-time finite element method (STFEM) which was based on a unified space-time discretization approach. A weak form of the governing equation which corresponds to the generalized law of conservation of impulse-momentum (the shock-momentum equation) was established, based on which STFEM equations were derived. A family of linear temporal shape functions was studied, which for linear elasticity, the ensuing STFEM algorithm was equivalent to the Newmark algorithm with $\gamma = 0.5$. Rate-independent plasticity was incorporated into the model. As a numerical example, a cantilever beam under shock loading was analyzed. It was found that the STFEM formulation is inherently suitable for handling the evolution equations of plastic flow. The results showed that the propagation of shock waves was drastically slowed down by the presence of plasticity. Also, because the plastic deformation tended to be localized in the vicinity of the impact, a full transient analysis was essential, in order to accurately determine the locations of the plastic hinges. Furthermore, it was shown that damping reduced the amplitude of the vibration, but did not, in general, affect the evolution and distribution of the plastic deformations significantly. Instead, it was the hardening parameter that played this role.

Ribeiro and Petyt (1999) investigated the geometrically non-linear multi-harmonic free and steady-state forced vibrations of uniform, slender beams with rectangular solid cross section using the hierarchical finite-element method (HFEM) and the harmonic balance method (HBM). The HFEM is a type of the p-version of the finite element

method (FEM) when the set of functions, corresponding to an approximation of lower order p, constitutes a subset of the set of functions corresponding to the approximation of order p+1. The HBM was applied to study the effect of internal resonances in the non-linear vibration of beams. Two cases for the end conditions of the beam were studied, both ends clamped or simply supported. The beam analogue of von Kármán's non-linear strain–displacement relationships was employed and the middle plane in-plane displacements were included in the model. The equations of motion were developed by applying the principle of virtual work and were solved by a continuation method. The ratios 1:3 and 1:5 for internal resonances were discovered and their consequences were discussed. The convergence properties of the HFEM were analyzed.

It was found that the internal resonances of order n exist if the ratio of the linear frequencies associated with the interacting different modes of vibration is approximately equal to n. Therefore, when analyzing a certain mode of vibration and when the nonlinear natural frequency becomes a submultiple of another natural frequency, it was necessary to include another harmonic in the time series. Below that point, the solution with only one harmonic produced data that was sufficiently accurate, as was confirmed by comparison with experimental results. On the other hand, the coupling with higher order modes also implied that more degrees of freedom were necessary in the spatial model for accuracy. Also, it was concluded that the non-linear mode shape changes with the amplitude and frequency of vibration because of two different causes. The first is the variation of the stiffness of the beam with the amplitude of vibration due to the axial forces. In this case, the alteration in the non-linear mode shape is moderate. The second cause of alteration is modal coupling. If there is commensurability of natural frequencies and internal resonance occurs, then the non-linear vibration of the beam is defined by the sum of the coupled modes vibrating at commensurable frequencies, and the mode shape varies significantly during the period of vibration.

When the HFEM model was favourably compared with FEM models presented in the literature, it was demonstrated that in order to achieve convergence the HFEM model required far fewer degrees of freedom (coarser mesh) than the h-version of the FEM models, the thing that significantly reduced the computational time. This turned out to

be of great importance if one wanted to analyze higher order modes or when higher order modes coupled with lower order modes due to internal resonance, if several harmonics must be included in the time series or if a structure composed of several beams was to be studied.

Pham (2000) analyzed the dynamic load-bearing capacity of elastic-plastic beams by the apparatus of shakedown theory. The reduced kinematic formulation for bending beams, which was equivalently deduced from Koiter's kinematic theorem, combined with the plastic collapse method of hinge mechanisms were employed. These analytical techniques appeared effective in solving practical beam problems especially beams subjected to quasiperiodic dynamic loading. The safety limits on the quasiperiodic dynamic loads as well as the respective collapse mechanisms for a number of practical cases of beams were determined. Also, some shakedown load amplitude-frequency diagrams that could serve various engineering design purposes were drawn.

Yankelevsky and Karinski (2000) presented an approximate model to analyze the dynamic elasto-plastic small or large deformation response of beams under various symmetrical loading. The present model extended the capabilities of the earlier model proposed by Yankelevsky and Boymel (1984) (which itself built on the analytical techniques and notes listed by Johnson (1972) for determining the response of beams subjected to impulsive loading), and considered the general symmetrical problem with loading along part of the beam. In this model, the beam was composed of two rigid parts interconnected by a gap of zero width, thus yielding a triangular deflection shape. The gap was built of fibers having imaginary length which governed strains and stresses in the beam and was determined by requiring equal deflections in both the real and model beams. This imaginary length was found to be almost constant in the elastic and in the elasto-plastic domains, but depended on the load distribution. Comparisons of maximum deflections predicted using this simplified model with results of a more accurate finite element analysis were done and showed very good correspondence. Apart from the permanent displacement which might easily be measured from test, this model could also calculate the time history of the dynamic reactions, bending moment and membrane force, displacement and velocity and acceleration as well as stress and strain distributions in the mid-section of the beam.

McEwan, Wright, Cooper and Leung (2001) proposed a method for modelling large deflection beam response involving multiple vibration modes. Significant savings in computational time could be obtained compared with the direct integration non-linear finite element method. The deflections from a number of static non-linear finite element test cases were transformed into modal co-ordinates using the modes of the underlying linear system. Regression analysis was then used to find the unknown coupled non-linear modal stiffness coefficients. The inclusion of finite element derived modal masses and an arbitrary damping model completed the governing non-linear equations of motion. The response of the beam to excitation of an arbitrary nature might then be found using time domain numerical integration of the reduced set of equations. The work presented here actually extended upon the work of previous researchers to include non-linearly coupled multi-modal response. The particular benefits of this approach were that no linearization is imposed and that almost any commercial finite element package might be employed without modification.

The proposed method was applied to the case of a homogeneous isotropic beam. Both fully simply supported and fully clamped boundary conditions were considered. For the free vibration case, results were compared to those of previous researchers. For the case of steady-state harmonic excitation, results were compared with the direct integration non-linear finite element method using ABAQUS. In all cases, excellent agreement was obtained.

Ribeiro (2001) analyzed the geometrically non-linear vibrations of beams by the Hierarchical Finite Element Method (HFEM) which is a p-version method. Two main points were of interest. The first was to compare polynomials, trigonometric functions and beam eigenfunctions as displacement shape functions for the beam hierarchical finite elements. The second was to examine the suitability of the HFEM for the geometrically nonlinear dynamic analysis of beams in the time domain. It was found that polynomials had in general more advantages than trigonometric functions and beam eigenfunctions as accuracy was achieved with a smaller number of degrees of freedom, continuity between elements was more guaranteed and the element matrices were

derived more quickly when polynomials were used. Also, the HFEM was found to be an efficient tool for time domain analysis as it quickly provided the response even when involving several modes of vibration. This was due to the small number of degrees of freedom required for fairly 'accurate' analysis by this method.

Gerstmayr and Irschik (2003) presented a numerical strategy for flexural vibrations of elasto-plastic beams with rigid-body degrees-of-freedom. Beams vibrating in the small-strain regime were considered and special emphasis was laid upon the development of plastic zones. An elasto-plastic beam performing plane rotatory motions about a fixed hinged end was used as example problem. Emphasis was laid upon the coupling between the vibrations and the rigid body rotation of the pendulum. Plastic strains were treated as eigenstrains acting in the elastic background (real) structure. The formulation led to a non-linear system of differential algebraic equations (DAEs) which was solved by means of the Runge–Kutta midpoint rule illustrated by Thomson (1993). A low dimension of this system was obtained by splitting the flexural vibrations into a quasi-static and a dynamic part. Plastic strains were computed by means of an iterative procedure tailored for the Runge–Kutta midpoint rule. The numerical results demonstrated a decay of the vibration amplitude due to plasticity and the development of plastic zones. Also, it was found that the pendulum approached a state of plastic shake-down after sufficient time. In general, the newly derived numerical algorithm turned out to be efficient and robust and would serve as a starting point for an extension of the present formulation in the case of large deformations, and also for studies concerning elasto-plastic multibody systems.

Ma, Liu, Zhao and Li (2005) investigated the dynamic instability of an elastic-plastic beam by employing a three-degree-of-freedom (3-DoF) Shanley-type beam model. Especially, asymmetrical instability induced by symmetrical load was discussed. The asymmetrical instability was considered as a second-order buckling mode. Four types of perturbations, i.e., geometrical misalignment, material property mismatch, unsymmetry of applied load and disturbance of boundary conditions, were introduced to activate the asymmetrical responses. The asymmetrical response was characterized by a modal participation factor which corresponded to an asymmetrical mode shape. The axial force over the beam model was assumed constant while the maximum axial force

experienced in the beam model increased with the increase of the transverse load. Phase plane trajectories and Poincaré map were used to illustrate the chaotic characteristics of the beam response. Results showed that if the perturbations were small enough, the perturbation type had negligible influence on the critical load for the occurrence of the asymmetrical instability, which implied that the asymmetrical instability was an intrinsic feature of the beam system. However, with the increase of the magnitude of perturbations, the influence of the asymmetrical vibration was expanded to a large range of the critical loading parameter. Also, it was derived in this study that, similar to the column instability theory, the dynamic buckling of an elastic-plastic beam under transverse load was also affected mainly by the axial compressive force. However, the bending moment in the beam was well below the yielding bending moment.

Calis, Laghrouche and Desmulliez (2007) proposed a nonlinear slender beam model for Micro-Electro-Mechanical-Systems (MEMS) structures used in haptic sensing technology that was based on Cosserat theory instead of the classical theory of elasticity. The model was to be used for real-time simulation of these microstructures in a Virtual Reality Environment (VRE), enabling their virtual design, prototyping and manufacturing. It also allows for microtesting including failure diagnosis and evaluation of process reliability. To demonstrate the feasibility of the model, a cantilever microbeam and a bridge microbeam undergoing bending were simulated in real time in VRE. Cosserat theory was used because it better represented stresses in the miniaturised components of Microtechnology, especially in the nonlinear spectrum. Also, the implementation of Cosserat theory led to a reduction in the complexity of the model thus increased its capability for real-time simulation, which is indispensable in Microtechnology. Another significant benefit of the present work is that the proposed model can also be expected to be useful in Nanotechnology.

Ece, Aydogdu and Taskin (2007) investigated the free vibration of an isotropic elastic beam with a variable cross-section. The governing equation of motion was reduced to an ordinary differential equation in spatial coordinates for a family of cross-section geometries with exponentially varying width. The analytical solutions of the vibration of the beam were obtained, using Euler-Bernoulli beam theory, for three different

boundary conditions, simply supported, fully clamped and free ends. The natural frequencies and the mode shapes were determined for each set of boundary conditions. The results of this investigation showed that the non-uniformity in the cross-section influenced the natural frequencies and the mode shapes, and that the amplitude of vibrations was increased for widening beams while it was decreased for narrowing beams. Also, it was found that the frequencies were independent from the exponential decrease or increase but the mode shapes were affected by the increase or decrease behaviour.

Based on the work of Lloyd Smith and Sahlit (1991), Khan (2008) studied the dynamic behaviour of beams under extreme impulsive loads such as blast and gas explosion using the rigid-plastic method in which the dynamic analysis was treated as a Linear Complementarity Problem (LCP). For this purpose, Lemke's algorithm, which was characterized by a semi-definite matrix, was proposed and adapted for the solution of the LCP. The capability of the LCP method was demonstrated by comparing the solutions with available theoretical plastic solutions in closed form to dynamic beam problems where plasticity resulted from bending deformations only. Comparisons showed that the LCP solution had a tendency to converge on the theoretical solution with very small errors, less than 2%, for the particular range of parameters considered. Results from the LCP method were also compared with results from elasto-plastic simulations provided by the nonlinear structural analysis software ADAPTIC for problems in which the elastic stiffness was assumed to be very large in order to investigate the effect of ignoring the presence of even a small amount of elastic deformations on the accuracy of the rigid-plastic analysis. It was found that neglecting elastic behaviour in the LCP analysis tended to give slightly different results despite the efforts made to ensure that the ratio of the total input energy imparted to the beam by the impulse to the maximum elastic strain energy the beam could store was high. Due to its simple formulation, the LCP method was a very efficient tool for the dynamic analysis of beams. However, it ignored the effects of axial force, which made it restricted to small displacement problems and thus implied the presence of some limitations on the maximum impulse that could be applied to a beam analysed using this method.

Chen and May (2009) investigated the dynamic response of reinforced concrete beams under a different type of impulsive loading, a high-mass low-velocity impact. A series of experimental studies which provided high-quality input data and results was described and used to validate a numerical model proposed for the beams. Fourteen 2·7 m and four 1·5 m span beams were tested under impact loads using a drop-weight facility. Measurements included the transient impact load, the acceleration at various points on the beam and strains in the steel reinforcement. Additionally, the impact events were recorded using a high-speed video camera operated at up to 4500 frames per second. The local failure pattern of the beam under the impact zone was also examined by correlating the images of the progression of cracks, spalling and scabbing with the time history of the impact load. In total, the work enabled a better understanding of the impact behaviour of reinforced concrete beams.

Gupta, Babu, Janardhan and Rao (2009) investigated large amplitude free vibration analysis of uniform, slender and isotropic beams using a relatively simple finite element formulation, applicable to homogenous cubic nonlinear temporal equation (homogenous Duffing equation). All possible boundary conditions where the von-Karman type nonlinearity was applicable and where the ends were axially immovable were considered. The finite element formulation began with the assumption of simple harmonic motion and was subsequently corrected using the harmonic balance method and was general for the type of nonlinearity mentioned earlier. The nonlinear stiffness matrix derived in the finite element formulation led to symmetric stiffness matrix as compared to other recent formulations in the literature. Empirical formulae for the nonlinear to linear radian frequency ratios, for the boundary conditions considered, were presented using the least square fit from the solutions of the same obtained from the finite element analysis for various central amplitude ratios. The numerical results attained using these empirical formulae compared very well with the results available from the literature for the classical boundary conditions such as the hinged–hinged, clamped–clamped and clamped–hinged beams. For the beams with nonclassical boundary conditions such as the hinged–guided and clamped–guided, the numerical results obtained, apparently for the first time, were in line with the physics of the problem.

Rebeiro and van der Heijden (2009) developed a model based on a Timoshenko beam *p*-version finite element to analyze forced vibrations of beams that are, simultaneously, elasto-plastic and geometrically nonlinear. In the so-called *p*-version FEM, the accuracy of the approximation is improved by increasing the number of shape functions over the elements, unlike the case for the h-version FEM where simple elements are used. The geometrical nonlinearity was represented by Von Kármán type strain–displacement relations and the stress–strain relation was of the bilinear type, with mixed strain hardening. The equations of motion were obtained using the principle of virtual work and were solved in the time domain by an implicit Newmark numerical method. The Von Mises yield criterion is employed and the flow theory of plasticity applied; if plastic flow is found at a point of the domain, the total plastic strain is determined by summation. Numerical examples were carried out in order to demonstrate that the *p*-version element here advocated has a number of advantages and to show the influence of the plastic and geometrically nonlinear terms on the oscillations of beams. To investigate the robustness of the proposed approach, different parameters were tried in numerical tests and compared either with published data or with results computed using ANSYS. The element and procedure here suggested appeared to be robust and able to provide accurate results. The main advantages of the beam *p*-version, hierarchical, element were that it required fewer degrees of freedom than the *h*-version beam and shell elements, and provided a more detailed description of stress and strain fields than the *h*-version beam elements.

Plasticity was found to occur in a thin beam ($h/L = 0.01$) vibrating with displacement amplitude around its thickness; in a thicker beam plasticity occurred at relatively lower amplitudes. It was noted that the appearance of plasticity could significantly change the dynamic behaviour of beams. In the first cycles of excitation, at the beginning of the transient phase, plastic zones that absorb energy developed and, therefore, the displacements could be significantly over predicted by models that solely consider geometrical nonlinearity. Once the plastic strains were established they were permanent and obviously interfered in the beam dynamics; the way in which they did that would depend on the previous history of the motion and loading. With a periodic load, the fact that the combined plasticity and geometrical nonlinearity changed the stiffness, and therefore the natural frequencies, might was significant in the dynamics of the beam.

When a material is loaded in tension and then compressed, as occurs in cyclic loading, the yield stress in compression can be smaller than the yield stress reached in tension. A similar behaviour occurs when the material is again subjected to tension, and so on. This phenomenon is known as the Bauschinger effect. This effect on beam dynamics was also considered by Rebeiro and van der Heijden (2009) and a first assessment of it was made by carrying out tests on a thick beam. In these tests, it was found that the Bauschinger effect led to smaller plastic strains but which changed more significantly and during more cycles than when the effect is neglected. As a consequence, energy dissipation due to plastic work increased and smaller displacements, as well as smaller total strains and stresses, occurred.

Yagci, Filiz, Romero and Ozdoganlar (2009) presented a spectral-Tchebychev technique for solving linear and nonlinear beam problems. The technique used orthogonal Tchebychev polynomials as spatial basis functions, and applied Galerkin's method to obtain the spatially discretized equations of motion. Unlike alternative techniques that required different admissible functions for each different set of boundary conditions, the spectral-Tchebychev technique incorporated the boundary conditions into the derivation, and thereby enabled the utilization of the solution for any linear boundary conditions without re-derivation. Furthermore, the proposed technique produced symmetric system matrices for self-adjoint problems. In this work, the spectral-Tchebychev solutions for Euler–Bernoulli and Timoshenko beams were derived. The convergence and accuracy characteristics of the spectral-Tchebychev technique were studied by solving eigenvalue problems with different boundary conditions. It was found that the convergence was exponential, and a small number of polynomials was sufficient to obtain machine-precision accuracy. The application of the technique was demonstrated by solving: 1) eigenvalue problems for tapered Timoshenko beams with different boundary conditions, taper ratios and beam lengths; 2) an Euler–Bernoulli beam problem with spatially and temporally varying forcing, elastic boundary and damping; 3) large-deflection (nonlinear) Euler–Bernoulli beam problems with different boundary conditions; and 4) a micro-beam problem with nonlinear electrostatic excitation.

The results obtained from the spectral-Tchebychev solutions were seen to be in excellent agreement with those presented in the literature. Also, the spectral-Tchebychev technique derived here was found to be a numerically efficient approximate solution which was fairly accurate and applicable to a wide range of linear, nonlinear, self-adjoint and nonself-adjoint beam problems. Furthermore, this solution was suitable to be applied to beams with nonuniformly varying parameters and different boundary conditions without need for re-derivation.

Kimberley, Lambros, Chasiotis, Pulskamp, Polcawich and Dubey (manuscript accepted 2010) studied the dynamic response of microelectromechanical systems (MEMS) under impulsive loading. Despite the lack of means to provide such extreme loading rates to these miniature devices, the increasing use of MEMS-based sensors and actuators in adverse environments, which include extreme strain rate loading, has motivated the investigation of the response of MEMS components under these conditions. Micro Au (gold) fixed-fixed beams and cantilevers of uniform cross-section, the basic and most commonly used MEMS members, were subjected to impulsive loads of 40 ns in duration, which were generated by a high power pulsed laser in order to achieve acceleration levels on the order of 10^9 g. This allowed for the response to be investigated at time scales that were of the order of wave transit times in the substrate and the microdevices. Comparisons with companion finite element simulations were done in order to gain insight into the mechanisms responsible for impulsive deformations at the microscale. The simulations investigated the effect of loading rate, boundary conditions, beam dimensions and material constitutive behaviour including strain rate dependence on the permanent deformed shape of the beam. It was found that the contact and momentum transfer mechanisms were responsible for the large permanent beam displacements which were measured postmortem.

2.7 Conclusions

Various methods of dynamic analysis of beams have been presented. These methods differ from each other in terms of safety, material economy, cost of analysis and accuracy. Numerous studies have shown that although some analytical methods provide results close to reality, they might be very expensive to run. Also, due to the many assumptions serving to simplify accurate methods, it has been found that these methods often produce solutions which are not exact making the description 'accurate' just relative. Therefore, simple approximate methods of analysis have been put into use due to their cheap running cost and fast outcomes. However, as approximate methods reduce the confidence in the analysis results, accurate methods remain necessary in many structural situations when comparisons with trusted benchmarks are needed whether in practical design or for research purposes.

This Chapter also provides an overview of the investigations that have been done over the past decades in order to offer an insight into the attempts made in the field of the dynamic analysis of beams. This includes, in addition to some empirical formulae for fast primary calculations for example equation (2.43), various approximate methods both analytical and numerical that show good efficiency and reliability. Also included are several finite element methods that have proven to provide highly accurate results at fairly low computational costs.

For consideration of plastic strains and geometrical nonlinearity terms, several methods for dynamic analysis of beams were proposed such as the h-version of the FEM or the p-version of the FEM which includes the HFEM. The HFEM has, amongst the other p-version FEMs, the following advantages over the h-version of the FEM:

1- The HFEM's linear matrices possess the embedding property and the non-linear matrices of an approximation of lower order can be used in the derivation of the non-linear matrices of the improved approximation.

2- Simple structures can be modeled accurately using just one element, or "super-element", thus there are no inter-element continuity requirements and the assemblage of the elements is avoided.

3- The HFEM tends to give accurate results with fewer degrees of freedom than the h-version of the FEM. This is particularly true for smooth solutions since fine mesh generation is advantageous in the vicinity of singular points.

As a consequence of these properties, the HFEM model of a structure potentially requires less time to be produced and to be solved than an h-version of the FEM's model of this structure for the same level of accuracy.

Among the different approximate methods of dynamic analysis, the rigid plastic method has been one of the most widely used methods due to its simplicity, accuracy and above all its applicability for a wide range of problems including some very complex ones such as those that include nonlinearity, whether geometric or in the material. However, this method ignores the presence of elasticity in the material. Thus, plastic deformations must be present and much larger than elastic deformations in order for this method to give any accurate results, and this means that the energy imparted by the dynamic load should be many times larger than the beam elastic capacity of energy absorption. Otherwise, the rigid plastic method would have a great disadvantage. Therefore, there has been a need to develop other methods that include the effect of elasticity while remaining as convenient, the thing that has led to introducing the elastic plastic methods, such as the one presented in Chapter 4 and well investigated throughout this Thesis, which are more accurate and suitable for a wider spectrum of situations like those where elasticity should be taken into account.

The dynamic behaviour of elastic-plastic beams can be very complicated especially with the presence of nonlinearity, whether geometric or in the material, in the dynamic system. Some of the evidence of this complexity are the different predictions that different computer codes give for the deflection response after the first deflection peak, which include some counterintuitive responses, and the sensitivity of the problem to both the physical parameters and the computational technique used.

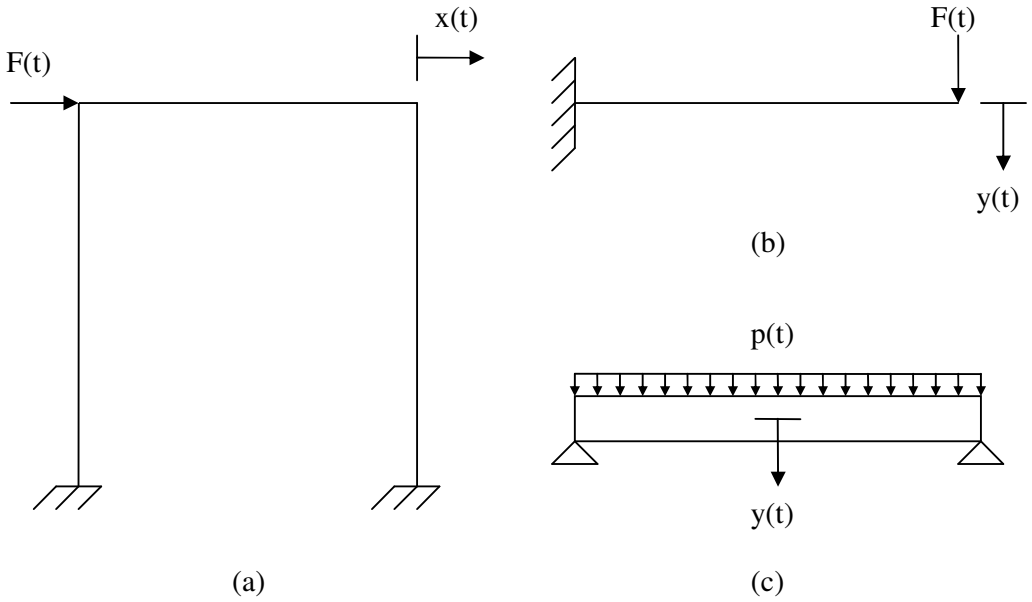

Figure 2.1: Various examples of structures modelled as having a single degree of freedom

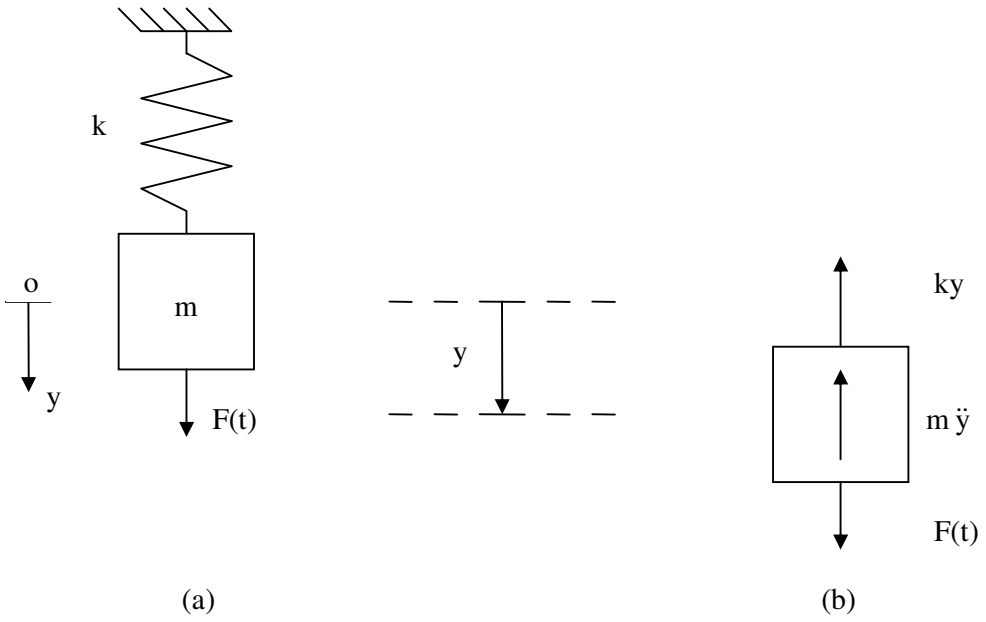

Figure 2.2: (a) Single degree of freedom model. (b) Free body diagram of this model mass

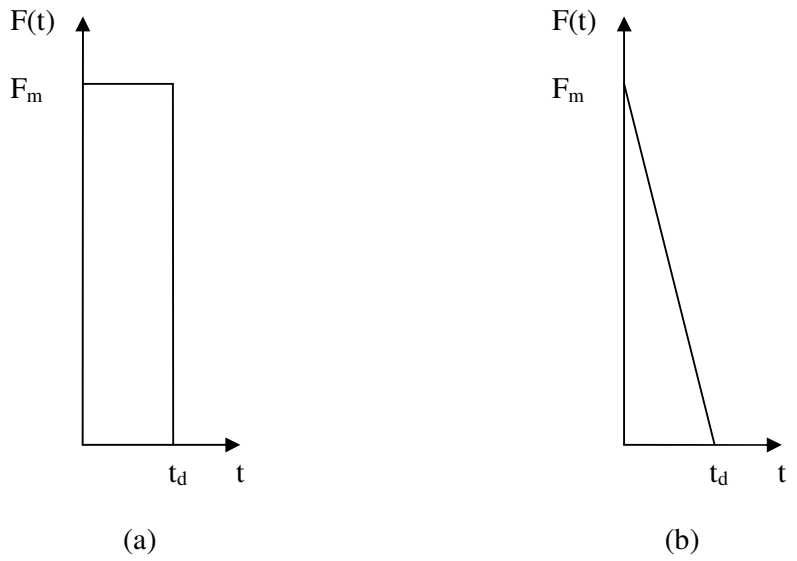

Figure 2.3: (a) Rectangular dynamic load. (b) Triangular dynamic load

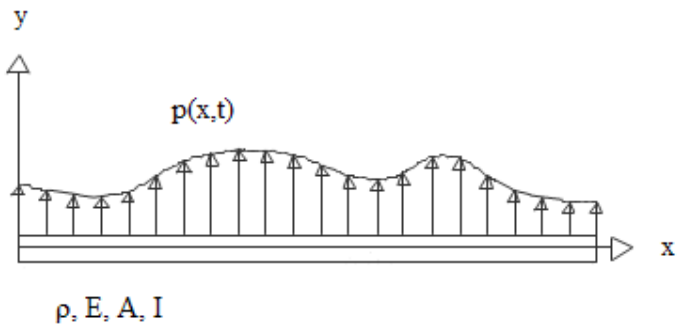

Figure 2.4: Beam under general dynamic load

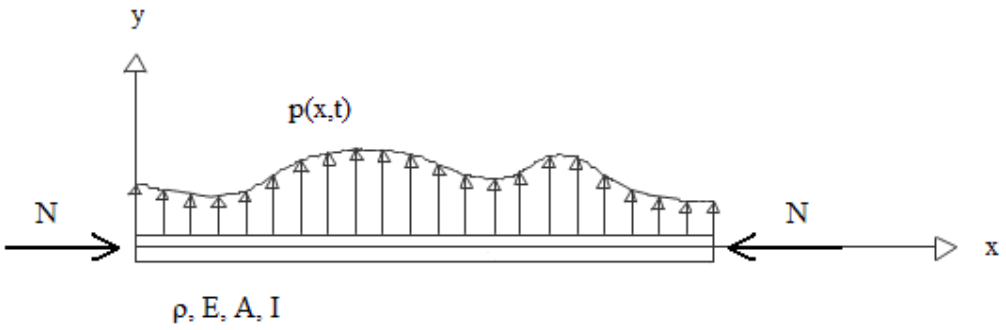

Figure 2.5: Axial force effect in beam dynamics

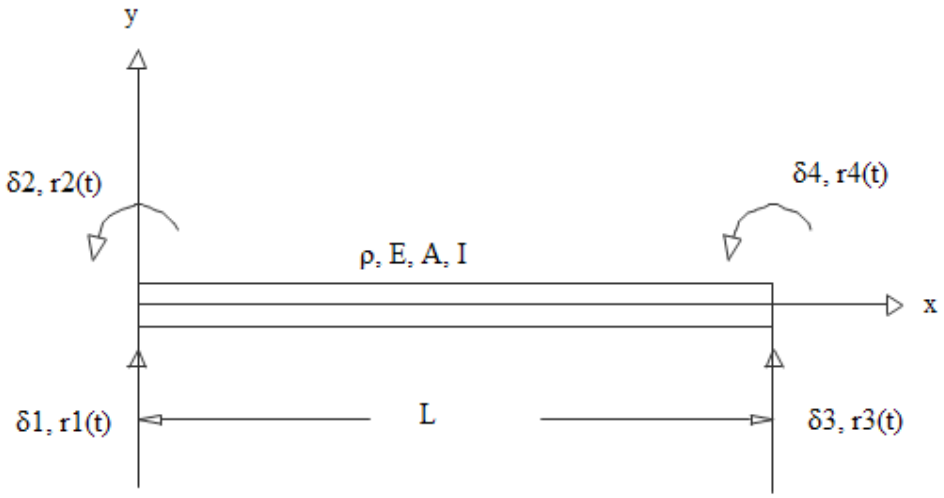

Figure 2.6: Beam element with its nodal displacements and forces

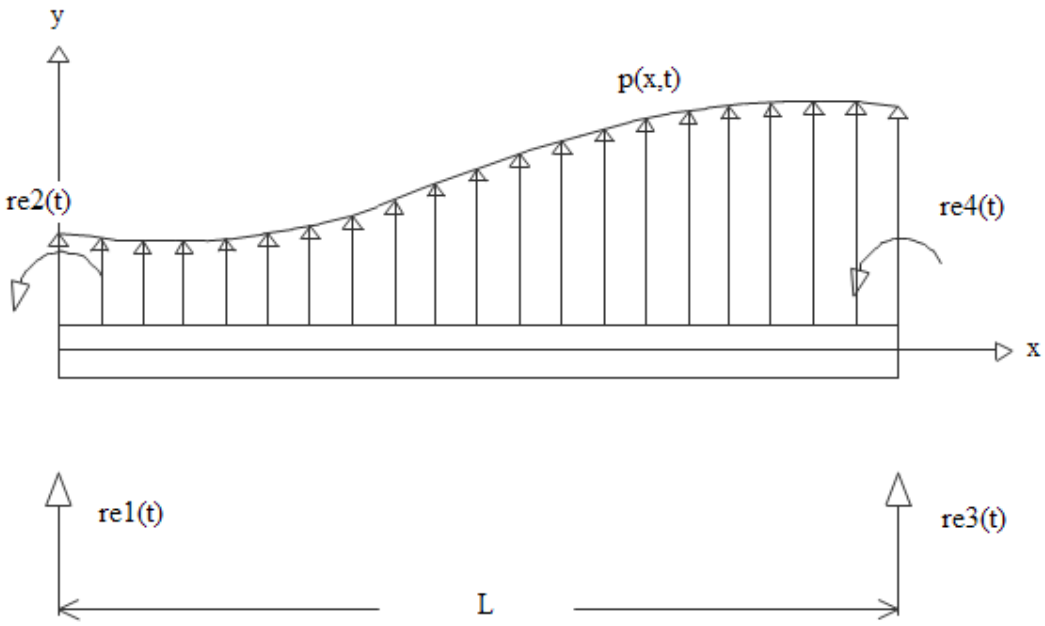

Figure 2.7: Equivalent nodal forces of beam element

Chapter 3 – Impulsive Loads

3.1 Introduction

In this Chapter, an introduction to the nature of impulsive loads is presented. In particular, one kind of these loads, the air blast of an explosion, is discussed. The importance of including explosive loads in the dynamic analysis and design of structures is revealed. The computational equations used for simulating the blast wave pressure applied to the exposed surface of a structure are detailed. Also, the principles of dynamic analysis and design of structures subjected to impulsive loads together with the various simplification techniques used in the simulation of these loads such as the pulse theorem are explained.

An impulsive load is a dynamic load that is applied very rapidly and maintained for a very short duration, less than one tenth of the fundamental natural period of the structure to which it is applied. In this case, the impulse, which is the time integral of pressure, is the dominant characteristic of loading.

3.2 Explosions as Source of Dynamic Loading

3.2.1 Introduction

Explosions produce one of the most common impulsive dynamic loads that structures could be subjected to. An explosion, or detonation, causes fast supersonic pressure waves called shock waves which are generated from a location called the centre of explosion. The waves propagate with a front like a sphere and reflect in the local medium around the centre. Thus, the medium is named the propagation medium. Also, an explosion causes an increase in the volume of the propagation medium, a release of various kinds of energies and high temperature. Figure 3.1 shows an example of explosions. More detailed information about explosions can be found in Baker, Cox,

Westine, Kulesz and Strehlow (1983), Bangash (1993), Bartknecht (1981, 1989), Lalanne (2002) and Wearne (1999).

3.2.2 Types of Explosions

Explosions are of various types and happen in different ways and from different sources. The most common type of explosions is the chemical explosion which is a fast chemical oxidation reaction that produces a large amount of hot gas. Examples of chemical explosives are gunpowder, ammonium nitrate fertilizer, guncotton (nitrocellulose), dynamite (stabilized nitroglycerin), natural gas (methane), petrol, etc. A second type of explosions is the nuclear reaction examples of which are atomic bomb and fusion bomb. Another type of explosions is the BLEVE, standing for Boiling Liquid Expanding Vapour Explosion, which happens when a container full of pressurized boiling liquid and hot vapour is ruptured causing the liquid and vapour to escape rapidly. Also, there are explosions that arise from natural causes. One example of this type of explosions is a volcano. This occurs when some magma that contains much dissolved gas rises from the depths of the earth. While the magma is rising, the pressure on it reduces and that allows the gas to bubble out resulting in a volcanic explosion. Another example of natural explosions is an Earth impact. This happens when a large cosmic body, such as an asteroid, travelling at a high velocity collides with planet Earth causing an enormous destructive explosion that could make life vanish from the face of the planet.

3.2.3 Examples of Explosion Incidents in the Past

Structures could be exposed to any of the explosions mentioned above. For example, a gas explosion could happen in a domestic building, which has gas supply, because of a

faulty boiler, leakage in pipes, lack of maintenance, human mistake, etc. Such an explosion took place in 1968 at the Ronan Point multi storey Building in Newham, East London and resulted in the complete collapse of one of its corners as shown in figure 3.2. Also, structures could be subjected to explosions due to terrorist attacks such as the one launched in 1995 by a booby-trapped truck on the Alfred P. Murrah Federal Building in Oklahoma City, figures 3.3a and b, where the severe damage induced to one of the key transfer beams in the building façade at the third floor above the open pedestrian plaza caused its failure, and thus resulted in the partial progressive collapse of the building as several columns were borne by this crucial beam, Wearne (1999).

3.3 Explosive Loads in Structural Design

3.3.1 Principle of Design

It is not practical to design all structures to resist all possible destructive forces because people would end up living and working in buildings like fortresses and bunkers. Instead, the structures vulnerability to destructive forces and potential threats should be assessed. What should then be made is a balance between the robustness and safety of the building on one side, its serviceability and architectural beauty on another side, and its cost on a third side as depicted in figure 3.4, a balance between using more and stronger and thicker structural elements and using heavy and expensive construction materials on one side, and providing more open spaces and more windows and using light and cheap construction materials on another side, a balance, in the general case, between the concern of the structural engineer, the concern of the architect, and the concern of the owner.

3.3.2 Occurrence vs. Loss Cost and Importance of Including Explosions in Design

For each of several kinds of potential hazardous accidents that could happen to structures, the yearly occurrence measured in number of incidents and the yearly loss cost in dollars due to the damage incurred by the accident, both as percentages of the total of all kind accidents, have been presented for comparison in a chart made by IRIS, the Industrial Risk Insurers Society, and shown in figure 3.5. The percentage yearly occurrence and the percentage yearly loss cost are presented in blue and red, respectively. Also, the yearly data actually represent the average of a 3-year period. The chart reveals a distinctive case for the explosion hazard where the occurrence is very low while the loss cost is very high, actually the highest among all hazards, indicating the importance of considering explosive loads in the design of vulnerable structures.

For illustration purpose, DIC perils in figure 3.5 refer to those covered by the DIC, Difference In Conditions, policy of business insurance, large industrial or commercial risks beyond those covered by standard insurance policies like earthquakes, floods, landslides and collapses. Sprinkler leakage hazard refers to damage to property due to untimely discharge of extinguisher from automatic fire sprinkler systems.

3.3.3 Design Criteria and Requirements

Designing structures against explosions consists of considering the following:

1. reduction of severity of injuries including those resulting from physical hazards
2. rescue facilitation
3. repair expedition
4. acceleration of the speed of return to full operation.

3.3.4 Explosion Hazards

Hazards during and post an explosion include:

1. direct bodily harm from air blast
2. flying and falling debris
3. broken glass
4. smoke and fire
5. power loss
6. communications breakdown
7. blocked exits and trapping
8. partial or total collapse of structure especially progressive.

3.4 Surface Pressure of Blast

3.4.1 Introduction

An explosion detonated on the surface of the ground affects a structure by both ground shock waves and air blast waves. These two kinds of waves arrive at the structure at different times because wave speeds in the air and in the ground are different. The ground shock acts first on the structure while the air blast has a greater effect on the structure (figure 3.3b) because, for the ground shock, the ground absorbs some of the explosion energy and damps the shock wave. Therefore, structural engineers are concerned more about the air blast in the analysis and design of structures. However, the time lag between the two waves could be very short and both waves would then affect the structure simultaneously, and that could sometimes result in the ground shock

wave magnifying the effect of the air blast wave especially when both waves are in resonance, having the same frequency, length and phase. Information about explosion waves, blast waves in particular, are given in the references introduced earlier in this chapter and also by Wu and Hao (2003).

3.4.2 Time History and Spatial Distribution of Blast Surface Pressure

The air blast applies pressure to the exposed surfaces of the structure. This pressure at any point of these surfaces is related to a number of variables. Among these variables are the distance of the point from the centre of the explosion, the strength of the explosion and of course the time.

Figure 3.6 presents the typical relation between the surface pressure p_s, resulting from the air blast, and time. The air blast wave reaches the surface at a time t_a after the explosion, the arrival time, and then t is set to 0. The pressure then begins to build up on the surface. Assuming that positive pressure is compression and negative pressure is tension, the blast surface pressure predicted by this typical constitutive model starts from zero and increases, as compression, linearly until reaching the maximum value p_{so}, the peak pressure, at $t = t_r$ which is called the pressure-rising time. Thereafter, it decays exponentially until reaching zero after a time t_d, the pressure-decreasing time, starting from $t = t_r$. It then continues to decay, as tension now, exponentially until reaching a minimum value, the maximum tension. After that, it increases again, exponentially and while remaining tensile, diminishing gradually but not vanishing according to this constitutive model.

In reality however, the surface pressure will eventually vanish at a finite time t_{ov}, the duration of blast pressure application, where ov stands for overall.

In order to provide values for the various parameters shown in figure 3.6, a lot of experiments were conducted. The results of these experiments led to the proposal of some empirical best-fitted-curve relations for these parameters. A set of such relations was presented by Wu and Hao (2003) and is used in this research and given below.

If R is the distance in meters between the explosion centre and the considered point on the structure exposed surface, Q is the weight of the TNT explosive in kilograms, c_a is the speed of sound in the air, in meters per second, which is equal to 340 m/s, and t_+ is the duration of application of the blast compressive pressure, then the following equations apply at the considered point:

$$p_{so} = \left[10.59 \left(\frac{R}{Q^{1/3}} \right)^{-2.56} - 0.51 \right] 10^5 \quad \text{N/m}^2 \qquad \text{when} \qquad 0.1 \le \frac{R}{Q^{1/3}} \le 1 \tag{3.1}$$

$$p_{so} = 10.08 \left(\frac{R}{Q^{1/3}} \right)^{-2.01} 10^5 \quad \text{N/m}^2 \qquad \text{when} \qquad 1 < \frac{R}{Q^{1/3}} \le 10 \tag{3.2}$$

$$t_a = 0.34 \frac{R^{1.4} Q^{-0.2}}{c_a} \quad \text{sec} \tag{3.3}$$

$$t_r = 0.0019 \left(\frac{R}{Q^{1/3}} \right)^{1.3} \quad \text{sec} \tag{3.4}$$

$$t_d = 0.0005 \left(\frac{R}{Q^{1/3}} \right)^{0.72} Q^{0.4} = 0.0005 R^{0.72} Q^{0.16} \quad \text{sec} \tag{3.5}$$

$$t_+ = t_r + t_d \quad \text{sec} \tag{3.6}$$

$$p_s(t) = p_{so} \left(\frac{t}{t_r} \right) \quad \text{N/m}^2 \qquad \text{for} \qquad 0 \le t \le t_r \tag{3.7}$$

$$p_s(t) = p_{so}\left(1-\frac{t-t_r}{t_d}\right)\exp\left(-a\frac{t-t_r}{t_d}\right) \qquad \text{N/m}^2 \qquad \text{for} \qquad t_r \le t \tag{3.8}$$

where a is the decrease rate constant and is determined by the following equations:

when $p_{so} \le 10^6$ N/m^2:

$$a = 1.26 p_{so}{}^{0.38} + 1.19 p_{so}{}^{0.79} \exp\left(-4.55\frac{t-t_r}{t_d}\right) \qquad \text{for} \quad t_r \le t \le t_+ \tag{3.9}$$

$$a = 1.1 p_{so}{}^{0.25} + 0.0176 p_{so} \exp\left(-2.27 p_{so}{}^{-0.49}\frac{t-t_+}{t_d}\right) \qquad \text{for} \quad t_+ < t \tag{3.10}$$

while when 10^6 N/m$^2 \le p_{so} \le 10^8$ N/m^2:

$$a = 0.8 p_{so}{}^{0.3} + 2.69 p_{so}{}^{0.28} \exp\left(-4.47\frac{t-t_r}{t_d}\right) \qquad \text{for} \quad t_r \le t \le t_+ \tag{3.11}$$

$$a = 0.5 p_{so}{}^{0.17} + 1.42 p_{so}{}^{0.28} \exp\left(-0.12 p_{so}{}^{-0.33}\frac{t-t_r}{t_d}\right) \qquad \text{for} \quad t_+ < t \tag{3.12}$$

3.5 Simplification of Spatial Distribution and Time History of Blast Pressure

3.5.1 Simplification of Spatial Distribution

Due to the high speed of the blast wave, the exposed surface, if it is relatively small, can be assumed to be subjected to a uniform blast pressure over its entire area. Thus, the blast pressure becomes a function of time only p_s (t) instead of a function of time and

space p_s (x,y,t), where (x,y) is the coordinates of any point on the exposed surface with reference to a local coordinate system.

3.5.2 Simplification of Time History

Referring back to the previous section and figure 3.6, the momentum imparted to the structure through its exposed surface by the negative pressure is usually very small and can often be neglected and the blast is assumed to generate compression wave only.

The first shape one would propose to simplify the curve of the blast pressure time history p_s (t) is the triangular shape where the pressure starts from zero and rises linearly to the peak pressure p_{so} and then falls linearly to zero again.

In a study of the dynamic response of several structural elements exposed to blast, Na and Librescu (2001) found that the blast pressure applied to the surface of the element reached the peak value very quickly. In other words, the rise time t_r was very short. That is one of the reasons why loads generated by the air blast of explosions are considered to be impulsive and sometimes called pulses. Therefore, the blast pressure can be assumed to jump to the peak value instantly at the start, and if the triangular representation was adopted for the time history of the blast pressure this pressure starts suddenly from the peak value and falls linearly to zero. In this case, the triangle of the pressure time history is right angled. This shape of dynamic loading and its effect on response were investigated in Chapter 2.

An alternative more convenient simplification of the blast pressure time history is to assume that the pressure jumps instantly to the peak value at the start as above but remains constant thereafter for a while and then falls suddenly to zero. In this case, the time history of the blast pressure is represented by a rectangle as shown in figure 3.7

where p_s is the constant pressure and t_{ov} is the duration of its application. The rectangular shape of dynamic loading was also discussed in Chapter 2.

For the rectangular representation, t_{ov} is assumed to remain the same and p_s can then be calculated, vice versa, or a suitable value is given to one of them and the other can then be calculated. Calculation of the unknown is by using the principle of impulse conservation which is:

$$I_{simplified} = I_{original} \tag{3.13}$$

where I is the impulse imparted by the blast pressure while the subscript refers to the representation of the pressure time history.

The above impulses are given by:

$$I_{simplified} = p_s t_{ov} \tag{3.14}$$

$$I_{original} = \int_{overall} p_s(t)dt \tag{3.15}$$

where overall under the integration symbol means that the integration is done over the overall duration of the pressure.

The substitution of equations (3.14) and (3.15) into equation (3.13) gives:

$$p_s t_{ov} = \int_{overall} p_s(t)dt \tag{3.16}$$

The last equation is used to calculate the unknown p_s or t_{ov} and is interpreted as the area under the curve depicting the time history of pressure is the same for both models, the simplified and the original.

3.6 The Initial Velocity and the Pulse Theorem

Once the pressure of the blast is applied to the surface of a structure, it responds by deforming and starts to gain velocity. By the end of the blast pressure duration t_{ov}, the structure would have absorbed its total momentum and have a velocity of a certain value, say V_0. As the blast pressure is an impulsive load, its duration t_{ov} is very short compared to the fundamental natural period of the structure. Thus, the velocity V_0 can be considered as a uniform initial velocity which the structure attains instantly at the start time t = 0, with zero initial displacements, which substitutes for the blast pressure.

The uniform initial velocity field of the structure above represents the only parameter of loading substituting for the blast pressure and can be determined using the principle of impulse conservation which says:

$$I_{initial} = I_{blast} \tag{3.17}$$

where $I_{initial}$ is the initial impulse of the structure while I_{blast} is the impulse imparted by the blast pressure.

Where m is the mass of the structure, the initial impulse is given by:

$$I_{initial} = mV_0 \tag{3.18}$$

If A_{expo} is the area of the structure surface exposed to the blast, the blast impulse is:

$$I_{blast} = A_{expo} p_s t_{ov} \tag{3.19}$$

Substituting equations (3.18) and (3.19) in equation (3.17) gives:

$$mV_0 = I_{blast} = A_{\exp o}\, p_s t_{ov} \tag{3.20}$$

From last equation, the uniform initial velocity is found as follows:

$$V_0 = \frac{I_{blast}}{m} = \frac{A_{\exp o}\, p_s t_{ov}}{m} \tag{3.21}$$

The last equation represents the basic idea behind the pulse theorem where the impulse of blast becomes the dominant characteristic of loading.

3.7 Blast Loading of Beams

If a beam of a rectangular solid cross section is subjected to blast, as the one shown in figure 3.8, the resulting pressure can be represented by a field of uniform initial velocity V_0. If the beam has a span of 2l, a width of b, a thickness of h and a material mass density of ρ and from equation (3.21), the initial velocity is given by:

$$V_0 = \frac{2lbp_s t_{ov}}{2lbh\rho} = \frac{p_s t_{ov}}{\rho h} \tag{3.22}$$

3.8 Conclusion

Impulsive loads, generated by the blast from explosions in particular, along with their effect on structural design have been discussed. Detailed equations of the blast pressure and the techniques used to simplify them including the pulse theorem have been given. The central role of the impulse and the initial velocity in the characterization of blast loading and in the dynamic analysis has also been explained.

Figure 3.1: Petrol explosions simulating bomb drops at an air show, after PD Photo

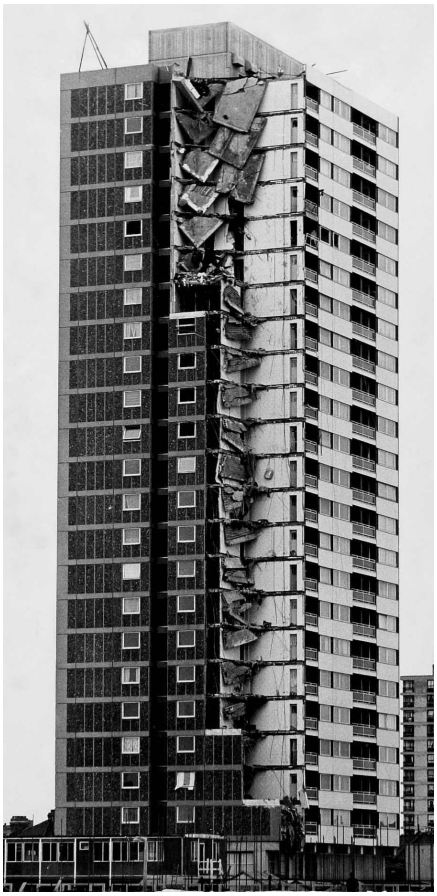

Figure 3.2: The Ronan Point Building after the gas explosion of 1968, taken from Macleod (2005)

Figure 3.3a: Damage to the Alfred P. Murrah Federal Building in Oklahoma City 1995, after AP the Associated Press

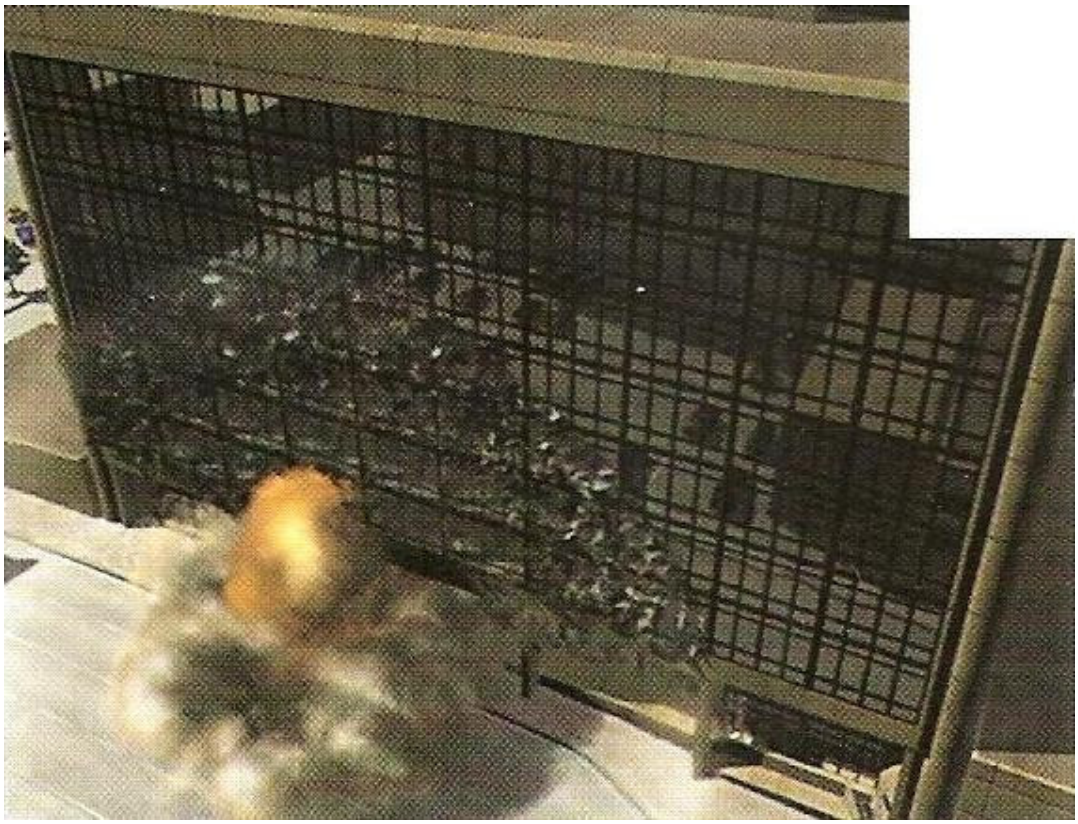

Figure 3.3b: Computerized simulation of blast wave as it shattered the glazed façade of the Alfred P. Murrah Federal Building, after Wearne 1999

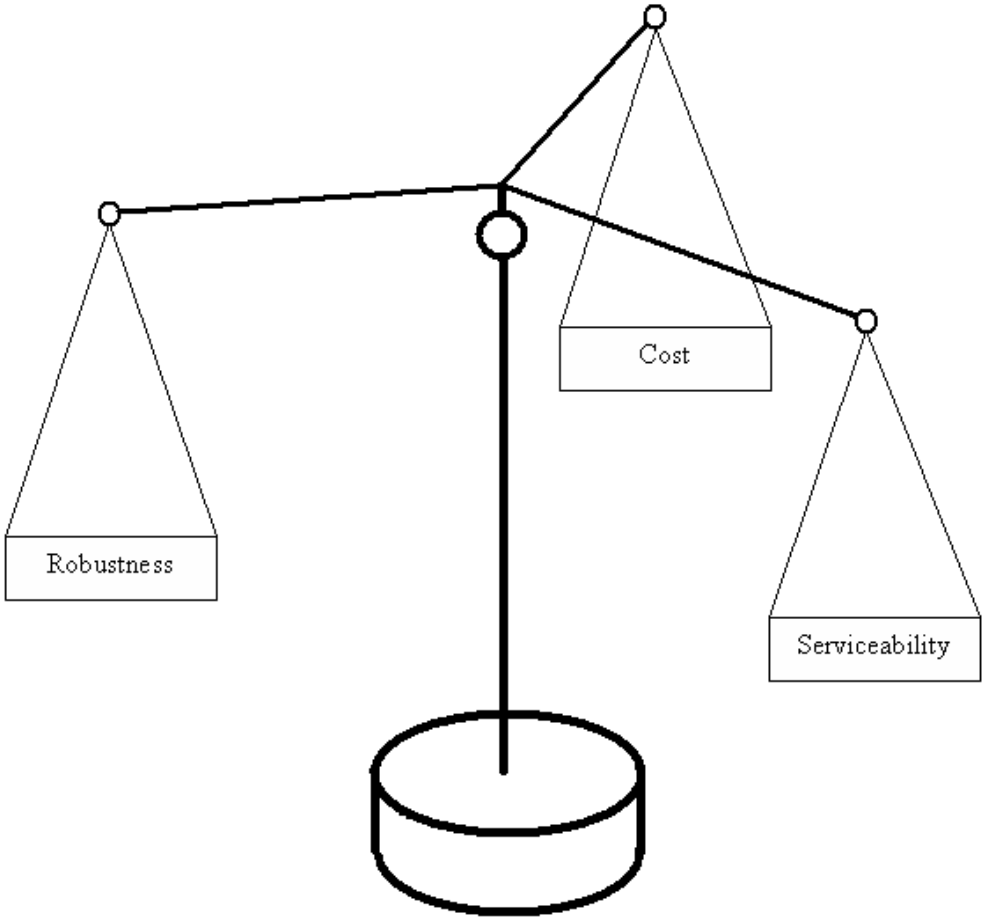

Figure 3.4: Depiction of the trinal balance between robustness, serviceability and cost

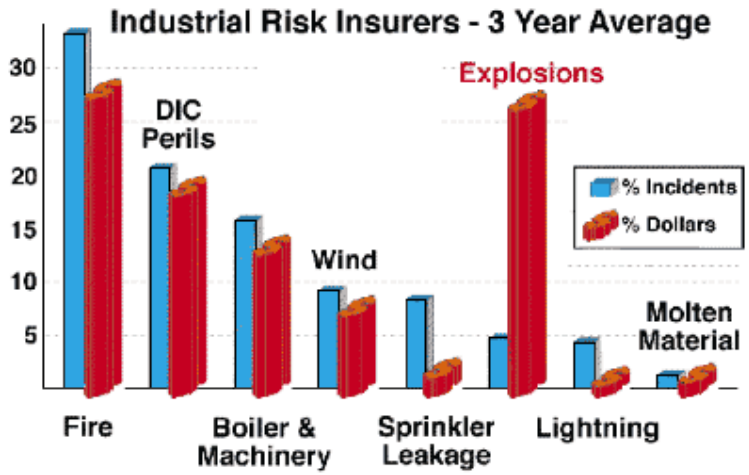

Figure 3.5: Percentage yearly occurrence and loss cost of various hazards, after IRIS the Industrial Risk Insurers Society

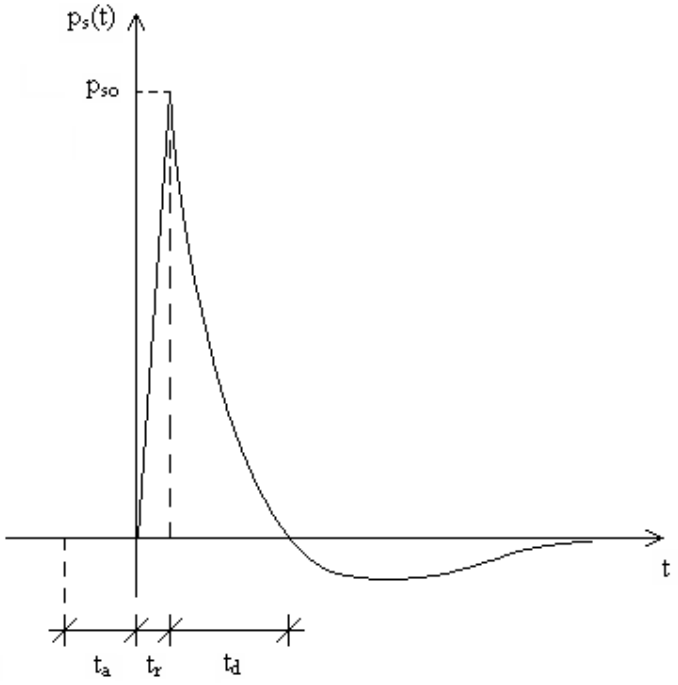

Figure 3.6: Typical time history of blast surface pressure

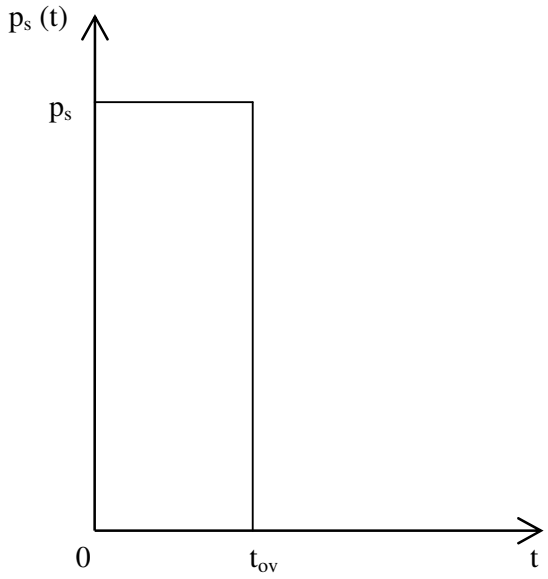

Figure 3.7: Simplification of blast pressure time history to rectangular shape

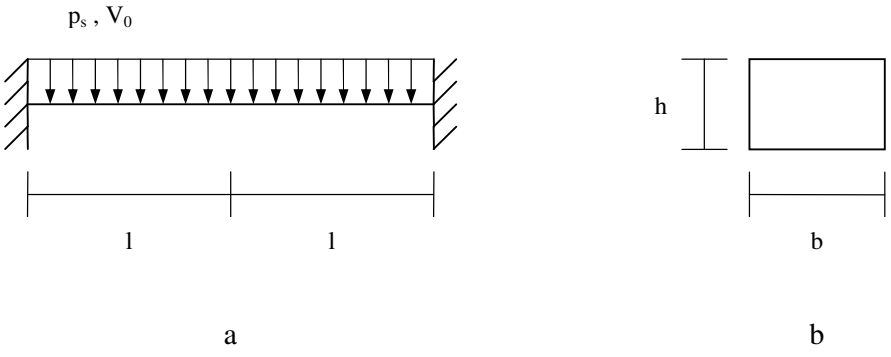

Figure 3.8: a. Beam subjected to blast. b. Cross section of beam

Chapter 4 – The SEP Method

4.1 Introduction

As previously discussed in Chapter 2, the difficulty of applying the accurate method for the dynamic analysis of beams has led researchers to propose approximate methods. The basic idea is that instead of dealing with the beam as an infinite degree of freedom dynamic system, which is governed by a differential equation of an unknown variable y that is a function of the coordinate x and time t, the beam is considered as a dynamic system having a finite number, for example two or even one, of degrees of freedom.

Symonds (1980a and b) has developed an efficient method for the dynamic analysis of beams called the Simplified Elastic Plastic Method (the SEP Method) which has given promising results when checked for accuracy and safety. This Chapter gives a detailed description of this method and includes an introduction to the theoretical assumptions made and an explanation of the analytical techniques used. In addition, the steps and the procedures for this method along with their various equations and relationships are detailed. This discussion assumes the general case of loading which is enough to cause plastic strains in the beam so the member exhibits both elastic and plastic behaviours.

In this method, the behaviour of the beam is considered to be modelled in a number of discrete stages which are described later.

4.2 Main Assumptions

The main assumption in this method is that the beam can be considered as a single degree of freedom system. This degree of freedom is the displacement "a" at a chosen point $\bar{x}$ of the beam. This displacement is a function of time only ($a(t)$).

Also, it is assumed that as the beam vibrates it takes an assumed shape which is constant through time in each stage of the response. This shape is expressed as a shape function in x, $\phi(x)$.

The displacement $y(x,t)$ of any point x of the beam at any time t is then given by the relation:

$$y(x,t) = \phi(x)a(t) \tag{4.1}$$

At $x = \bar{x}$:

$$\phi(\bar{x}) = 1 \tag{4.2}$$

which leads to:

$$y(\bar{x},t) = \phi(\bar{x})a(t) = 1 * a(t) = a(t) \tag{4.3}$$

This single degree of freedom system is called the equivalent SDOF system which is governed by a differential equation of the unknown variable "a" which is, in this case, a function of time t only. Using this differential equation and depending on the initial conditions of the beam (the displacement and velocity), the degree of freedom $a(t)$ can be found, and because $\phi(x)$ is assumed so it is known then $y(x,t)$ can be identified from equation (4.1). This solution of $y(x,t)$ is a mode form solution, that is why this method is described as a mode simulation technique or as a mode form method.

In reality, when a beam is subjected to a large dynamic load, it goes through a number of stages. At the beginning, when the deformations are small and the stresses are less than the yield stress, the beam is fully elastic. Thereafter, the deformations increase and the stresses increase and in some sections they reach the yield stress so the beam is elastic plastic in these sections. These increments continue until that all the stresses in

some sections reach the yield stress so the beam is fully plastic in these sections. So in reality there is not a separation between elastic and plastic stages but they interfere with each other. A main idea in the SEP method is that it assumes that a cross-section of the beam is either fully elastic or fully plastic. Thus, the simplified method assumes an artificial separation between the elastic and the plastic stages.

This method assumes different mode form solutions (different shape functions) for the beam during the different stages. This causes discontinuity at the time that separates two succeeding stages. So if the solution of the first stage is known the conditions (the displacements and the velocities) at the end of this first stage, which is also the beginning of the next second stage, can be found. Even though, these conditions cannot just be simply used as direct initial conditions for the second stage.

To find these direct initial conditions, other assumptions need to be employed. To find the initial velocity particularly, a special advanced technique called the "Δ_0 minimum" device is used. These assumptions and this device help to overcome the discontinuity between the two successive different mode form stages and to connect them together.

4.3 Analytical Techniques

4.3.1 Introduction

If two successive stages are considered, the mode form solution during the first one can be determined by the following relation:

$$y_1(x,t) = \phi_1(x)a_1(t) \tag{4.4}$$

and the solution during the second stage by:

$$y_2(x,t) = \phi_2(x)a_2(t) \tag{4.5}$$

where $a_1(t)$ and $a_2(t)$ are the displacements of the point $\bar{x}$ of the beam during the first and second stages, respectively. $\phi_1(x)$ and $\phi_2(x)$ are respectively the shape functions of the beam for the first and second stages and they are not identical.

If t_0 is assumed to be the time when the first stage terminates and the next one begins, then at $t = t_0$:

$$a_1(t_0) = a_{10} \tag{4.6}$$

$$\dot{a}_1(t_0) = \dot{a}_{10} \tag{4.7}$$

Thus, from equation (4.4):

$$y_1(x,t_0) = \phi_1(x)a_1(t_0) = \phi_1(x)a_{10} \tag{4.8}$$

$$\dot{y}_1(x,t_0) = \phi_1(x)\dot{a}_1(t_0) = \phi_1(x)\dot{a}_{10} \tag{4.9}$$

These last two functions are assumed to be known.

Also, at $t = t_0$:

$$a_2(t_0) = a_{20} \tag{4.10}$$

$$\dot{a}_2(t_0) = \dot{a}_{20} \tag{4.11}$$

Therefore, from equation (4.5):

$$y_2(x,t_0) = \phi_2(x)a_2(t_0) = \phi_2(x)a_{20} \tag{4.12}$$

$$\dot{y}_2(x,t_0) = \phi_2(x)\dot{a}_2(t_0) = \phi_2(x)\dot{a}_{20} \tag{4.13}$$

In the last two equations, all values are known except a_{20}, $\dot{a}_{20}$ which are the initial conditions of the second stage that need to be identified.

4.3.2 Determination of a_{20} and $\dot{a}_{20}$

It can be clearly seen that the equality $\phi_1(x)a_{10} = \phi_2(x)a_{20}$ cannot be achieved with any value of a_{20} as $\phi_1(x)$ and $\phi_2(x)$ are not identical. So there is an inevitable discontinuity. However, this discontinuity can be accepted and a_{20} is assumed to be:

$$a_{20} = a_{10} \tag{4.14}$$

Also, it is obvious that the equality $\phi_1(x)\dot{a}_{10} = \phi_2(x)\dot{a}_{20}$ cannot be always true for any value of $\dot{a}_{20}$. Therefore, another discontinuity cannot be evitable. However, the discontinuity is accepted and $\dot{a}_{20}$ can be determined by making use of a special analytical tool developed for this purpose; the "Δ_0 minimum" device.

So to summarise, at the interface of the two stages $a_{20} = a_{10}$ but $\dot{a}_{20} \neq \dot{a}_{10}$.

4.3.3 The Δ_0 Minimum Device

The best way to connect the two velocity fields $\phi_1(x)\dot{a}_{10}$ and $\phi_2(x)\dot{a}_{20}$ of the two successive stages is by trying to conserve, as much as possible, the kinetic energy and the translational momentum of the beam between the two stages at the separation time t_0. The most suitable technique to achieve the "as much as possible" conservation is the "Δ_0 minimum" device which represents the minimum of the mean of the difference squares at $t = t_0$. The mean of the difference squares at $t = t_0$, Δ_0, is given by:

$$\Delta_0 = \Delta_0(\dot{a}_{20}) = \frac{1}{2}\int_L \overline{\rho}(\phi_1\dot{a}_{10} - \phi_2\dot{a}_{20})^2\, dx \tag{4.15}$$

where L is the whole length of the beam, and $\overline{\rho}$ is the mass per unit length of the beam material.

It can be noted from the last equation that Δ_0 is a function of only the one unknown which is $\dot{a}_{20}$. From this, the desired value of $\dot{a}_{20}$ would be that which makes Δ_0 minimum, that is, the value which satisfies the following condition:

$$\frac{d\Delta_0}{d\dot{a}_{20}} = 0 \tag{4.16}$$

If $\dot{a}_{20}$ satisfies the last equation then Δ_0 would be minimum and it can be shown that this value is given by:

$$\dot{a}_{20} = \frac{\int_L \phi_1\phi_2\, dx}{\int_L \phi_2{}^2\, dx}\dot{a}_{10} \tag{4.17}$$

4.3.4 Summary

After determining a_{20} and $\dot{a}_{20}$, they are used as direct initial conditions in the next stage for $a_2(t)$ by which, along with using the differential equation of $a_2(t)$, the function $a_2(t)$ can be completely determined and then used in its turn to determine the general response function $y_2(x,t)$ during the second stage.

4.4 Steps and Procedures of the SEP Method

4.4.1 Introduction

To illustrate the SEP Method, the case of a fully clamped beam subjected to an impulsive dynamic load, as shown in figure 4.1, is discussed.

The mechanical properties of the beam material are:

The mass density ρ
Young's modulus of elasticity E
The yield stress σ_y

The dimensions of the beam are illustrated in figure 4.1. The second moment of area of the cross section of the beam is I.

At the start time t = 0, there is no deformation in the beam and it is assumed to be at rest.

The impulsive dynamic load per unit length of the beam is given by:

$$p(t) = p_0 \quad \text{for} \quad t \leq t_0$$
$$p(t) = 0 \quad \text{for} \quad t > t_0 \tag{4.18}$$

where t_0, the duration of the load, is very small compared to the fundamental natural period of the beam and thus the load is impulsive.

During the response, the beam goes through a number of stages depending on the state of the material (elastic or plastic). During each stage, the beam has a unique shape function. These stages are explained and their differential equations of motion are given in the following with the aid of figure 4.6.

4.4.2 Stage I – Fully Elastic

The first stage of the response of the beam is when it remains fully elastic. The response for the beam during this stage can be written in the following mode form expression:

$$y(x,t) = \phi(x)a(t) \tag{4.19}$$

where, as shown in figure 4.2, $a(t)$ is the displacement at the midpoint of the beam and $\phi(x)$ is the modal shape function of the beam during the first stage and is given by:

$$\phi(x) = 3\left(\frac{x^2}{l^2}\right) - 2\left(\frac{x^3}{l^3}\right) \qquad 0 \le x \le l \tag{4.20}$$

It should be noted that the value of the shape function at the mid point of the beam is $\phi(l) = 1$.

Because the duration of application t_0 for the distributed impulsive load p_0 is short, this load can be conveniently substituted by a field of initial velocity V_0 of the beam, as illustrated in figure 4.3, where the scalar momentum (pulse) of the beam resulting from this velocity field V_0 is equal to the scalar momentum (pulse) of the beam resulting from the distributed load p_0, that is:

$$p_0(2l)t_0 = \rho bh(2l)V_0 \tag{4.21}$$

$$\Rightarrow V_0 = \frac{p_0 t_0}{\rho bh} \tag{4.22}$$

V_0 is the value that should be assigned to the initial velocity of the beam.

In this case of impulsive load substitution, there would be no external forces of excitation acting on the beam. Therefore, the differential equation of motion of the beam during this stage becomes an equation of free vibration. Applying the approximate method detailed in Chapter 2 for the dynamic analysis of beams using the shape function determined above, the equation of motion is given by:

$$\frac{156}{420}\rho bhl\ddot{a} + 12\frac{EI}{l^3}a = 0 \tag{4.23}$$

A similar equation was reported by Symonds but it was not correct as it lacked few variables and thus it was not dimensionally compatible. This is corrected here.

The direct initial conditions for this stage at the midpoint of the beam are a_{10} and $\dot{a}_{10}$ for the displacement and velocity, respectively. The value of the initial displacement is:

$$a_{10} = 0 \tag{4.24}$$

The initial velocity of this stage $\dot{a}_{10}$ on the other hand can be determined from the original initial velocity of the beam V_0 by making use of the "Δ_0 minimum" device which can analytically connect the two discontinuous fields of initial velocity of the beam; the original field and the field for the assumed first stage. Upon substitution in equations (4.15), (4.16) and (4.17), the result is:

$$\dot{a}_{10} = 1.346 V_0 \tag{4.25}$$

The solution of the last differential equation considering these initial conditions is given by:

$$a = \dot{a}_{10}\left(\frac{1}{\omega}\right)\sin \omega t \tag{4.26}$$

where

$$\omega^2 = \frac{35}{13}\left(\frac{E}{\rho}\right)\left(\frac{h^2}{l^4}\right) \tag{4.27}$$

The beam response during the first stage is now determined. This stage actually terminates at the time when the beam starts to yield and the second stage starts. If the termination time is assumed to be t_1 and because the separation between the elastic first

stage and the plastic second stage is artificial, as stated previously, t_1 depends on the assumption. Many ways can be suggested in order to estimate t_1. One of these is to find out the time history of the absolute value of the elastic bending moment at the critical sections of the beam (the maximum value of the bending moment whether positive or negative) $M_c(t)$ and then determine the time when this value becomes equal to the fully plastic pure bending moment M_p of the cross section of the beam. This time would be a good estimation of t_1.

The time history of the critical bending moment of the beam is given by:

$$M_c(t) = \left|M(l,t)\right| = \left|M(0,t)\right| \tag{4.28}$$

where M(l,t) and M(0,t) are respectively the bending moments at the time t at the mid span x = l and at the support x = 0 of the beam (the critical sections) which are determined from the beam bending relationship M = -EI y``.

The fully plastic bending moment is given by:

$$M_p = \sigma_y \frac{bh^2}{4} \tag{4.29}$$

Finally, to determine t_1, the following equation needs to be solved for t:

$$M_c(t) = M_p \tag{4.30}$$

4.4.3 Stage II – Fully Plastic Pure Bending

At the second stage of the beam response, plastic hinges form at the critical cross sections of the beam. Thus, each half of the beam can be assumed to move as a rigid bar during this stage with fully plastic hinges formed at both ends of this bar (at the ends and the midpoint of the beam), as shown in figure 4.4. At each of these hinges, there is a bending moment which is equal to M_p.

The beam response during this stage is given by:

$$y(x,t) = \phi(x)a(t) \tag{4.31}$$

where $\phi(x)$, the beam modal shape function for the second stage, is:

$$\phi(x) = \frac{x}{l} \qquad 0 \le x \le l \tag{4.32}$$

The last relation shows that the value of the shape function at the mid point of the beam is $\phi(l) = 1$.

The differential equation of the beam during this stage is of uniformly decelerated motion and is given by:

$$\ddot{a} = -\frac{6M_p}{\rho bhl^2} \tag{4.33}$$

Substituting the value of M_p in the last equation gives:

$$\ddot{a} = -\frac{3}{2}\frac{\sigma_y h}{\rho l^2} \tag{4.34}$$

a_{21} and $\dot{a}_{21}$ are assumed to represent the initial displacement and velocity, respectively, for this second stage at time t = t_1, while a_{11} and $\dot{a}_{11}$ are assumed to represent the same quantities at the same time but for the first stage and which can be calculated from its equations at t = t_1. As the shape functions of the beam motion for the first and second stages are different, there are discontinuities in both the displacement and velocity fields of the beam, at the time t_1 that separates these stages. a_{21} can be determined from a_{11} as follows:

$$a_{21} = a_{11} \tag{4.35}$$

and $\dot{a}_{21}$ can be determined from $\dot{a}_{11}$, by using the "Δ_0 minimum" technique, as follows:

$$\dot{a}_{21} = 1.050\dot{a}_{11} \tag{4.36}$$

After determining the initial conditions a_{21} and $\dot{a}_{21}$, the solution of the last differential equation is found from the following relation:

$$a = a_{21} + \dot{a}_{21}(t - t_1) - \frac{3}{4}\frac{\sigma_y h}{\rho l^2}(t - t_1)^2 \tag{4.37}$$

Hence, the beam response during the second stage is found. This stage terminates at a time t_2 when the deformation of the beam reaches values large enough that the axial tension in the beam becomes significant and plasticity spreads throughout the beam, and all the stresses are at yield and tensile so that instead of the plastic bending moment M_p there is a fully plastic pure axial tension N_p at all the cross sections of the beam. The deformation at which this occurs is assumed to be given by:

$$a = h \tag{4.38}$$

where h is the depth of the beam. Solving equation (4.38) for t gives the termination time t_2.

4.4.4 Stage III – Fully Plastic Pure Axial Tension

This stage, figure 4.5, is characterized by pure internal axial tension without any bending moment at all cross sections of the beam equal to the fully plastic tension N_p which is given by:

$$N_p = \sigma_y bh \tag{4.39}$$

Thus, the beam in this stage is at its maximum capacity of resistance.

The response of the beam for this stage is:

$$y(x,t) = \phi(x)a(t) \tag{4.40}$$

where $\phi(x)$ is the shape function in the third stage and is given by:

$$\phi(x) = \sin\left(\frac{\pi}{2} \cdot \frac{x}{l}\right) \qquad 0 \le x \le l \tag{4.41}$$

where it can be seen that at the beam mid span $\phi(l) = \sin\frac{\pi}{2} = 1$.

In this stage, the differential equation of the beam motion is the equation of free vibration of a cable, that is:

$$\rho bh\ddot{y} = N_p y'' \tag{4.42}$$

where $''$ indicates to the second derivative with respect to the position coordinate x.

Substituting N_p and y and then $\phi(x)$ into equation (4.42) yields after removing shared terms:

$$\rho\ddot{a} + \frac{\pi^2}{4}\frac{\sigma_y}{l^2}a = 0 \tag{4.43}$$

At the time $t = t_2$, the displacement and velocity are respectively a_{32} and $\dot{a}_{32}$ for this stage representing its initial conditions, and a_{22} and $\dot{a}_{22}$ for the previous stage calculated from its equations. a_{32} and $\dot{a}_{32}$ are found from a_{22} and $\dot{a}_{22}$ by the following relations:

$$a_{32} = a_{22} = h \tag{4.44}$$

$$\dot{a}_{32} = \frac{8}{\pi^2}\dot{a}_{22} \tag{4.45}$$

where the "Δ_0 minimum" device is employed to get the second one as the fields are discontinuous between the third and second stages, as with the previous stages.

After determining the initial conditions a_{32} and $\dot{a}_{32}$, the solution of the differential equation of motion is given as:

$$a = a_{32}\cos\ \omega(t - t_2) + \frac{\dot{a}_{32}}{\omega}\sin\ \omega(t - t_2) \tag{4.46}$$

where

$$\omega^2 = \frac{\pi^2}{4}\frac{\sigma_y}{\rho l^2} \tag{4.47}$$

The beam response during the third stage is now known. This stage terminates at the time t_f at which the motion of the beam reverses direction when reaching to the maximum amplitude of displacement. At this point, the beam stops gaining more plastic deformation and its velocity becomes zero, that is:

$$\dot{a} = 0 \tag{4.48}$$

Solving the last equation for t gives t_f which is also called the final time of response. The maximum displacement of the beam a_{max} is then determined from:

$$a_{max} = a(t_f) \tag{4.49}$$

4.4.5 Stage IV – Elastic Recovery

In this stage, which is the final one, the beam moves back while keeping the plastic strains it has previously gained as residual permanent deformation, and goes into an elastic vibration about the position where it only has the plastic permanent deformation. This position is called the residual permanent position or the rest position of the beam. With the passage of time, this elastic vibration will finally be damped out leaving just the permanent displacements in the beam which will then be at rest, and at the beam midpoint then the permanent displacement is given the notation a_p.

The maximum displacement a_{max} of the beam consists of two components: the elastic displacement a_{11} previously calculated at the end of the elastic first stage and the plastic permanent displacement a_p. Thus, a_p can actually be found from the following relation:

$$a_p = a_{max} - a_{11} \tag{4.50}$$

In the last equation, a_{11} represents the elastic recovery of the beam during this stage.

4.5 Conclusion

The SEP Method is an efficient practical tool for analysis which provides solutions in mode form to the beam dynamic problem even when it is necessary to include those effects that are difficult to consider in the accurate method such as nonlinearity, plasticity or the effect of axial force.

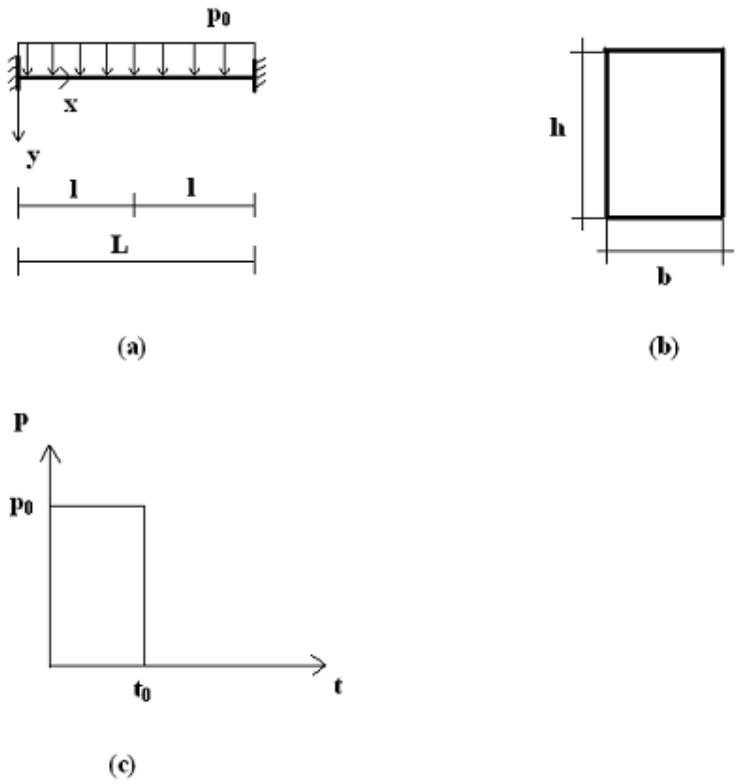

Figure 4.1: (a) The beam and the load. (b) The cross-section of the beam. (c) The load time-history.

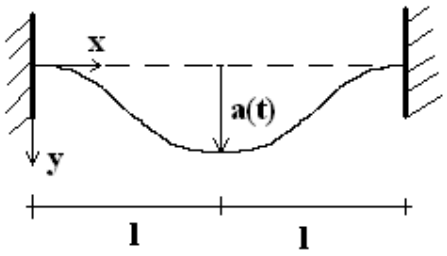

Figure 4.2: The beam during stage I

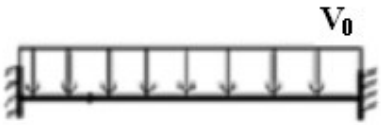

Figure 4.3: Substitution of the distributed impulsive load p_0 by the velocity field V_0

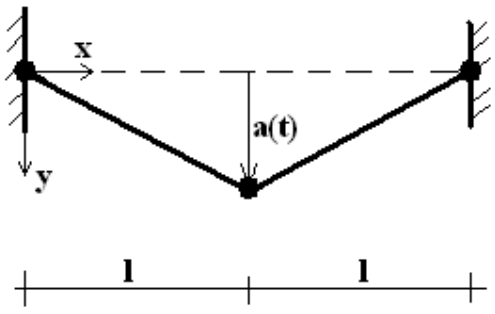

Figure 4.4: The beam during stage II

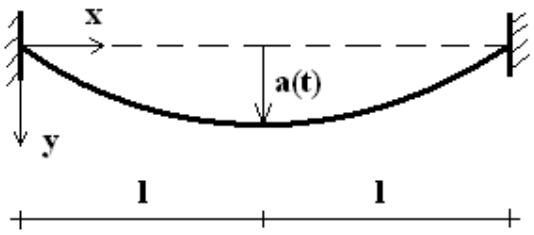

Figure 4.5: Stage III of the beam response

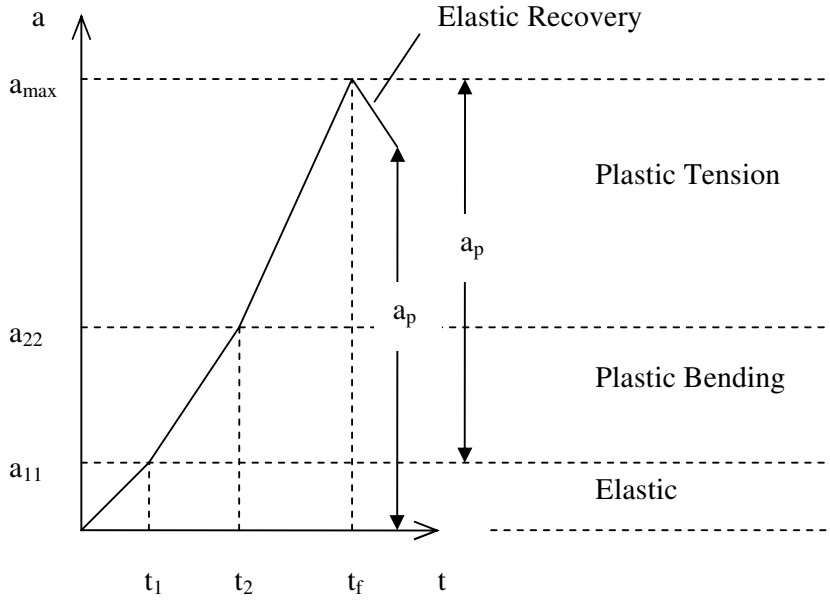

Figure 4.6: An illustrative graph showing the successive stages of the SEP Method

Chapter 5 – Finite Element Modelling and Numerical Analysis

5.1 Introduction

The analytical accurate method of dynamic analysis presented in Chapter 2 serves to formulate structural problems in terms of partial differential equations. Solving such equations is very expensive in terms of effort and time while engineers cannot devote long hours to it when each new problem arises. Also, the method is unable to model anything other than simple shapes, boundary conditions, loads, etc. Therefore, there is a need for other methods which are also accurate and can model complex problems and whose solutions can be obtained at a reasonable cost. Numerical methods, such as the finite element method, have shown to satisfy those requirements in addition to their potency for programming on computer.

This Chapter presents a survey of various numerical methods used in the solution of dynamic problems. These included the numerical integration of a differential equation of a dynamic motion, for linear and nonlinear problems. The finite element method is also presented with various time stepping techniques. Last, a finite element model of ABAQUS, used in the analysis of a fully clamped beam subjected to a uniformly distributed impulsive load, is presented.

The finite element method was first introduced by Turner, Clough, Martin and Topp (1956) when it was suggested that triangular plane stress elements could be used to model the skin of delta wings in the airplanes of the Boeing Company. However, the term 'finite element' was coined by Ray W. Clough in 1960. In this method, conventional engineering structures which are of continuous nature can be modelled as an assemblage of structural elements interconnected at a number of discrete nodes. Therefore, structures in this method are considered as having a finite number of degrees of freedom which are the displacements of these nodes. If the force-displacement relationships for the individual finite elements are known, it is possible to derive the properties and determine the behaviour of the entire structure by using the various well-known techniques of structural analysis.

The finite element method has been developed enormously. It began as a numerical method for stress analysis and is still widely used for this purpose. Also, it has become useful in many other areas such as heat conduction, seepage flow, fluid dynamics and electric and magnetic fields. One of the main factors that have been behind the wide spread of this method is the massive revolution in computer technology in recent years. Therefore, it has been a significant area of research. Reviews of the method are given by, for example, Cook (1995), Cook, Malkus and Plesha (1989), Smith and Griffiths (1988) and Zienkiewicz and Taylor (1989 and 1991).

5.2 Numerical Methods of Dynamic Analysis

5.2.1 Introduction

Numerical methods are found to be accurate enough for the solution of most dynamic structural problems. In fact, some numerical methods can be exact in certain situations such as structures subjected to excitation forces described by functions of linear segments, when linear approximation is used in the method. In some of these methods, the process of numerical solution requires for convenience that the excitation function be calculated at equal time intervals Δt, then the excitation function during each interval can be estimated by various interpolations, for example linear interpolation, between the points separating the intervals. Thus, the time duration of the excitation, including a suitable extension of time after cessation of the excitation, is divided into N equal time intervals of duration Δt.

In the numerical method of linear interpolation, the response, for each time interval Δt, is determined from the initial conditions at the beginning of the interval and the linear excitation during the interval. The initial conditions are, in this case, the displacement and velocity at the end of the preceding time interval.

Some numerical methods are more sophisticated than the method above. Griffiths and Smith (1991) provide a broader explanation of the various methods of numerical analysis.

5.2.2 Numerical Integration of the Differential Equation of Motion

For a single degree of freedom model subjected to a general excitation force F(t), the force can be approximated by a piecewise linear function, during each time interval Δt, as follows:

$$F(t) = \left(1 - \frac{t - t_i}{\Delta t}\right) F_i + \left(\frac{t - t_i}{\Delta t}\right) F_{i+1} \ , \qquad t_i \le t \le t_{i+1} \tag{5.1}$$

in which

$$t_i = i.\Delta t \tag{5.2}$$

for equal intervals of time Δt and i = 1, 2, 3, … , N.

Then, the differential equation of motion would be as follows:

$$m\ddot{y} + ky = \left(1 - \frac{t - t_i}{\Delta t}\right) F_i + \left(\frac{t - t_i}{\Delta t}\right) F_{i+1} \ , \qquad t_i \le t \le t_{i+1} \tag{5.3}$$

The solution y can be expressed as the sum of the complementary solution y_c for which the right-hand side of this equation is set equal to zero, and the particular solution y_p, that is:

$$y = y_c + y_p \tag{5.4}$$

The complementary solution is given in general by:

$$y_c = C_i \cos \omega(t - t_i) + D_i \sin \omega(t - t_i) \tag{5.5}$$

The particular solution takes the same form of the excitation function, that is:

$$y_p = B_i + A_i(t - t_i) \tag{5.6}$$

which, upon substitution into the differential equation of motion, gives:

$$k[B_i + A_i(t - t_i)] = \left(1 - \frac{t - t_i}{\Delta t}\right)F_i + \left(\frac{t - t_i}{\Delta t}\right)F_{i+1} \tag{5.7}$$

Establishing the identity of terms between the left-hand and right-hand sides of the last equation, that is, between the constant terms and the terms with a factor $(t - t_i)$ and then solving the resulting equations, A_i and B_i are determined as follows:

$$A_i = \frac{F_{i+1} - F_i}{k\Delta t} \tag{5.8}$$

and

$$B_i = \frac{F_i}{k} \tag{5.9}$$

From the preceding equations, the total solution y can be rewritten as follows:

$$y = C_i \cos \omega(t - t_i) + D_i \sin \omega(t - t_i) + B_i + A_i(t - t_i) \tag{5.10}$$

The velocity is then given by the derivative of the last equation as:

$$\dot{y} = \omega D_i \cos\omega(t - t_i) - \omega C_i \sin\omega(t - t_i) + A_i \tag{5.11}$$

The constant of integration C_i and D_i can be determined from the initial conditions of the system. These include the displacement y_i and the velocity $\dot{y}_i$ at the beginning of the current time interval Δt, that is, at time t_i. By introducing these initial conditions into the previous equations of displacement and velocity and solving for the constants C_i and D_i in the resulting relations yields:

$$C_i = y_i - B_i \tag{5.12}$$

and

$$D_i = \frac{\dot{y}_i - A_i}{\omega} \tag{5.13}$$

The evaluation of equations (5.10) and (5.11) at the end of the current time interval, that is, at time $t_{i+1} = t_i + \Delta t$ results in the displacement y_{i+1} and the velocity $\dot{y}_{i+1}$ at the end of the interval as follows:

$$y_{i+1} = C_i \cos\omega\Delta t + D_i \sin\omega\Delta t + B_i + A_i\Delta t \tag{5.14}$$

and

$$\dot{y}_{i+1} = \omega D_i \cos\omega\Delta t - \omega C_i \sin\omega\Delta t + A_i \tag{5.15}$$

Finally, the acceleration at time t_{i+1} is obtained by substituting y_{i+1} and $\dot{y}_{i+1}$ from the last two equations into the differential equation (5.3) at time $t = t_{i+1}$. Namely:

$$\ddot{y}_{i+1} = \frac{1}{m}\left(F_{i+1} - k y_{i+1}\right) \tag{5.16}$$

The substitution of the coefficients A_i, B_i, C_i and D_i previously determined into equations (5.14) and (5.15) results in the following formulae to calculate the displacement, velocity and acceleration at time $t = t_{i+1}$:

$$y_{i+1} = N_1 y_i + N_2 \dot{y}_i + N_3 F_i + N_4 F_{i+1} \tag{5.17}$$

$$\dot{y}_{i+1} = N_5 y_i + N_6 \dot{y}_i + N_7 F_i + N_8 F_{i+1} \tag{5.18}$$

$$\ddot{y}_{i+1} = N_9 y_{i+1} + N_{10} F_{i+1} \tag{5.19}$$

where the coefficients N_1, N_2, N_3, N_4, N_5, N_6, N_7, N_8, N_9 and N_{10} are given by the following expressions:

$$N_1 = \cos \omega \Delta t \tag{5.20}$$

$$N_2 = \frac{\sin \omega \Delta t}{\omega} \tag{5.21}$$

$$N_3 = \frac{\dfrac{\sin \omega \Delta t}{\omega \Delta t} - \cos \omega \Delta t}{k} \tag{5.22}$$

$$N_4 = \frac{1 - \dfrac{\sin \omega \Delta t}{\omega \Delta t}}{k} \tag{5.23}$$

$$N_5 = -\omega \sin \omega \Delta t \tag{5.24}$$

$$N_6 = \cos \omega \Delta t \tag{5.25}$$

$$N_7 = \frac{\dfrac{\cos \omega \Delta t - 1}{\Delta t} - \omega \sin \omega \Delta t}{k} \tag{5.26}$$

$$N_8 = \frac{1 - \cos \omega \Delta t}{k \Delta t} \tag{5.27}$$

$$N_9 = -\omega^2 \tag{5.28}$$

$$N_{10} = \frac{1}{m} \tag{5.29}$$

Equations (5.17), (5.18) and (5.19) are recurrence formulas to calculate, respectively, the displacement, velocity and acceleration at the next time step t_{i+1} from the previously calculated values for these quantities at the preceding time step t_i. Because these recurrence formulae are exact, the only restriction in selecting the length of the time step Δt is that it allows a close approximation to the excitation function and that equally spaced time intervals do not miss the peaks of this function. This numerical procedure is highly efficient due to the fact that the coefficients N_1, N_2, N_3, N_4, N_5, N_6, N_7, N_8, N_9 and N_{10} need to be calculated only once.

5.3 Nonlinearity in Structural Dynamics

5.3.1 Introduction

For linear dynamic problems, structures are represented by models in which the restoring forces are proportional to the displacements. Therefore, the governing equations of motion of structures for such dynamic problems are, as shown in Chapter 2 and in the previous Section, linear, second order ordinary differential equations with constant coefficients. Solving such equations has been shown to be relatively simple for particular excitation functions such as harmonic functions. Furthermore, general solutions of these equations always exist for any kind of forcing functions and can be found numerically by the method described in the previous section.

However, there are physical situations for which this linear model does not adequately represent the dynamic characteristics of the structure. Instead, the dynamic analysis in such cases requires the introduction of a nonlinear model in which the spring forces do not remain proportional to the displacements. Consequently, the resulting equations of motion are no longer linear and their closed form solutions are generally not possible and therefore require numerical procedures. A more detailed theoretical investigation of nonlinearity in structural dynamics can be found in Worden and Tomlinson (2001).

5.3.2 Nonlinear Modelling

The dynamic equilibrium of a system is established by equating the inertial force $F_I(t)$ and the spring force $F_S(t)$ to the external force $F(t)$. This, at time t, results in the following equation:

$$F_I(t) + F_S(t) = F(t) \tag{5.30}$$

The inertial force is $F_I(t) = m\ddot{y}$. Consider the case when the spring force is not necessarily proportional to the displacement y by the factor k but is a function of the displacement, $F_S(y)$, equation (5.30) becomes:

$$m\ddot{y} + F_S(y) = F(t) \tag{5.31}$$

Equation (5.31) is the nonlinear differential equation of motion of the structure. Hence, at time t_i, the beginning of the time step Δt chosen for the analysis, this equation results in:

$$m\ddot{y}_i + F_{Si} = F_i \tag{5.32}$$

At the end of the time step, $t_{i+1} = t_i + \Delta t$, the equation of motion gives:

$$m\ddot{y}_{i+1} + F_{Si+1} = F_{i+1} \tag{5.33}$$

Subtracting equation (5.33) from equation (5.32) results in the difference equation of motion in terms of increments, namely:

$$m\Delta\ddot{y}_i + \Delta F_{Si} = \Delta F_i \tag{5.34}$$

where $\Delta\ddot{y}_i$, ΔF_{Si} and ΔF_i are respectively the incremental acceleration, incremental spring force and incremental external force and are given by the following relations:

$$\Delta\ddot{y}_i = \ddot{y}_{i+1} - \ddot{y}_i \tag{5.35}$$

$$\Delta F_{Si} = F_{Si+1} - F_{Si} \tag{5.36}$$

$$\Delta F_i = F_{i+1} - F_i \tag{5.37}$$

The stiffness coefficient k_i of the time step is defined as the current value of the spring force per unit displacement which may be taken as the slope of the tangent of the nonlinear spring force – displacement function $F_S(y)$ at the initiation of the current time step Δt, or as the slope of the secant line for the interval Δt. The value of this coefficient is assumed to remain constant during the current increment of time Δt.

From the previous discussion, it can be concluded that the incremental spring force is proportional to the incremental displacement, even though the spring force itself is not necessarily proportional to the corresponding displacement. Therefore:

$$\Delta F_{Si} = k_i \Delta y_i \tag{5.38}$$

where Δy_i refers to the incremental displacement and is defined by the following relationship:

$$\Delta y_i = y_{i+1} - y_i \tag{5.39}$$

Substituting equation (5.38) into equation (5.34) finally gives the incremental governing equation of motion of the structure, that is:

$$m\Delta\ddot{y}_i + k_i \Delta y_i = \Delta F_i \tag{5.40}$$

5.3.3 Numerical Evaluation of Nonlinear Solutions

Among the many methods available for the solution of the nonlinear equation of motion, probably one of the most effective is the step-by-step integration method. In this method, the response is evaluated at successive increments Δt of time, usually taken as equal lengths of time for computational convenience. At the beginning of each interval, the condition of dynamic equilibrium is established. Then, the response for the time increment Δt is evaluated based on the assumption that the stiffness coefficient k_i remains constant during the interval Δt. However, the nonlinear characteristics of this coefficient are considered in the numerical analysis by re-evaluating this coefficient at the beginning of each time increment. The response is then obtained progressively using the displacement and velocity calculated at the end of each time interval as the initial conditions for the next time step.

In nonlinear numerical methods, the dynamic coefficients generally vary over the successive time intervals. Therefore, the nonlinear behaviour of the structure is actually composed of a sequence of responses of systems with changing dynamic characteristics. Also, it is obvious that the assumption of constant mass is unnecessary as it could just as well be represented by another changing coefficient.

There are many procedures available for performing the step-by-step integration of the incremental equation of motion. Two of the most popular methods are the constant acceleration method and the linear acceleration method. As the names of these methods imply, in the first method the acceleration is assumed to remain constant during the time interval Δt, while in the second method the acceleration is assumed to vary linearly during the interval. The constant acceleration method is cheaper to run but less accurate compared to the linear acceleration method for the same value of the time increment. In the following, the two methods are presented.

5.3.4 Constant Acceleration Step-by-Step Integration Technique

In the constant acceleration method, it is assumed that acceleration remains constant for the time step between times t_i and $t_{i+1} = t_i + \Delta t$. The value of the constant acceleration during the interval Δt is taken as the average of the values of the acceleration $\ddot{y}_i$ at the initiation of the time step and $\ddot{y}_{i+1}$, the acceleration at the end of the time step. Thus, the acceleration $\ddot{y}(t)$ at any time t during the time interval Δt is given by:

$$\ddot{y}(t) = \frac{1}{2}\left(\ddot{y}_i + \ddot{y}_{i+1}\right) \tag{5.41}$$

Integration of this equation twice with respect to time between the limits t_i and t results in:

$$\dot{y}(t) = \dot{y}_i + \frac{1}{2}\left(\ddot{y}_i + \ddot{y}_{i+1}\right)\left(t - t_i\right) \tag{5.42}$$

and

$$y(t) = y_i + \dot{y}_i\left(t - t_i\right) + \frac{1}{4}\left(\ddot{y}_i + \ddot{y}_{i+1}\right)\left(t - t_i\right)^2 \tag{5.43}$$

The evaluation of equations (5.42) and (5.43) at the end of the time step $t_{i+1} = t_i + \Delta t$ results in:

$$\dot{y}_{i+1} = \dot{y}_i + \frac{\Delta t}{2}\left(\ddot{y}_i + \ddot{y}_{i+1}\right) \tag{5.44}$$

and

$$y_{i+1} = y_i + \dot{y}_i \Delta t + \frac{\Delta t^2}{4}\left(\ddot{y}_i + \ddot{y}_{i+1}\right) \tag{5.45}$$

Moving the first term in the right-hand side of each of the last two equations to the left-hand side gives:

$$\Delta\dot{y}_i = \frac{\Delta t}{2}\left(\ddot{y}_i + \ddot{y}_{i+1}\right) \tag{5.46}$$

and

$$\Delta y_i = \dot{y}_i \Delta t + \frac{\Delta t^2}{4}\left(\ddot{y}_i + \ddot{y}_{i+1}\right) \tag{5.47}$$

where Δy_i is the incremental displacement defined by equation (5.39) and $\Delta\dot{y}_i$ is the incremental velocity defined by:

$$\Delta\dot{y}_i = \dot{y}_{i+1} - \dot{y}_i \tag{5.48}$$

To use the incremental displacement in the analysis, equation (5.47) is solved for $\ddot{y}_{i+1}$ and substituted into equation (5.46) to obtain:

$$\ddot{y}_{i+1} = \frac{4}{\Delta t^2}\Delta y_i - \frac{4}{\Delta t}\dot{y}_i - \ddot{y}_i \tag{5.49}$$

and

$$\Delta\dot{y}_i = \frac{2}{\Delta t}\Delta y_i - 2\dot{y}_i \tag{5.50}$$

Also, substitution of $\ddot{y}_{i+1}$ from equation (5.49) into equation (5.35) gives:

$$\Delta\ddot{y}_i = \frac{4}{\Delta t^2}\Delta y_i - \frac{4}{\Delta t}\dot{y}_i - 2\ddot{y}_i \tag{5.51}$$

Substituting $\Delta\ddot{y}_i$ from the last equation into the incremental equation of motion results in:

$$m\left(\frac{4}{\Delta t^2}\Delta y_i - \frac{4}{\Delta t}\dot{y}_i - 2\ddot{y}_i\right) + k_i \Delta y_i = \Delta F_i \tag{5.52}$$

The last equation is then solved for the incremental displacement as follows:

$$\Delta y_i = \frac{\Delta F_{ei}}{k_{ei}} \tag{5.53}$$

where k_{ei} is the effective stiffness and is given by:

$$k_{ei} = \frac{4m}{\Delta t^2} + k_i \tag{5.54}$$

and ΔF_{ei} is the effective incremental force determined as follows:

$$\Delta F_{ei} = \frac{4m}{\Delta t}\dot{y}_i + 2m\ddot{y}_i + \Delta F_i \tag{5.55}$$

From equation (5.53), Δy_i can be determined and from which $\Delta\dot{y}_i$ and $\Delta\ddot{y}_i$ can be calculated from equations (5.50) and (5.51). Thus, the displacement and the velocity at the end of the current time step can be found from the following relations:

$$y_{i+1} = y_i + \Delta y_i \tag{5.56}$$

and

$$\dot{y}_{i+1} = \dot{y}_i + \Delta\dot{y}_i \tag{5.57}$$

The acceleration at the end of the time step is calculated directly from the nonlinear differential equation of motion, rather than using equation (5.49) or equation (5.35), as follows:

$$\ddot{y}_{i+1} = \frac{1}{m}\left(F_{i+1} - F_{S\,i+1}\right) \tag{5.58}$$

where $F_{S\,i+1}$ is the restoring force evaluated at time t_{i+1} from the following relation using the value determined above of the displacement y_{i+1}:

$$F_{S\,i+1} = F_S(y_{i+1}) \tag{5.59}$$

After the displacement, velocity and acceleration have been determined at time $t_{i+1} = t_i + \Delta t$, the procedure is repeated to calculate these quantities at the end of the next time step $t_{i+2} = t_{i+1} + \Delta t$, and the process is continued to any desired final value of time.

5.3.5 Linear Acceleration Step-by-Step Integration Technique

In the linear acceleration method, it is assumed that the acceleration may be expressed by a linear function of time during the time interval Δt. In this type of analysis, the structural properties of the dynamic system such as the stiffness coefficient k_i may include any form of nonlinearity. Thus, it is not necessary for the restoring force to be only a function of the displacement. The only restriction in the analysis is that these properties are evaluated at an instant of time t_i and then assumed to remain constant during the increment of time Δt. When the acceleration is assumed to be a linear function of time for the interval between t_i and t_{i+1}, it may be expressed as:

$$\ddot{y}(t) = \ddot{y}_i + \frac{\Delta \ddot{y}_i}{\Delta t}\left(t - t_i\right) \tag{5.60}$$

Integrating the last equation twice with respect to time between the limits t_i and t yields:

$$\dot{y}(t) = \dot{y}_i + \ddot{y}_i(t - t_i) + \frac{1}{2}\frac{\Delta\ddot{y}_i}{\Delta t}(t - t_i)^2 \tag{5.61}$$

and

$$y(t) = y_i + \dot{y}_i(t - t_i) + \frac{1}{2}\ddot{y}_i(t - t_i)^2 + \frac{1}{6}\frac{\Delta\ddot{y}_i}{\Delta t}(t - t_i)^3 \tag{5.62}$$

The evaluation of the last two equations at the end of the time step $t_{i+1} = t_i + \Delta t$ results in:

$$\dot{y}_{i+1} = \dot{y}_i + \ddot{y}_i\Delta t + \frac{1}{2}\Delta\ddot{y}_i\Delta t \tag{5.63}$$

and

$$y_{i+1} = y_i + \dot{y}_i\Delta t + \frac{1}{2}\ddot{y}_i\Delta t^2 + \frac{1}{6}\Delta\ddot{y}_i\Delta t^2 \tag{5.64}$$

Moving the first term in the right-hand side of each of the last two equations to the left-hand side gives:

$$\Delta\dot{y}_i = \left(\ddot{y}_i + \frac{1}{2}\Delta\ddot{y}_i\right)\Delta t \tag{5.65}$$

and

$$\Delta y_i = \dot{y}_i\Delta t + \left(\frac{1}{2}\ddot{y}_i + \frac{1}{6}\Delta\ddot{y}_i\right)\Delta t^2 \tag{5.66}$$

To use the incremental displacement as the basic variable in the analysis, the last equation is solved for $\Delta\ddot{y}_i$ and then substituted into equation (5.65) to obtain:

$$\Delta\ddot{y}_i = \frac{6}{\Delta t^2}\Delta y_i - \frac{6}{\Delta t}\dot{y}_i - 3\ddot{y}_i \tag{5.67}$$

and

$$\Delta\dot{y}_i = \frac{3}{\Delta t}\Delta y_i - 3\dot{y}_i - \frac{\Delta t}{2}\ddot{y}_i \tag{5.68}$$

Substituting $\Delta\ddot{y}_i$ from equation (5.67) into the incremental equation of motion results in:

$$m\left(\frac{6}{\Delta t^2}\Delta y_i - \frac{6}{\Delta t}\dot{y}_i - 3\ddot{y}_i\right) + k_i\Delta y_i = \Delta F_i \tag{5.69}$$

The last equation is then solved for the incremental displacement as follows:

$$\Delta y_i = \frac{\Delta F_{ei}}{k_{ei}} \tag{5.70}$$

where k_{ei} is the effective stiffness and is given by:

$$k_{ei} = \frac{6m}{\Delta t^2} + k_i \tag{5.71}$$

and ΔF_{ei} is the effective incremental force determined as follows:

$$\Delta F_{ei} = \frac{6m}{\Delta t}\dot{y}_i + 3m\ddot{y}_i + \Delta F_i \tag{5.72}$$

From equation (5.70), Δy_i can be determined and then $\Delta \dot{y}_i$ and $\Delta \ddot{y}_i$ can be calculated from equations (5.68) and (5.67). Thus, the displacement and the velocity at the end of the current time step can be found from the following relationships:

$$y_{i+1} = y_i + \Delta y_i \tag{5.73}$$

and

$$\dot{y}_{i+1} = \dot{y}_i + \Delta \dot{y}_i \tag{5.74}$$

The acceleration at the end of the time step is calculated directly from the nonlinear differential equation of motion, rather than using equation (5.35), as follows:

$$\ddot{y}_{i+1} = \frac{1}{m}\left(F_{i+1} - F_{S\,i+1}\right) \tag{5.75}$$

where $F_{S\,i+1}$ is the restoring force evaluated at time t_{i+1} from the following relation using the value determined above of the displacement y_{i+1}:

$$F_{S\,i+1} = F_S(y_{i+1}) \tag{5.76}$$

After the displacement, velocity and acceleration have been determined at time $t_{i+1} = t_i + \Delta t$, the application of the previously outlined iterative formulae is repeated to calculate these quantities at the end of the next time step $t_{i+2} = t_{i+1} + \Delta t$, and the process is continued to any desired final value of time.

5.3.6 Accuracy of the Recurrence Formulae and Selection of the Time Step

The previous numerical procedures involve two kinds of approximations. First, the acceleration is assumed either to remain constant or to vary linearly during the time increment Δt. Second, the nonlinear stiffness properties of the structure are evaluated at the initiation of each time step and assumed to remain constant during the time increment. In general, these two assumptions introduce errors that are small if the chosen time step is short. However, these errors tend to accumulate from step to step. This accumulation of errors can be avoided by imposing the total dynamic equilibrium condition in the analysis at the end of each time step. This can be accomplished by calculating the acceleration at the end of each time step using, as shown previously, the nonlinear differential equation of motion in which the displacement and velocity as well as the restoring and external forces are calculated at the end of that time step.

Special care has to be given to the task of choosing the proper time step Δt for the numerical analysis. The accuracy of the step-by-step integration method depends upon the magnitude of the time increment selected. The following factors should be considered in the selection of Δt:

1- The smallest natural period excited of the structure

2- The rate of variation of the excitation function

3- The complexity of the stiffness function and the functions of the other dynamic properties of the structure

Practically, it has been found that to satisfy 1 above with sufficiently accurate results the time increment chosen should be no longer than one tenth of the smallest natural period excited of the structure. The second consideration is that the time step should be small enough to represent properly the variation of the excitation function with respect to time. The third point that should be taken into account is any abrupt change in the rate of variation of the stiffness function or of any other dynamic property function, for

example in the case of elastoplastic materials when the stiffness suddenly changes from linear elastic to a yielding plastic phase. In these cases, to obtain the best accuracy, it is more appropriate to choose smaller time intervals in the neighbourhood of such drastic changes.

5.4 Finite Element Method and Time Stepping Schemes

5.4.1 Introduction

The numerical methods of solving the differential equation of motion for single degree of freedom systems have been presented in the previous sections of this chapter. The extension of these methods for the numerical analysis of structures modelled as multi degree of freedom systems using the finite element methods is described in this section.

Over the past fifty years, the finite element method has been studied intensively and many numerical integration schemes have been developed for different types of physical problems. However, researchers often do not agree on the choice of method for a given class of problems even though they tend to have the same preferences for certain kinds of engineering situations.

In the following, a brief explanation of the different schemes for time-history finite element analysis is provided. These include the Wilson-θ method, Newmark-β method, and both the explicit and implicit algorithms of numerical integration. More detailed information on the subject has been given by Wood (1990).

5.4.2 Governing Equation of Motion in Nonlinear Finite Element Analysis

The governing equation of motion of structures modelled as multi degree of freedom nonlinear systems takes the form of a differential matrix equation as follows:

$$[M]\{\ddot{y}\}+\{F_S(\{y\})\}=\{F(t)\} \tag{5.77}$$

where

[M] is the mass matrix of the structure

$\{y\}$, $\{\ddot{y}\}$ and $\{F(t)\}$ are respectively the displacement, acceleration and dynamic load vectors of the structure

$\{F_S(\{y\})\}$ is the stiffness restoring force vector of the structure which is a function of the displacement vector $\{y\}$.

5.4.3 Wilson−θ Time Stepping Scheme

The Wilson-θ time stepping scheme is a modification, of the nonlinear step-by-step acceleration method presented in Section 5.3, in which the time step is multiplied by a factor necessary to render the method unconditionally stable, that is, numerical errors do not tend to accumulate during the integration process regardless of the magnitude selected for the time step. This extension of the numerical method was introduced and developed by Wilson et al. (1973). Without Wilson's modification, the step-by-step acceleration method is only conditionally stable which means that in order to guarantee the numerical stability of the solution it may require very small time steps. For some dynamic problems, this conditional time step can be so small as to make the solution impractical.

The basic assumption of the Wilson-θ method is that the acceleration varies over the extended time increment θ.Δt where θ is a factor greater than 1. The value of this extension factor θ should be determined to obtain optimum stability of the numerical process and accuracy of the solution. It was shown by Wilson et al. (1973) that for $\theta \geq 1.38$ the method becomes unconditionally stable.

The Wilson-θ method is similar to the step-by-step acceleration method, Section 5.3, except that the calculations are carried out for the extended time interval θ.Δt instead of the normal time interval Δt. After obtaining the incremental acceleration vector $\{\hat{\Delta}\ddot{y}_i\}$ for the extended time step from these calculations, the incremental acceleration vector $\{\Delta\ddot{y}_i\}$ for the normal time step can then be determined by a simple linear interpolation as follows:

$$\{\Delta\ddot{y}_i\} = \frac{1}{\theta} \cdot \{\hat{\Delta}\ddot{y}_i\} \tag{5.78}$$

After finding $\{\Delta\ddot{y}_i\}$, the process of numerical analysis can be continued in a similar way to before for the normal time interval in order to determine the displacement, velocity and acceleration vectors at the end of the normal time step and then moving to the next time step and so on.

5.4.4 Newmark–β Time Stepping Scheme

The Newmark-β time stepping scheme is a generalization, of the step-by-step linear-acceleration method, in which the acceleration is assumed to vary nonlinearly in time during each time step Δt. This method includes, in its formulation, several time-step

methods used for the numerical solution of linear and nonlinear equations. It uses a parameter designated as β. The method, as originally proposed by Newmark (1959), contained, in addition to β, a second parameter γ. Particular numerical values assigned to these parameters lead to well-known methods for the solution of the governing equation of motion such as the constant or linear acceleration methods. These parameters actually replace the numerical coefficients $\frac{1}{6}$ and $\frac{1}{2}$ of the terms containing the incremental acceleration $\Delta\ddot{y}_i$ in equations (5.66) and (5.65), respectively.

The Newmark equations are given by:

$$\{\Delta\dot{y}_i\} = (\{\ddot{y}_i\} + \gamma\{\Delta\ddot{y}_i\})\Delta t \tag{5.79}$$

and

$$\{\Delta y_i\} = \{\dot{y}_i\}\Delta t + \left(\frac{1}{2}\{\ddot{y}_i\} + \beta\{\Delta\ddot{y}_i\}\right)\Delta t^2 \tag{5.80}$$

where Δt, $\{\dot{y}_i\}$, $\{\ddot{y}_i\}$, $\{\Delta y_i\}$, $\{\Delta\dot{y}_i\}$ and $\{\Delta\ddot{y}_i\}$ represent the constant time step, the velocity vector at the beginning of the current time step, the acceleration vector at the beginning of the current time step, the incremental displacement vector, the incremental velocity vector and the incremental acceleration vector, respectively.

It has been found that for values of γ other than $\frac{1}{2}$, the method introduces an unwanted artificial damping in the system which is sometimes referred to as numerical damping. Therefore, γ is generally set as $\frac{1}{2}$ and the Newmark relations become:

$$\{\Delta\ddot{y}_i\} = \frac{1}{\beta\Delta t^2}\{\Delta y_i\} - \frac{1}{\beta\Delta t}\{\dot{y}_i\} - \frac{1}{2\beta}\{\ddot{y}_i\} \tag{5.81}$$

and

$$\{\Delta\dot{y}_i\} = \frac{1}{2\beta\Delta t}\{\Delta y_i\} - \frac{1}{2\beta}\{\dot{y}_i\} + \left(1 - \frac{1}{4\beta}\right)\Delta t\{\ddot{y}_i\} \tag{5.82}$$

In the implementation of the Newmark-β method, the process begins by selecting a numerical value for the parameter β. Newmark has suggested a value in the range $\frac{1}{6} \le \beta \le \frac{1}{2}$. It can be clearly seen from the previous equations that for $\beta = \frac{1}{6}$ the method is exactly equivalent to the linear acceleration method and is only conditionally stable.

An important special case of the Newmark-β method is when $\beta = \frac{1}{4}$ for which the method becomes unconditionally stable while providing satisfactory accuracy and is exactly equivalent to the constant acceleration method.

5.4.5 Explicit Integration Schemes

The explicit method of numerical integration approximates the velocity and acceleration vectors by the following relations:

$$\{\dot{y}_i\} = \frac{1}{2\Delta t}\left(\{y_{i+1}\} - \{y_{i-1}\}\right) \tag{5.83}$$

and

$$\{\ddot{y}_i\} = \frac{1}{\Delta t^2}\left(\{y_{i+1}\} - 2\{y_i\} + \{y_{i-1}\}\right) \tag{5.84}$$

in which Δt is the time step chosen for the numerical analysis, while $\{y\}$, $\{\dot{y}\}$ and $\{\ddot{y}\}$ represent the displacement, velocity and acceleration vectors respectively, and the subscripts i, i+1 and i−1 indicate to the successive time instants at which these vectors are evaluated.

The explicit method analyses the structure element by element and thus it is known for being computationally cheap. However, one of its major disadvantages is that being conditionally stable means it requires very small time steps to ensure its numerical stability. Therefore, the explicit method is more suitable for use in wave propagation analysis and for the solution of dynamic problems of short durations such as structures subjected to impulsive dynamic loads like impact or explosion.

The condition of numerical stability in the explicit method is imposed upon the time step chosen for the analysis and is given by the following inequality:

$$\Delta t \leq \frac{2}{\omega_{\max}} \tag{5.85}$$

where $\omega_{\max}$ is the highest natural frequency of the model.

5.4.6 Implicit Integration Schemes

The velocity and acceleration vectors in the implicit method of numerical analysis are given by the following equations:

$$\{\dot{y}_{i+1}\} = \frac{2}{\Delta t}(\{y_{i+1}\} - \{y_i\}) - \{\dot{y}_i\} \tag{5.86}$$

and

$$\{\ddot{y}_{i+1}\} = \frac{4}{\Delta t^2}(\{y_{i+1}\} - \{y_i\}) - \frac{4}{\Delta t}\{\dot{y}_i\} - \{\ddot{y}_i\} \tag{5.87}$$

The advantage of the implicit method of numerical integration is its unconditional stability which means that it is numerically stable regardless of the length chosen for the time step duration Δt. So, there is no restriction on the time step size other than that required for accuracy. This method considers the structure as a whole during the analysis and therefore it is computationally expensive. Consequently, the implicit method is more appropriately employed in the numerical analysis of dynamic problems of long durations such as structures subjected to, for example, wind loading or earthquakes.

5.5 Finite Element Modelling and Analysis of Beams Using ABAQUS

5.5.1 Introduction

For simulating the beams investigated in the research, figure 5.1, a finite element model was built. For this purpose, ABAQUS, a powerful software for nonlinear finite element simulation, was used. The software was also used for the analysis of the model and visualization of results. The ABAQUS Model is described in this Section.

The beams modelled are fully clamped, of solid rectangular cross section, made from mild steel and subjected to uniformly distributed impulsive loads.

5.5.2 Description of the Model Geometry

For the beam and the impulsive load applied to it transversely, a two dimensional modelling space was chosen. The beam was modelled as a one dimensional deformable body.

As the beam, its boundary conditions and dynamic load are symmetric and in order to reduce the cost and time of the analysis, only half of the beam was modelled.

5.5.3 Strain Rate Sensitivity and Modelling of the Material

As the dynamic loads applied to the beams described and studied in the Thesis can sometimes be very large, there is a need to include plasticity in the finite element analysis. Also, because the beams are made of steel and due to the impulsive nature of the dynamic loads, strain rates in the beam can be very high to the extent that can alter the yield strength of the steel as it is a highly strain rate sensitive material as mentioned in Chapter 2.

ABAQUS has an extensive set of material models that can simulate the behaviour of most typical engineering materials. It also offers several constitutive models for the plastic analysis of strain rate sensitive metals including steel, ABAQUS vr.6.8 User's Manuals (2008). A convenient elasto-plastic steel model with isotropic hardening and defined power law for strain rate dependency was chosen for the material. The numerical parameters of the power law, equation (2.41), were assigned the values for steel, that is, D = 40 and q = 5.

5.5.4 Boundary Conditions

As half the beam only was modelled, the boundary conditions were modelled as fully fixed at the end of the beam and as a symmetric support at the middle of the beam.

5.5.5 Modelling of Dynamic Loads

As the dynamic load is uniform and impulsive, it was modelled as a predefined field of uniform initial translational velocity along the beam as shown in figure 5.1.

5.5.6 The Numerical Integration Scheme Used in the Nonlinear Analysis

Explicit schemes are computationally efficient for the dynamic analysis of structures with a relatively short response time. Thus, an explicit scheme used in ABAQUS/Explicit Solver was chosen for the analysis of the beam as it is under impulsive loading and the precision of the calculation was set to double. The explicit scheme was also a Newmark-β type scheme.

ABAQUS/Explicit operates an explicit central-difference time integration rule where the acceleration is calculated at the start of the increment for time t and used to advance the velocity solution to time $t+\Delta t/2$ and the displacement solution to time $t+\Delta t$. The dynamic equilibrium is then checked at the end of the increment $t+\Delta t$, ABAQUS vr.6.8 User's Manuals (2008).

5.5.7 The Time Step Chosen for the Analysis

ABAQUS can automatically estimate the most efficient size for the time increment and continuously adjust it during the analysis in terms of computational cost and numerical convergence, ABAQUS vr.6.8 User's Manuals (2008). The software was set to do that when analysing the beam model.

5.5.8 Effect of Axial Forces and Geometric Nonlinearity

Large deformations were included in the ABAQUS model. In this case, elements are normally formulated in the initial configuration using the initial nodal positions. Most elements however distort from their initial shapes as deformations increase. With sufficiently large deformations, these elements may become so distorted that they are no longer suitable for use; for example, the volume of an element at an integration point may become negative. In this situation, ABAQUS will issue a warning message indicating the problem and cut back the time increment before making further attempts to continue the solution.

5.5.9 Type of Finite Elements and Meshing Techniques

ABAQUS contains an extensive library of finite elements. For beam problems, ABAQUS offers a wide range of beam elements including Euler-Bernoulli-type beams and with linear, quadratic or cubic interpolation formulation.

The model for this research was built using 3-node Euler-Bernoulli beam elements of quadratic geometric order, type B22, chosen from the ABAQUS library of explicit elements. The utilisation of these beam elements allows for wave propagation in the analysis.

For meshing the half symmetric beam in the model, one hundred elements were used. As found from the convergence studies carried out for the meshing, using this number of elements gave accurate results and was not very expensive computationally.

5.6 Conclusions

The solution of the differential equation of motion can be found using numerical methods. In these methods, the forcing functions are approximated by segmental linear functions between defining points. Based on this assumption and by choosing time steps that are small enough, the numerical integration is straight forward and the solution obtained can be reasonably accurate. The response is calculated at each time increment for the conditions existing at the end of the preceding time interval which would be the initial conditions of the system for the new time interval and the action of the excitation applied during the time interval, which is assumed to be linear.

There are many numerical methods for solution of nonlinear differential equations of motion. The step-by-step acceleration method presented in this Chapter provides satisfactorily accurate results with recurrence calculations which can be performed on a computer. However, these calculations are tedious and time consuming if they were to be run manually.

The finite element method is a powerful tool that is widely used for the static or dynamic analysis of structures especially with complex geometrical configurations, material properties or loading conditions, and which can be easily programmed for computers. This numerical method has proven to be highly efficient in cost and time and has also shown at the same time very good accuracy and numerical stability in the solutions it provides. When applied to solve dynamic problems particularly, the finite element method needs to include a suitable time stepping scheme adopted for the numerical integration such as the Wilson-θ, the Newmark-β, the explicit or the implicit schemes.

For the finite element modelling and analysis in this research, the ABAQUS suite of computer programmes was employed. In particular, three were used; ABAQUS CAE for modelling, ABAQUS Explicit for the finite element analysis using the explicit method and ABAQUS Viewer to investigate the results.

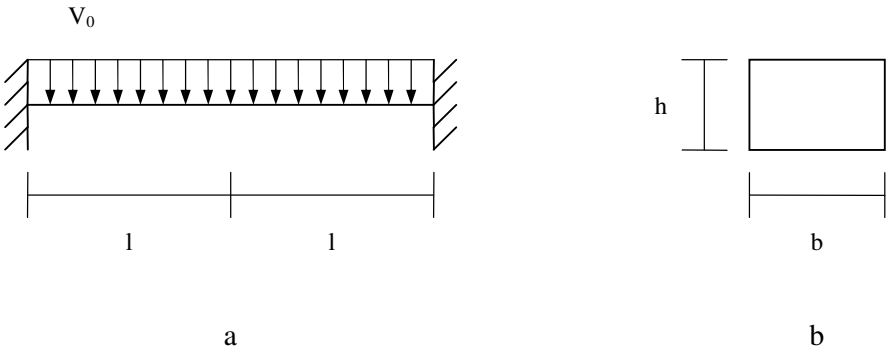

Figure 5.1: a. Model of beam subjected to impulsive load. b. Cross section of beam

Chapter 6 – Symonds and Jones' Experiments

6.1 Introduction

In order to validate the methods presented in the previous chapters, a highly accurate benchmark to compare their results with is needed. The experimental investigation of Symonds and Jones (1972) was used. It consisted of twenty experiments done on five groups of steel beams with different thicknesses which were subjected to explosive loads of various intensities that were high enough to cause permanent plastic deformations in all the beams. The initial momentum imparted to the beam and the permanent shape of the beam after each test were recorded.

In this Chapter, a description of the Symonds and Jones' experimental work, dealing with beams subjected to air blast of explosive loads, is presented. The aim is to use the experimental results as benchmark tests.

6.2 Test Rig

6.2.1 Ballistic Pendulum

Figure 6.1 illustrates the experimental arrangement for this investigation where the test rig is shown along with the accompanying instrumentation. The main part of the test rig was the ballistic pendulum which consisted of an I beam hanged by string steel wires, a head welded to one of the I beam ends while holding the specimen being tested, and few ballasts resting on the I beam including one at the opposite side to that of the head to ensure stability for the I beam.

6.2.2 Experimental Instrumentation

The accompanying instrumentation shown in figure 6.1 included a Minidet electrical detonator and a heat-sensitive paper. The detonator had a leader coming from it towards the explosives at the specimen onto which it was firmly attached and was used to trigger the explosion by means of an electric blasting cap attached to its end. The detonator was put a short distance away from the specimen and was protected from the explosion by a shield. The heat-sensitive paper was located on the other side of the ballistic pendulum I beam to record the amplitude of its swing on the paper by a hot wire attached to the I beam.

In order to measure the permanent plastic displacements of the beam specimen, the specimen was removed from the head of the ballistic pendulum after the test and was placed on a flat surface. A slip gauge with 0.00001 m dial indicator was then used to measure the displacements relative to the ends of the specimen.

6.2.3 Imparted Explosive Momentum

The innovative experimental technique employed provided the ability to determine the momentum imparted to a test specimen due to explosion directly from the amplitude of the initial swing of the ballistic pendulum which was recorded on the heat-sensitive paper by a hot wire as they were related by the following equation:

$$V_0 = K \Delta \tag{6.1}$$

where

V_0 is the uniform initial velocity of the beam specimen due to the explosion

Δ is the amplitude of the initial swing of the ballistic pendulum from its initial position due to the explosion

K is a constant which was determined from the specimen and test rig data

6.3 Experimental Specimens

6.3.1 Introduction

Each tested specimen was a fully clamped beam made from mild steel and subjected to uniformly distributed pressure to model the air blast of an explosion. The specimen was held in place by the head of the ballistic pendulum.

6.3.2 Details of Specimens and Head of the Ballistic Pendulum

A detailed sketch of the specimen and the ballistic pendulum head with dimensions is shown in figure 6.2. The specimen consisted of the beam being tested in between two enlarged ends that were part of it. The enlargement of each end was of thickness c and the thickness of the beam was h, the width of the end, b, was the same as that of the beam. The enlargement was to ensure rotational fixity of the beam ends. The enlarged ends were attached to the specimen supports by steel bolts as well as case hardened serrated surfaces as first suggested by Nonaka (1967) who designed this gripping device to ensure axial fixity of the beam end by prohibiting it from slipping along the support

surface. To ensure a high level of friction was exerted between the support surface and the specimen end, high tensile steel bolts were used in order to apply a large pressure on the surfaces. As a result, the enlarged ends and the support serrated surfaces with the high-tensile steel bolts ensured fully clamped beam ends.

The thickness of the enlarged end for the smallest two beam thicknesses was doubled for the larger beam thicknesses. The length of the enlarged end was a little smaller than half of the beam span. The above dimensions were to ensure that there was no rotation of the beam end.

Each test beam, figure 6.3, had a solid rectangular cross section and the dimensions were:

Half span $l = 0.06367$ m

Span $2l = 0.12733$ m

Width $b = 0.00954$ m

Thicknesses $h = 0.0023$ m, 0.0028 m, 0.0040 m, 0.0048 m and 0.0060 m

6.3.3 Mechanical Properties of Specimen Material

The specimens were made from mild steel which is a highly strain rate sensitive material. The mild steel had the following mechanical properties:

Mass density $\rho = 7820$ kg/m^3

Young's elasticity modulus $E = 2.1*10^{11}$ N/m^2

Yield stress $\sigma_y = 210*10^6$ N/m^2

Power law multiplier of strain rate sensitivity D = 40

Power law exponent of strain rate sensitivity q = 5

6.3.4 Sheet Explosives

To apply the explosive load to the specimen, Du Pont Detasheet explosive was utilized. As shown in figure 6.2, the sheet explosive covered the entire top surface area of the specimen and underneath it a thin layer of neoprene, 0.00318 m thick, was spread in order to protect the specimen from spalling by the explosion. Different numbers of layers of sheet explosive were applied to the specimen to vary the intensity of the explosive load.

6.4 The Experiments

In each experiment, an explosive load was applied to the beam specimen as shown in figure 6.3 where it is represented by the field of uniformly distributed initial velocity V_0. The load was obtained by triggering the sheet explosives on the specimen using the Minidet electrical detonator, the displacement of the beam was measured and the velocity was determined with the aid of equation (6.1).

Table 6.1 lists the experiments done on the different beam specimens and the various intensities of loads applied. Twenty specimens divided into five groups of different thicknesses were tested. In all the experiments, the load had an intensity which was high enough to cause a permanent plastic displacement in the beam specimen which was in many of the tests up to several times the beam depth. The recorded permanent displacements are also included in table 6.1.

6.5 Conclusion

The experimental work of Symonds and Jones was described in this Chapter. Details of the test rig, specimens and experiments conducted on them were included. These tests form a highly accurate benchmark that is used in the results comparison process presented in Chapter 7.

Table 6.1: The experiments and their results

Experiment number	Specimen thickness h m	Explosive load V_0 m/s	Permanent displacement a_p m
1	0.0023	35.31	0.00749
2		47.75	0.00889
3		64.52	0.01265
4		67.16	0.01516
5		72.19	0.01605
6	0.0028	32.13	0.00640
7		38.25	0.00729
8		49.91	0.01052
9		55.37	0.01105
10	0.0040	21.54	0.00340
11		24.31	0.00445
12		25.07	0.00427
13		30.30	0.00607
14		34.57	0.00724
15		41.61	0.00983
16	0.0048	21.69	0.00302
17		27.94	0.00495
18		30.25	0.00638
19		35.84	0.00701
20	0.0060	13.87	0.00142

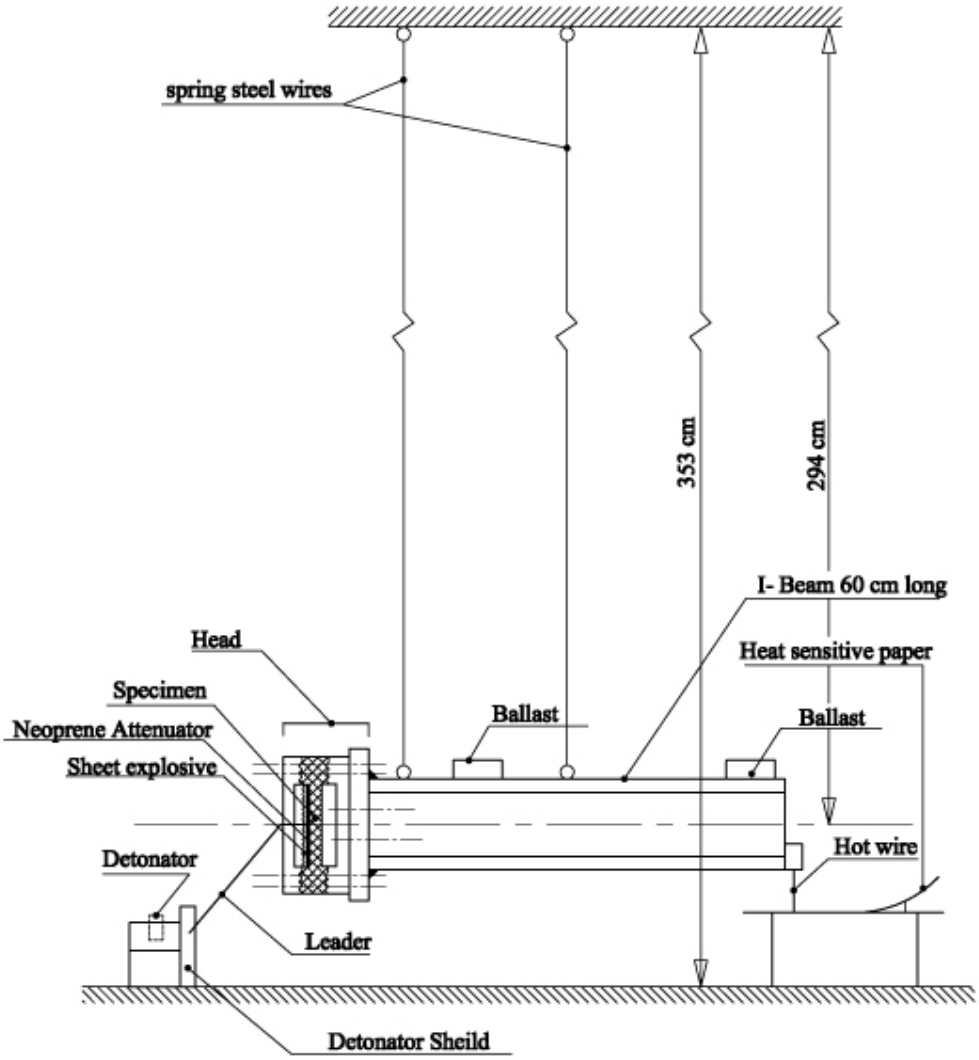

Figure 6.1: Test rig including ballistic pendulum and accompanying instrumentation

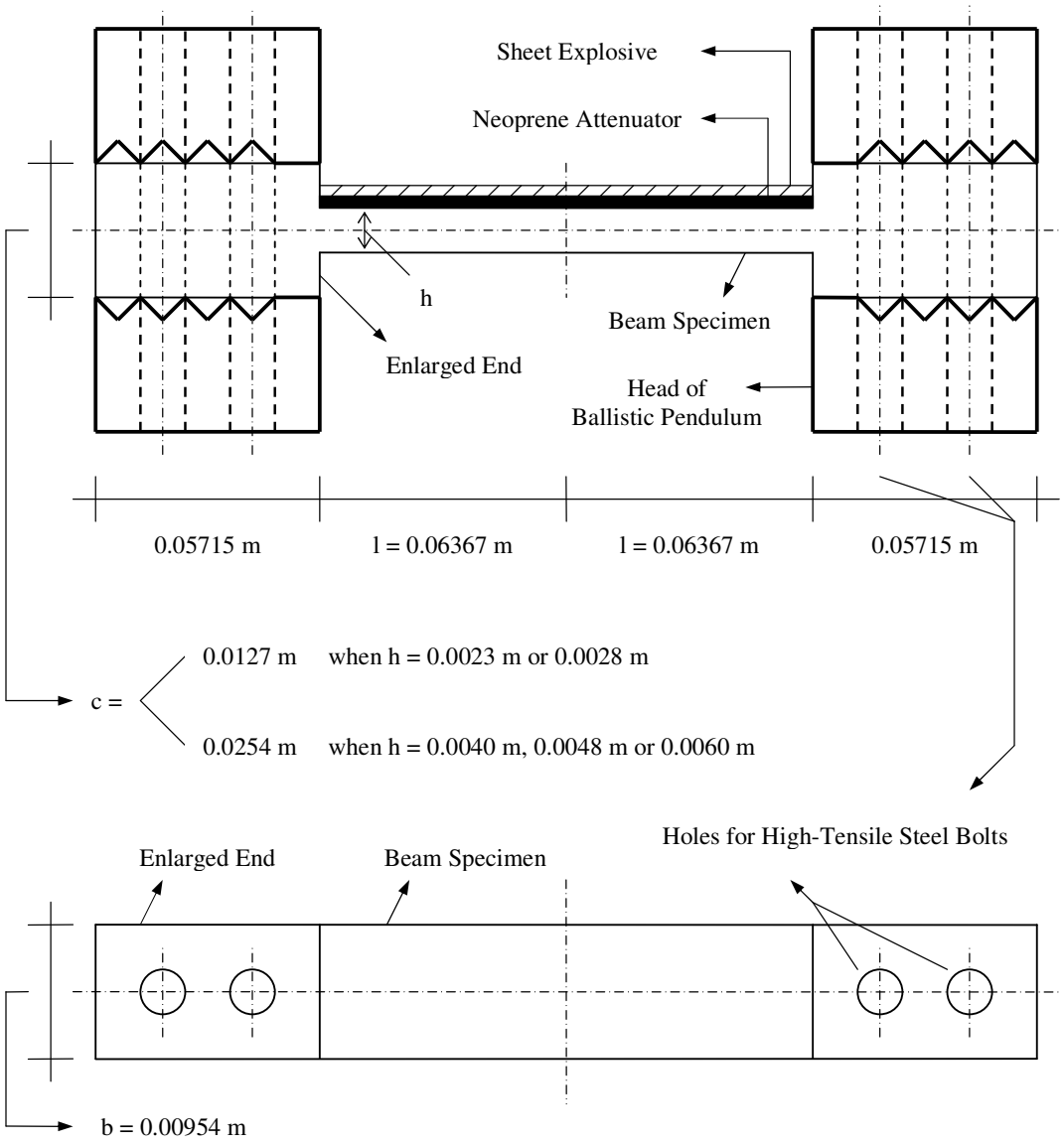

Figure 6.2: Specimen and head of ballistic pendulum

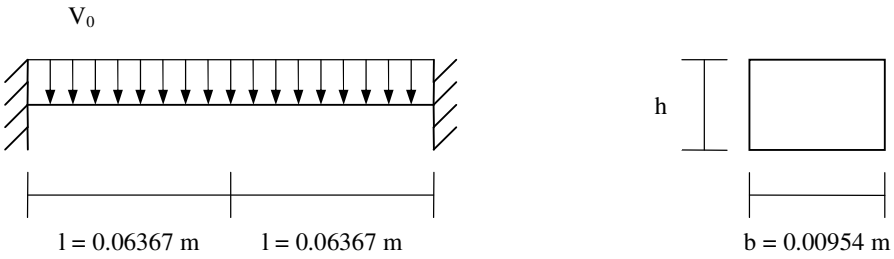

Figure 6.3: (a) Beam and its explosive load represented by an initial velocity field (b) Cross section of beam

Chapter 7 – Analysis, Results and Discussion

7.1 Introduction

The dynamic behaviour of beams can be very complicated especially with the presence of nonlinearity. Actually for the most complex dynamic analyses it may be necessary to include both material and geometric nonlinearities in a time history analysis. In all but the simplest of cases this would involve the use of a numerical method such as the finite element method.

However in design it may be possible to use simplified methods. For example in many cases the effects of material and geometric nonlinearities can be ignored and an elastic analysis is carried out.

In practice it might be best to carry out an analysis for dynamic problems which is elastic. However, in certain conditions, the effect of elasticity in the response becomes very small and thus can be neglected in order to simplify the solution if the energy imparted by the dynamic load is many times larger than the elastic energy absorption of the structure. In this case, a purely plastic dynamic analysis of the structure would suffice as the effect of plasticity is very significant because the plastic deformations are much larger than the elastic deformations.

Among the different approximate methods for plastic dynamic analysis, the rigid plastic method has been one of the most commonly used methods due to its simplicity, accuracy and above all its applicability to a wide range of plastic problems. Also, the rigid plastic method can be extended to include geometric nonlinearity and other forms of material nonlinearity such as nonlinear stress-strain relationship, strain hardening and strain rate sensitivity.

However, there has been a need to improve the rigid-plastic method so it includes the effect of both elasticity and plasticity while remaining convenient to use. This has led to introducing the elastic-plastic methods, such as the one presented in Chapter 4, which

are more accurate and allow for a wider spectrum of problems, for example those in which elasticity should be taken into account.

The simplified elastic plastic, SEP, method presented in Chapter 4 is an efficient practical tool for analysis which provides relatively easy solutions in the mode form for the beam dynamic problem. The method is able to include those effects that are difficult to consider in the analytical accurate methods, for example the Euler-Bernoulli analysis, such as material and geometric nonlinearity.

The finite element analysis which was carried out using ABAQUS has been described in Chapter 5. This, along with the SEP Method, was used for the dynamic analysis of beams similar to those tested under impulsive loads by Symonds and Jones (1972) which were presented in Chapter 6. The results from the tests have been used as a benchmark for comparison with the results from the finite element analysis which are presented in this Chapter.

Under certain conditions, in order to simplify the analysis, the dynamic load is converted into an initial velocity field. The load can be replaced by an initial velocity if its duration is smaller than approximately one tenth of the fundamental natural period of the beam. The analysis of beams under impulsive loads and the role of the impulse and the initial velocity in the modelling of these loads were discussed in Chapter 3.

The validation of the finite element model and the simplified elastic plastic method has been carried out by comparing the results from the model/method with those of a benchmark whether analytical or experimental. Through the comparison, the accuracy or the conservatism of the model/method has been investigated.

The finite element model has been validated against the experimental results. The validation is described in this Chapter. Once the validation has been done, the finite

element model can then be used as an 'accurate' benchmark to validate other methods of dynamic analysis such as the SEP Method and to compare the results.

The accuracy of the SEP Method for the dynamic analysis of beams is checked in this Chapter. The checking is done by comparing the results from the SEP Method against those from ABAQUS as the benchmark. Beams loaded impulsively, similar to those tested by Symonds and Jones (1972) but with a wider range of variables, have been analysed using ABAQUS. The dimensions of the beams, mechanical properties of the material and intensities of impulsive loads are given in this Chapter.

For the cases studied, the permanent displacements of the beam predicted using ABAQUS and the SEP Method, together with the available experimental results are given in this Chapter. The results are compared and discussed. Good agreement is found between the experimental results and ABAQUS. The SEP Method is shown to be conservative when compared to ABAQUS. The percentage differences between the various results are detailed in this Chapter and these provide guidance for proposing the calibration factors to improve the SEP Method.

Finally, a design procedure using the SEP Method is developed in this Chapter. The steps in the SEP Method, the determination of the fundamental natural period of the beam, checking the nature of the dynamic load whether impulsive or not, choosing the analysis path, then describing the various stages of the response until the determination of the displacement of the beam are discussed. A flow chart for this design procedure with the equations used are given. Recommendations for the possible applications of the SEP Method in practice, which establishes its engineering significance, are also presented.

7.2 Methodology

7.2.1 Introduction

This section explains the methodology adopted to validate the ABAQUS Model and then to check the accuracy of the SEP Method. The methodology is built upon the concept of choosing an 'accurate' benchmark, whether experimental or analytical, and then making comparisons between this benchmark and results of the desired model. By this methodology, both the safety and accuracy of the checked method can be assessed.

A variable is defined, the percentage difference of the permanent displacement that represents the comparison process. This variable can be used as an indicator of the level of safety and accuracy of the desired method.

7.2.2 Percentage Difference of Permanent Displacement

The percentage difference, Δa_p %, is the difference between two values of the permanent displacement, a_p, calculated in different ways, for example by the analytical methods, the SEP Method and ABAQUS Model, or the results from the tests. Thus, Δa_p % is defined as follows:

$$\Delta a_p \% = \frac{a_{p2} - a_{p1}}{a_{p1}} 100 = \left(\frac{a_{p2}}{a_{p1}} - 1 \right) 100 \tag{7.1}$$

where a_{p1} and a_{p2} are the permanent displacements obtained from the less accurate way and the more accurate way, respectively.

The percentage difference is useful in the comparison between the two values of the variable where the value obtained from the more accurate way is considered a benchmark.

The reason behind using the less accurate value as the value for which the difference is estimated as a percentage is that a designer would normally use the less accurate way, such as the SEP Method, to predict the sought variable as it is easier to use than the more accurate ways such as using ABAQUS or testing. Predicting the value a_{p1} of the variable using the less accurate way, the designer can then use the percentage difference to calibrate this less accurate value by adding the difference to it in order to get the value a_{p2} of that variable predicted using the more accurate way, as shown in the following equation assuming that the value of a_{p1} will be available:

$$a_{p2} = a_{p1} + \frac{\Delta a_p \%}{100} a_{p1} = \left(1 + \frac{\Delta a_p \%}{100}\right) a_{p1} \tag{7.2}$$

As the permanent displacement a_p in this research is determined in three ways, the SEP Method, the ABAQUS Model and the experiments, there are three different permanent displacement percentage differences, Δa_p %. Keeping in mind that the ABAQUS Model and the experiments can be used as benchmarks, the three percentage differences are:

1. $\Delta a_{p\,(AS)}$ % between $a_{p\,(SEP)}$ and $a_{p\,(ABAQUS)}$ as a benchmark

2. $\Delta a_{p\,(ES)}$ % between $a_{p\,(SEP)}$ and $a_{p\,(Experiment)}$ as a benchmark

3. $\Delta a_{p\,(EA)}$ % between $a_{p\,(ABAQUS)}$ and $a_{p\,(Experiment)}$ as a benchmark

where they are respectively defined by the following:

$$\Delta a_{p(AS)}\% = \frac{a_{p(ABAQUS)} - a_{p(SEP)}}{a_{p(SEP)}} 100 = \left(\frac{a_{p(ABAQUS)}}{a_{p(SEP)}} - 1 \right) 100 \tag{7.3}$$

$$\Delta a_{p(ES)}\% = \frac{a_{p(Experiment)} - a_{p(SEP)}}{a_{p(SEP)}} 100 = \left(\frac{a_{p(Experiment)}}{a_{p(SEP)}} - 1 \right) 100 \tag{7.4}$$

$$\Delta a_{p(EA)}\% = \frac{a_{p(Experiment)} - a_{p(ABAQUS)}}{a_{p(ABAQUS)}} 100 = \left(\frac{a_{p(Experiment)}}{a_{p(ABAQUS)}} - 1 \right) 100 \tag{7.5}$$

Figure 7.1 illustrates the relationship between the sign and values of Δa_p % determined, and the nature and level of both safety and accuracy of the method of analysis, whether it is the SEP Method compared with either the ABAQUS Model (by the variable $\Delta a_{p\ (AS)}$ %) or the experiments (by the variable $\Delta a_{p\ (ES)}$ %), or the ABAQUS Model compared with the experiments (by the variable $\Delta a_{p\ (EA)}$ %). When Δa_p % is negative or zero the checked method is safe, while when Δa_p % is positive the method is unsafe. Also, when the value of Δa_p % decreases, the safety level of the method increases. The accuracy of the method is related to the absolute value of Δa_p % regardless of its sign. So, when this absolute value decreases the accuracy increases, and when this value becomes zero the method is exact.

7.2.3 Validation of the ABAQUS Model

To validate the ABAQUS Model, the permanent displacement a_p computed using this model is compared with that measured in the experiment and which is considered as an 'accurate' benchmark.

Such validation serves two purposes the first of which is to determine the level of confidence in the ABAQUS Model when used for the dynamic analysis of beams. The second purpose is to enable the ABAQUS Model to be used as an analytical benchmark for validating the solutions provided by the SEP Method in addition to using the experimental benchmark, especially for those study cases described in the next Section for which experiments have not been carried out.

As part of the validation process, values of $\Delta a_{p\,(EA)}$ % are determined to assess the level of safety and accuracy of the ABAQUS Model as this variable represents the percentage difference in the permanent displacement a_p results given by ABAQUS compared to its results measured from the experiments which act as the benchmark. Also, these percentage differences can be used for assessing the level of scatter in the experimental results.

7.2.4 Validation of the SEP Method

In order to validate the SEP Method, the predictions of the permanent displacement a_p are compared with those predicted by the ABAQUS Model previously validated as an analytical benchmark, and also with the test results considered to be the experimental benchmark.

As part of the validation process, values of $\Delta a_{p\,(AS)}$ % and $\Delta a_{p\,(ES)}$ % are determined to assess the level of safety and accuracy of the SEP Method in comparison to the two benchmarks, the ABAQUS Model and the experiments, respectively. These percentage differences will assist in the proposal of suitable calibration factors for the SEP Method in order to increase its accuracy.

7.3 Data and Study Cases

7.3.1 Introduction

In this Section, detailed information for the cases considered is provided. The cases which include the experimental results have also been extended in order to cover a wider range of impulsive load intensities than that covered in the tests. The data consists of the geometry and dimensions of the beams, the mechanical properties of the material and the different intensities of the impulsive load applied.

7.3.2 General Description

As shown in figure 7.2, each case is a fully clamped mild steel beam and is subjected to a uniformly distributed impulsive load.

7.3.3 Geometry and Dimensions of Beam

The beam geometry is illustrated in figure 7.2, the cross section is solid and rectangular, and the dimensions are:
Span, 2l = 0.12733 m
Width, b = 0.00954 m
Thicknesses, h = 0.0023 m, 0.0028 m, 0.0040 m, 0.0048 m or 0.0060 m

7.3.4 Mechanical Properties of Beam Material

The beams are made from mild steel, which is a highly strain rate sensitive material. The mild steel has the following mechanical properties:

Mass density, $\rho = 7820$ kg/m^3

Young's elasticity modulus, $E = 2.1*10^{11}$ N/m^2

Yield stress, $\sigma_y = 210*10^6$ N/m^2

Power law multiplier of strain rate sensitivity, $D = 40$

Power law exponent of strain rate sensitivity, $q = 5$

7.3.5 Intensities of Impulsive Load

The impulsive load applied to the beam is shown in figure 7.2 as a field of uniformly distributed initial velocity V_0. In all the experiments, this load had an intensity which was high enough to cause a permanent plastic displacement in the beam which was, in many experiments, up to several times the beam depth. The initial velocity in the tests was in the range of 21 m/s to 73 m/s forcing the beam to reach the plastic third stage, except in the case of the thickest beam where the initial velocity was about 13 m/s, this beam only reached the plastic second stage. Thus, these values do not cover the entire range of possible beam responses.

In order to fill the gaps, a wide range of initial velocities up to 100 m/s was applied to the beams analysed using the SEP Method and the ABAQUS Model. This velocity range therefore covered cases in which the beam responded elastically only, through to beams for which the response included all four stages, Chapter 4. In total, about four hundred analyses for about two hundred cases were carried out using the SEP Method and the ABAQUS Model, including the experiments.

7.3.6 Summary

The choice of cases to broaden the responses investigated experimentally has been discussed. Details of the geometry and dimensions, the mechanical properties of material and the intensities of impulsive load have also been given.

7.4 Results

7.4.1 Overview

This section gives the values of the permanent displacement of the beam for the cases previously detailed. These include the results from the experiments, those computed using the ABAQUS Model and the results calculated using the SEP Method. These results are discussed and comparisons between them are made in order to validate the ABAQUS Model and the SEP Method. An important part of the process has been to calculate the relative percentage difference between the two results and to discuss it in terms of figure 7.1.

7.4.2 The Permanent Displacement a_p

In this section, the permanent displacements, a_p, are presented, for each beam thickness h, as a function of the initial velocity V_0, the impulsive loading intensity applied to the beam. This relationship between a_p and V_0 is plotted and then discussed for three ranges of V_0 which represent the range of velocities for the elastic first stage of the beam's response, the range for the plastic second stage and the range for the plastic third stage.

It should be recalled that if the permanent displacement predicted by the method being validated is greater than or equal to that of the benchmark the method is considered to be safe, while if it is smaller than the benchmark the method is unsafe. Also, when both displacements are close to or equal to each other the method is considered to be accurate.

Figures 7.3 to 7.7 show the variation of a_p, calculated by the SEP Method ($a_{p\ (SEP)}$) and the ABAQUS Model ($a_{p\ (ABAQUS)}$) and the experimental result ($a_{p\ (Experiment)}$), against V_0 for the different thicknesses, h, of the beam. Figures 7.8 to 7.10 shows the variation of a_p against V_0 for all the thicknesses when a_p is calculated by the SEP Method, the ABAQUS Model or measured experimentally. These results will be discussed in the following sections.

7.4.3 The Permanent Displacement Percentage Difference Δa_p %

In this section, values of $\Delta a_{p\ (AS)}$ %, $\Delta a_{p\ (ES)}$ % and $\Delta a_{p\ (EA)}$ % are presented, for the different thicknesses of the beam, as a function of the initial velocity. This relationship between the percentage difference and V_0 is plotted and then discussed for the three ranges of V_0 values mentioned earlier.

Figures 7.11 to 7.15 show the variation of $\Delta a_{p\ (AS)}$ %, $\Delta a_{p\ (ES)}$ % and $\Delta a_{p\ (EA)}$ % against V_0 for different thicknesses of the beam. Figures 7.16 to 7.18 show the variation of each difference independently against V_0 for all the thicknesses. These results will be discussed in the following sections.

7.5 Validation of the ABAQUS Model

7.5.1 Introduction

As described earlier, one of the objectives of this research was to develop and validate a finite element model, built using ABAQUS, for beams which are subjected to dynamic loads, particularly impulsive loads. The intention was that once validated it could also be used as an 'accurate' benchmark to compare with and validate other methods of dynamic analysis. The validation process is carried out by making comparisons between the experimental results and those computed by ABAQUS.

7.5.2 Comparison of Results and Discussion

Table 7.1 presents the experimental results and the results from the ABAQUS Model for the permanent displacement, a_p, for each of the beams tested. The ratio between the ABAQUS Model results and the experimental results is also provided.

By comparing the permanent displacements from the tests and the ABAQUS Model for all the thicknesses, table 7.1 and figures 7.3a, 7.4a, 7.5a, 7.6a, 7.7a and b, it can be observed that they are always very close, and sometimes equal, to each other. This shows clearly the ability of the ABAQUS Model to accurately predict the permanent displacement and thus it can be used as a benchmark.

In order to get a better understanding of the accuracy of the ABAQUS Model compared to the experimental benchmark, a statistical analysis for the values of the ratio between

a result from the ABAQUS Model and the corresponding experimental result is given in table 7.1.

The mean and the standard deviation for all the ratios are 1.043 and 0.105, respectively. The mean value which is close to one indicates that the ABAQUS Model is accurate on average, while the small value for the standard deviation indicates that the accuracy of the ABAQUS Model is consistent and the scatter in the experimental results is relatively small.

The mean of the ratio is given for the group of tested beams for each thickness in table 7.1. Each group is discussed in turn in the following.

Comparing $a_{p\ (ABAQUS)}$ with $a_{p\ (Experiment)}$ for the smallest thickness, h = 0.0023 m, table 7.1 and figure 7.3a, it is observed that $a_{p\ (ABAQUS)}$ is greater than $a_{p\ (Experiment)}$ for four experiments, and is slightly smaller than $a_{p\ (Experiment)}$ for the fifth experiment where V_0 = 67.16 m/s, $a_{p\ (ABAQUS)}$ = 0.01513 m, $a_{p\ (Experiment)}$ = 0.01516 m and their ratio is 0.998. The mean for the result ratio for this thickness group is 1.077 which indicates that the ABAQUS Model is accurate and slightly overpredicts the permanent displacement. However, this overprediction is obviously insignificant and is likely due to the scatter in the experimental results.

Comparing $a_{p\ (ABAQUS)}$ and $a_{p\ (Experiment)}$ for h = 0.0028 m, table 7.1 and figure 7.4a, it is seen that $a_{p\ (ABAQUS)}$ is always greater than $a_{p\ (Experiment)}$. The mean for the result ratio for this thickness group is 1.082 thus the ABAQUS Model is accurate and slightly overpredicts the permanent displacement.

However, comparing $a_{p\ (ABAQUS)}$ and $a_{p\ (Experiment)}$ for the two thicknesses h = 0.0040 m and h = 0.0048 m, table 7.1 and figures 7.5a and 7.6a, it is observed that $a_{p\ (ABAQUS)}$ is smaller than $a_{p\ (Experiment)}$ for three experiments for h = 0.0040 m and two experiments for h = 0.0048 m, while $a_{p\ (ABAQUS)}$ is greater than $a_{p\ (Experiment)}$ for the other three

experiments for h = 0.0040 m and the other two experiments for h = 0.0048 m. The means for the result ratio for each group for these thicknesses are, respectively, 1.013 and 1.044 and the ABAQUS Model is accurate and slightly overpredicts the permanent displacement.

Finally, comparing $a_{p\ (ABAQUS)}$ and $a_{p\ (Experiment)}$ for h = 0.0060 m, table 7.1 and figures 7.7a and b, shows that $a_{p\ (ABAQUS)}$ is smaller than $a_{p\ (Experiment)}$. The mean for the result ratio for this thickness group is 0.887 which is close to one and the ABAQUS Model is accurate but slightly underpredicts the permanent displacement.

As discussed above, the result ratios for the groups for the different thicknesses all show that the ABAQUS Model is able to predict the experimental results relatively accurately. However, the slight differences, which indicate that the level of the agreement is slightly different for each thickness, are likely to be due to the scatter in the experimental results. The experimental scatter might also be the reason for the ratios not being equal to one and thus the agreement not being exact.

From the comparison between $a_{p\ (ABAQUS)}$ and $a_{p\ (Experiment)}$ an indication of how safe the ABAQUS Model as an analysis and design tool can be made. As $a_{p\ (ABAQUS)}$ is not always greater than $a_{p\ (Experiment)}$, especially for the highest initial velocities V_0 for the thicknesses h = 0.0023 m, 0.0040 m and 0.0048 m, table 7.1 and figures 7.3a, 7.5a and 7.6a, which lay in the design range of the initial velocity where plasticity spreading reaches much so far through the body of the beam, it could indicate that the results of the ABAQUS Model need to be treated with a little caution when the Model is used for the design of beams. However, because that is likely to be due to the scatter in the experimental results, the ABAQUS Model is actually satisfactory.

If the predication of the ABAQUS Model were to be a benchmark for checking the accuracy and safety of the SEP Method, then from the comparison between $a_{p\ (ABAQUS)}$ and $a_{p\ (Experiment)}$ for all the thicknesses since $a_{p\ (ABAQUS)}$ is always very close to

$a_{p\ (Experiment)}$, it is concluded that the ABAQUS Model is a fairly accurate benchmark against which to compare the SEP Method.

It is noted from figures 7.11a, 7.12a, 7.13a, 7.14a, 7.15a, b and 7.18 that $\Delta a_{p\ (EA)}$ % can be negative or positive. However, its value is always relatively small, up to about 20 %. This means that even though the experimental results are slightly scattered, the ABAQUS Model is able to predict them reasonably accurately.

As shown in figure 7.18, the absolute value of $\Delta a_{p\ (EA)}$ %, which represents the level of accuracy for the ABAQUS Model, is not simply related to V_0. This is likely due to the scatter in the experimental results.

7.5.3 Discussion on the Percentage Difference

Figure 7.18 presents the variation of $\Delta a_{p\ (EA)}$ % for the ABAQUS Model prediction and the experimental results with V_0 for the various thicknesses. As expected with the experimental results, there is some scatter in the variation of $\Delta a_{p\ (EA)}$ %.

For h = 0.0023 m and 0.0028 m, the variation of $\Delta a_{p\ (EA)}$ % and V_0 is scattered as expected. So, as V_0 increases $\Delta a_{p\ (EA)}$ % decreases, increases then decreases. In numbers, $\Delta a_{p\ (EA)}$ % is -3 %, -16 %, -13 %, 0 % then -1 % for the small thickness while it is -5 %, -11 %, -4 % then -9 % for the other thickness. As seen, all the values are negative, except for experiment 4 with a zero hence an exact prediction for the experimental result by the ABAQUS Model.

For h = 0.0040 m, the variation of $\Delta a_{p\ (EA)}$ % and V_0 is also scattered, but the difference between the case for this thickness and that for the smaller thicknesses above is that as

V_0 increases $\Delta a_{p\ (EA)}$ % increases. However, there is an exception where $\Delta a_{p\ (EA)}$ % decreases by 7 % between a couple of experiments, no 11 and 12 of V_0 = 24.31 and 25.07 m/s, respectively. That is an expected consequence of the same exception seen in figure 7.5a for the $a_{p\ (Experiment)}$ variation. Nonetheless, those exceptions could be due to the experimental scatter. In numbers, $\Delta a_{p\ (EA)}$ % is orderly -15 %, -3 %, -10 %, 4 %, 6 % and 16 %. As seen, the values are negative then positive.

For h = 0.0048 m, the variation of $\Delta a_{p\ (EA)}$ % and V_0 is scattered and as V_0 increases $\Delta a_{p\ (EA)}$ % increases then decreases. In numbers, $\Delta a_{p\ (EA)}$ % is orderly -20 %, -5 %, 13 % and 2 %. As seen, the values are negative first then positive.

However, for h = 0.0060 m, a single experiment was done, not enough to establish the variation of $\Delta a_{p\ (EA)}$ % which has a single positive value of 13 %.

In general, as seen in figure 7.18, the mean of $\Delta a_{p\ (EA)}$ % tends to be negative and possibly the ABAQUS Model is relatively less capable of predicting the experimental results when the velocities are high and the thicknesses are low.

7.6 Validation of the SEP Method

7.6.1 Introduction

A further objective of this research was to discuss in detail one of the most developed approximate methods for the dynamic analysis of beams, the Simplified Elastic Plastic Method (the SEP Method) which has been described in Chapter 4, and to validate this method. The validation process was conducted by making comparisons between the experimental results, the predictions of the ABAQUS Model and those of the SEP Method.

7.6.2 Comparison of Results and Discussion

The results are presented in figures 7.3-7.7 for the full range of the initial velocities V_0. Figures 7.3b, 7.4b, 7.5c, 7.6c and 7.7c present the results for the lower velocities for all the thicknesses. At the lower velocities, there is a narrow range at the commencement of the plastic behaviour and for which $a_{p\ (SEP)}$ is, unlike for the higher velocities, less than $a_{p\ (ABAQUS)}$. This indicates that the SEP Method is not safe in this range. Fortunately, in practice, the design of the beams is likely to be such that they will have adequate strength to enable them to go beyond this range and into the second and third plastic stages, at which stage the SEP Method is safe.

Outwith that narrow range, figures 7.3, 7.4, 7.5, 7.6 and 7.7, $a_{p\ (SEP)}$ is always more than $a_{p\ (ABAQUS)}$ for all the beam thicknesses. This is an important result as it shows that the SEP Method is safe.

When $a_{p\ (SEP)}$ is compared with $a_{p\ (Experiment)}$, figures 7.3a, 7.4a, 7.5a and b, 7.6a and b, and 7.7a and b, it is seen that $a_{p\ (SEP)}$ is always greater than $a_{p\ (Experiment)}$ for all the thicknesses. This confirms the conclusion above that the SEP Method is safe.

The difference between $a_{p\ (SEP)}$ and $a_{p\ (ABAQUS)}$ increases as V_0 increases and thus the conservatism of the SEP Method increases, as shown in figures 7.3-7.7. The rate of change of the difference as V_0 increases is higher in the second plastic stage than that in the third plastic stage.

Figures 7.11a, b, 7.12a, b, 7.13a, b, 7.14a, b, 7.15a, b, 7.16a and b show that the percentage difference $\Delta a_{p\ (AS)}$ % is always negative with a value of at least -20 % indicating that the SEP Method is safe.

The absolute value of $\Delta a_{p\ (AS)}$ % generally decreases as V_0 increases indicating that the safety level, if defined as a percentage difference, of the SEP Method generally decreases, but still satisfactory though, as V_0 increases.

Figures 7.11a, 7.12a, 7.13a, 7.14a, 7.15a, b and 7.17 show that $\Delta a_{p\ (ES)}$ % is always negative with a value of at least -20 % confirming the conclusion above that the SEP Method is safe.

There is not a simple relationship between $\Delta a_{p\ (ES)}$ % and V_0, which represents the level of safety for the SEP Method. This is likely to be due to the scatter expected in the experimental benchmark.

Comparing $\Delta a_{p\ (AS)}$ % and $\Delta a_{p\ (ES)}$ % in figures 7.11a, 7.12a, 7.13a, 7.14a, 7.15a and b, it is noted that they are relatively close indicating that the safety level of the SEP Method does not vary much when a different benchmark is used, for example when using the ABAQUS Model instead of the experiments.

Also, comparing $\Delta a_{p\,(EA)}$ % with $\Delta a_{p\,(AS)}$ % and $\Delta a_{p\,(ES)}$ % in the previous figures, the absolute value of $\Delta a_{p\,(EA)}$ % is found to be smaller than the absolute values of $\Delta a_{p\,(AS)}$ % and $\Delta a_{p\,(ES)}$ % and relatively close to zero. This indicates that the safety level of the ABAQUS Model is lower than the safety level of the SEP Method regardless of the benchmark. However, the accuracy level of the ABAQUS Model is relatively high and higher than the accuracy level of the SEP Method no matter what the benchmark is. The accuracy of the ABAQUS Model in predicting the experimental results agrees with what was noted in the previous paragraph.

In summary, the SEP Method is conservative and the ABAQUS Model is reasonably accurate. Therefore, the SEP Method can be used with confidence in structural design and the ABAQUS Model can be confidently used to give accurate predictions in structural design and additionally for research purposes.

7.6.3 Calibration Factors

Figures 7.16a and b present the variation of $\Delta a_{p\,(AS)}$ % for the SEP Method prediction and the ABAQUS Model prediction with V_0 and h. In the following, the variation is discussed for the second plastic stage and the third plastic stage separately as the variation is complex, particularly with h, and the curves have different characteristics in the second stage while the variation is simple and the curves have similar characteristics in the third stage.

For the smallest thicknesses h = 0.0023 m and 0.0028 m in the second stage, the variation of $\Delta a_{p\,(AS)}$ % and V_0 is generally nonlinear. $\Delta a_{p\,(AS)}$ % decreases as V_0 increases until reaching a minimum. For h = 0.0023 m, the minimum value is -57 % at V_0 = 5 m/s and it is actually the minimum value for all the stages, a global minimum for

this thickness, and the point at which the SEP Method provides the safest prediction for all the stages. For h = 0.0028 m, the minimum value is -56 % at the same V_0 = 5 m/s, though it is not the global minimum for this thickness. As V_0 increases, $\Delta a_{p\ (AS)}$ % increases until reaching a maximum then decreases to a minimum at the end of the second stage. For h = 0.0023 m, the minimum value is -56 % at V_0 = 6.51 m/s. For h = 0.0028 m, the minimum value is -57 % at V_0 = 8.23 m/s and it is the global minimum for this thickness, the point at which the SEP Method prediction is the safest for all the stages.

For h = 0.0040 m in the second stage, the variation of $\Delta a_{p\ (AS)}$ % and V_0 is generally nonlinear. $\Delta a_{p\ (AS)}$ % increases as V_0 increases until reaching a maximum whose value is -55 % at V_0 = 7 m/s. As V_0 increases further, $\Delta a_{p\ (AS)}$ % decreases to a minimum at the end of the second stage with a value of -58 % at V_0 = 12.21 m/s.

For the largest thicknesses h = 0.0048 m and 0.0060 m in the second stage, the variation of $\Delta a_{p\ (AS)}$ % and V_0 is generally nonlinear. $\Delta a_{p\ (AS)}$ % increases as V_0 increases until reaching a maximum whose value is, for these thicknesses respectively, -57 % and -58 % at V_0 = 8 m/s and 10 m/s. As V_0 increases more, $\Delta a_{p\ (AS)}$ % decreases to a minimum then increases to a maximum at the end of the second stage with a value of -59 % and -58 % at V_0 = 14.80 m/s and 18.65 m/s, for the two thicknesses respectively.

At the end of the second stage, it is noticeable that the $\Delta a_{p\ (AS)}$ % curves have a sharp transition to the third stage depicted by a sharp turning point. This discontinuity is due to that seen in the $a_{p\ (SEP)}$ curves.

$\Delta a_{p\ (AS)}$ % at the sharp curving point slightly varies as h varies. It has the value of -56 %, -57 %, -58 %, -59 % and -58 % for h = 0.0023 m, 0.0028 m, 0.0040 m, 0.0048 m and 0.0060 m, respectively, so it slightly decreases then slightly increases as h increases. As shown, the SEP Method safest prediction at the end of the second stage is for h = 0.0048 m.

V_0 at the sharp transition increases as h increases. This is due to the same relationship seen for the sharp transitions of the $a_{p\,(SEP)}$ curves.

For the smallest thickness h = 0.0023 m in the third stage, the variation of $\Delta a_{p\,(AS)}$ % and V_0 is generally nonlinear. As V_0 increases, $\Delta a_{p\,(AS)}$ % increases to a maximum whose value is -25 % at V_0 = 40 m/s. The maximum is global for all the stages for this thickness and the SEP Method provides the least safe prediction at this point, though it is still safe. As V_0 further increases, $\Delta a_{p\,(AS)}$ % slightly decreases at a low decreasing rate until becoming constant with a horizontal curve and a value of -27 %.

For the other thicknesses h = 0.0028 m, 0.0040 m, 0.0048 m and 0.0060 m in the third stage, the variation of $\Delta a_{p\,(AS)}$ % and V_0 is generally nonlinear. As V_0 increases, $\Delta a_{p\,(AS)}$ % increases then remains constant with a horizontal curve and a value of -28 %, -31 %, -33 % and -35 %, respectively for the four thicknesses. This value for each thickness is the global maximum for all the stages at which the SEP Method prediction is the least safe prediction, though it is still safe.

The constant value of $\Delta a_{p\,(AS)}$ % stated above is evidence of the consistency of the accuracy level for the SEP Method, determined in comparison with the ABAQUS Model prediction, in predicting beams response to high impulsive loads.

As seen in figures 7.16a and b, the variation of $\Delta a_{p\,(AS)}$ % and h in the second stage is complex. As h increases from 0.0023 m to 0.0028 m, from 0.0023 m to 0.0040 m, from 0.0028 m to 0.0040 m or from 0.0048 m to 0.0060 m, $\Delta a_{p\,(AS)}$ % decreases, remains constant, increases, remains constant then decreases as V_0 increases. As h increases from 0.0023 m to 0.0048 m, from 0.0023 m to 0.0060 m, from 0.0028 m to 0.0048 m, from 0.0028 m to 0.0060 m, from 0.0040 m to 0.0048 m or from 0.0040 m to 0.0060 m, $\Delta a_{p\,(AS)}$ % decreases indicating an increasingly safe prediction using the SEP Method.

The variation of $\Delta a_{p\,(AS)}$ % and h in the third stage is simpler. As h increases, $\Delta a_{p\,(AS)}$ % decreases and the SEP Method becomes safer.

In the third stage, the difference of $\Delta a_{p\,(AS)}$ % for two values of h generally decreases then remains constant with the horizontal curves as V_0 increases. This indicates that the variation of the accuracy level for the SEP Method prediction of beams response to high impulsive loads, when the ABAQUS Model is the benchmark, due to a given variation of h is constant.

Figure 7.17 presents the variation of $\Delta a_{p\,(ES)}$ % for the SEP Method prediction and the experimental results with V_0 for the various thicknesses. As expected with the experimental results, there is scatter in the variation.

For h = 0.0023 m and 0.0028 m and as V_0 increases, $\Delta a_{p\,(ES)}$ % decreases, increases then decreases. In numbers, $\Delta a_{p\,(ES)}$ % is -28 %, -38 %, -36 %, -26 % then -27 % for the small thickness and it is -33 %, -36 %, -30 % then -34 % for the other thickness.

For h = 0.0040 m and as V_0 increases, $\Delta a_{p\,(ES)}$ % increases and the accuracy for the SEP Method improves. However, there is an exception where $\Delta a_{p\,(ES)}$ % decreases by 4 % between a couple of experiments, no 11 and 12 of V_0 = 24.31 and 25.07 m/s, respectively. That is an expected consequence of the same exception seen in figure 7.5a for the $a_{p\,(Experiment)}$ variation. Nonetheless, those exceptions could be due to the experimental scatter. In numbers, $\Delta a_{p\,(ES)}$ % is orderly -47 %, -39 %, -43 %, -34 %, -31 % and -23 %.

For h = 0.0048 m and as V_0 increases, $\Delta a_{p\,(ES)}$ % increases then decreases. In numbers, $\Delta a_{p\,(ES)}$ % is orderly -54 %, -42 %, -31 % and -36 %.

However, for h = 0.0060 m, a single experiment was done, not enough to establish the variation of $\Delta a_{p\,(ES)}$ % which has a single value of -53 %.

In general, as seen in figure 7.17, the mean of $\Delta a_{p\,(ES)}$ %, which is negative, tends to increase and the SEP Method is possibly more accurate as the velocity increases and the thickness decreases.

7.7 Some Comments on the Permanent Displacement of the Beams

7.7.1 The Permanent Displacement as Predicted by the ABAQUS Model

A beam whose dynamic response is predicted using the ABAQUS Model does not go through the same distinct stages of response as predicted using the SEP Method with the exception of the initial elastic stage. This is because the ABAQUS Model does not artificially separate the elastic state from the plastic state of the material and thus elasticity and plasticity can coexist simultaneously in the beam, and in the same cross section. Thus, the ABAQUS Model simulates the problem more realistically.

Figures 7.9a and b present the variation of $a_{p\ (ABAQUS)}$ with V_0 and h. As expected, $a_{p\ (ABAQUS)}$ increases as V_0 increases when the beam is elasto plastic and $a_{p\ (ABAQUS)}$ is zero for the V_0 values in the elastic stage which are below about 2 m/s.

For V_0 values from approximately 2 m/s to 20 m/s, the variation of $a_{p\ (ABAQUS)}$ and V_0 is nonlinear for all the h values. For V_0 values above about 20 m/s, the variation is linear and parallel for all the h values. This prediction from the ABAQUS Model, which is similar to that from the SEP Method, is an evidence for the linear response of the beam to high impulsive loads.

The $a_{p\ (ABAQUS)}$ curves are smooth throughout the elasto plastic stage indicating that their equations, resulting from the ABAQUS analysis, are continuous. This continuity can be observed in the equations of the finite element analysis used in ABAQUS and detailed in Chapter 5.

Comparing the $a_{p\ (ABAQUS)}$ curves for the different thicknesses and the $a_{p\ (SEP)}$ curves, it is found that the two sets are slightly different. This is due to the nature of the

assumptions, described in previous Chapters, for the SEP Method and those for the ABAQUS Model.

As seen from figures 7.9a and b, $a_{p\ (ABAQUS)}$ decreases as h increases for a given V_0, as expected, with an exception for h = 0.0023 m and 0.0028 m whose $a_{p\ (ABAQUS)}$ curves meet, coincide then separate for V_0 between approximately 13 m/s and 24 m/s.

The parallel straight $a_{p\ (ABAQUS)}$ lines for all the h values and high V_0 values indicates that the rate of increase of the displacement is constant. That is evidence of the independence of the rate of change of the displacement under high impulsive loads of the velocity and the thickness.

A further conclusion from the parallelisation discussed above is that for high V_0 values, the difference of $a_{p\ (ABAQUS)}$ for two values of h is constant. The difference of $a_{p\ (ABAQUS)}$ is larger than that of $a_{p\ (SEP)}$ for the same values of h.

In figure 7.9, the curves are close to each other and the variation of the permanent displacement predicted using the ABAQUS Model with the thickness is relatively small. The reason for that is that the impulsive load increases as the thickness increases for a given initial velocity according to equation (3.22). These increments of the thickness and the load would have contradicting effects on the permanent displacement, decreasing and increasing, respectively. Also, the behaviour is mainly plastic and thus the prediction for elastic problems does not necessarily apply. The approximate plastic analysis discussed in Section 7.7.3 explains the phenomenon.

7.7.2 The Permanent Displacement as Predicted by SEP Method

Figures 7.8a and b present the variation of $a_{p\,(SEP)}$ for V_0 and h. For all the h values and as expected, $a_{p\,(SEP)}$ increases as V_0 increases in the second and third plastic stages and $a_{p\,(SEP)}$ is zero for the V_0 values in the elastic stage which are below about 3 m/s.

In the second plastic stage, the variation of $a_{p\,(SEP)}$ and V_0 is nonlinear representing the bending plasticity effect in the beam. Thus, the rate of increase of $a_{p\,(SEP)}$ increases as V_0 increases showing the increasing ductility the beam exhibits as plasticity spreads through when it becomes less stiff and gains extra displacement helping to resist the impulsive load and to absorb its imparted energy. Thereafter, in the third plastic stage, the variation becomes linear, and parallel for V_0 values above about 18 m/s, for all the h values representing the axial tension plasticity effect in the beam. Thus, the rate of $a_{p\,(SEP)}$ increase stops increasing as V_0 increases and becomes constant because the beam looses some ductility when moving to the third plastic stage, becomes stiffer and has smaller displacement when absorbing the energy of the impulsive load. This prediction from the SEP Method is an evidence for the linearity of the beam response to high impulsive loads.

The decrease in gradient discussed above is sudden. Thus, the $a_{p\,(SEP)}$ curves have a sharp transition from the second plastic stage to the third plastic stage indicating that the assumptions in the analysis are different either side of this point, in other words, for the second stage and the third stage. This discontinuity can be seen from the equations of the SEP Method detailed in Chapter 4.

In the second plastic stage, the increasing $a_{p\,(SEP)}$ as V_0 increases reaches a maximum at the sudden decrease in gradient, the end of the second stage. The maximum value at the end of the second stage is greater for a greater h and happens also at a higher V_0 causing the regular dislocation of $a_{p\,(SEP)}$ curves observed in figures 7.8a and 7.8b when h increases.

As seen from figures 7.8a and b, $a_{p\ (SEP)}$ decreases as h increases for a given V_0 in the second plastic stage. After that, in the third plastic stage, the variation reverses and $a_{p\ (SEP)}$ increases as h increases.

The parallel straight $a_{p\ (SEP)}$ lines for all the h values and high V_0 values indicates that the rate of increase of the displacement is constant. That is evidence of the independence of the rate of change of the displacement under high impulsive loads of the velocity and the thickness.

A further conclusion from the parallelisation discussed above is that for high V_0 values, the difference of $a_{p\ (SEP)}$ for two values of h is constant.

In figure 7.8, the curves are close to each other and the variation of the permanent displacement predicted using the SEP Method with the thickness is relatively small and in the third plastic stage increases as the thickness increases. A similar phenomenon was predicted using the ABAQUS Model and that predicted using the SEP Method can be explained likewise.

The $a_{p\ (SEP)}$ variation has many characteristics in common with the $a_{p\ (ABAQUS)}$ variation. Thus, the SEP Method prediction well compares with the benchmark, the ABAQUS Model prediction.

7.7.3 The Permanent Displacement Measured Experimentally

As for the ABAQUS Model, the response of the beam of the experiment does not go through the same distinct plastic stages of the SEP Method because in reality, elasticity would still be present when plasticity starts forming.

Figure 7.10 presents the variation of $a_{p\ (Experiment)}$ with V_0 and h. For an h value and as expected, $a_{p\ (Experiment)}$ increases as V_0 increases despite the scatter in the experimental results. However, for h = 0.0060 m, a single experiment was done, not enough to establish the variation experimentally. Also, for h = 0.0040 m, there is an exception where $a_{p\ (Experiment)}$ slightly decreases, by 4 %, for two experiments, no 11 and 12 of V_0 = 24.31 and 25.07 m/s and $a_{p\ (Experiment)}$ = 0.00445 and 0.00427 m, respectively. Nonetheless, that could be due to the experimental scatter.

It is clear from figure 7.10 that a straight line could be fixed through all the slightly scattered experimental results with a fairly good correlation. Thus, the variation of $a_{p\ (Experiment)}$ and V_0 could possibly be linear and independent of h if the scatter was to virtually be removed. That finding is compatible with the predictions of the ABAQUS Model and the SEP Method.

An approximate analysis which considered only the plastic axial tension behaviour of the beam in the third stage was carried out by equating the external energy of the beam to its internal energy. The displacement of the beam was given by

$$a_p = l\sqrt{\frac{\rho}{\sigma_y}}V_0 \tag{7.6}$$

As shown in equation (7.6), the approximate analysis above predicted that the displacement is related linearly to the velocity and independent of the thickness. The

relationship is drawn in figure 7.20. That prediction is in a good agreement with the experimental results and the predictions of the ABAQUS Model and the SEP Method.

In figure 7.20, the ABAQUS Model prediction is also shown for comparison with the prediction from the above membrane analysis. Although both predictions are linear in the plastic membrane stage, the ABAQUS Model prediction is lower. That is mainly due to the inclusion of the strain rate sensitivity of the material in the ABAQUS analysis.

The variation of $a_{p\ (Experiment)}$ has many characteristics in common with the variations of $a_{p\ (ABAQUS)}$ and $a_{p\ (SEP)}$. Thus, the predictions of the ABAQUS Model and the SEP Method are in a good agreement with the experimental benchmark.

7.8 Practical Use of the SEP Method and its Engineering Significance

In section 7.6 it was shown that the SEP Method is a suitable tool for simplified dynamic analysis. The conditions which have to be satisfied for the application of the method are that the beam must have a rectangular cross section and fully fixed boundaries. There is no restriction on the h/b ratio as Poisson's ratio is ignored in the elastic analysis, nor on the h/l ratio as the axial force effect is included.

In addition to beams, the SEP Method is suitable for other structural members, for example plates and slabs, which span predominantly in one direction. Thus, the method could be used for the dynamic analysis of flat cladding to buildings.

The SEP Method is mainly used for impulsive loads where their duration, t_d, is less than one tenth of the fundamental natural period, T, of vibration of the member. In this case, the load is replaced by an initial velocity.

The SEP Method can also be used for other dynamic loads of any variation and duration. In this case, the actual load will be used under which the beam starts to move elastically in Stage I. Thus, the elastic motion will be forced and its governing equation will be similar to the equation of free motion but with a forcing function on the right hand side. The forcing function can be derived from equation (2.34) for the approximate method which has been explained in Chapter 2. Once the beam starts to become plastic, the relevant steps of the SEP Method will be carried out as normal. So, the governing equation of motion will be found from the dynamic equilibrium of the beam.

In the prediction of the dynamic response, the SEP Method accounts for the elastic deformations and plastic deformations. Thus, this method is more accurate than approximate methods which ignore elasticity, for example the rigid plastic method. Also, the SEP Method accounts for geometric nonlinearity and includes the effect of the

axial force in the third stage of response which involves plastic tensile membrane behaviour.

Whilst all the tests and the relevant analyses described in the Thesis have been carried out on small scale specimens, it is envisaged that the procedures of the SEP Method can be applied to structures of any scale. This can be done by the generalisation of the results presented in this Chapter.

Cross sections other than rectangular cross sections could be analysed using the SEP Method, for example "I" sections, by taking into account the interaction between the internal bending moment M and the internal axial force N, and the second moment of area I and the area A. This means a relationship between M and N for the particular cross section in the fully plastic state different from the relationship for the rectangular cross section would need to be used.

Beams with boundary conditions other than full fixity, for example simply supported beams, can be analysed using the SEP Method by using suitable shape functions for the elastic stage and a suitable number of plastic hinges and possibly excluding the plastic tension stage from the response if there is no axial restraint.

The SEP Method could be extended in order that it could be used for other members, for example cantilevers, plates and slabs, and for more complex structures, for example multi span beams, frames and three dimensional systems of interacting slabs and frames. This would be done by making some amendments for the SEP Method, such as those described above, so that it would reasonably model the dynamic behaviour of these structures.

As explained in Chapter 4, in the SEP Method the response of the beam is considered to consist of several distinct stages based on whether the beam material is elastic or plastic and on the resistance action dominating the behaviour of the beam whether it is bending

or axial tension. In each stage, the beam takes a shape distinct to the stage. If the dynamic load applied to the beam is high enough, the stages of the SEP Method are:

1- Stage I – elastic deformation
2- Stage II – plastic bending
3- Stage III – plastic tension
4- Stage IV – elastic recovery

A flow chart that explains how the SEP Method can be used in practice is given in figure 7.19. It shows the different successive steps of the SEP Method for a given beam and loading where T is the fundamental natural period of free vibration of the beam, given by equation (2.16) and t_d is the duration of the dynamic load.

A full description of the SEP Method is given in Chapter 4. What follows is a brief description of how it can be applied in practice.

Initially, the duration of the dynamic load t_d has to be compared with the fundamental natural period of the beam, T. If t_d is found to be smaller than or equal to T/10, then the dynamic load is impulsive and thus can be converted according to the pulse theorem presented in Chapter 3 to an initial velocity V_0 using equation (3.22). This initial velocity should be considered as the loading causing the beam to move elastically in Stage I. In this case, the elastic motion is free and it is governed by equation (4.23) where the deformed shape of the symmetric beam half is assumed to be that of an unloaded fully fixed beam which is used in the approximate method explained in Chapter 2. This shape is given by equation (4.20).

Following Stage I, the beam motion starts to become plastic. In Stage II, the beam behaves in bending with a plastic hinge in the middle dividing the beam into two rigid halves and a plastic hinge at each of the two boundaries, and the governing equation of motion is equation (4.34). For this motion, the initial displacement is the displacement at the end of Stage I. However, the initial velocity is not the same because the beam

takes a new deformed shape in Stage II. To connect the two stages, the initial velocity of Stage II is determined from the velocity at the end of Stage I using the Δ_0 minimum technique, equation (4.36).

In Stage III, the beam behaves as a tendon in tension, which is plastic throughout, and the motion is governed by equation (4.43). The initial conditions are found using the velocity and displacement from the end of Stage II in a similar way to that explained above.

Finally, the beam recovers elastically in Stage IV until it comes to rest leaving only the permanent plastic deformations. At this stage, the permanent displacement of the beam a_p can be determined using equation (4.50).

However, if t_d is larger than T/10, then the dynamic load is non-impulsive. This load will then be that under which the beam starts to move elastically in Stage I. In this case, the elastic motion is forced and its governing equation is similar to the equation of free motion but with a forcing function on the right hand side. The forcing function can be derived from equation (2.34) for the approximate method which is explained in Chapter 2. Once the beam becomes plastic, the analysis moves to Stage II and is carried out as above using the displacement and the velocity in Stage II determined from these at the end of Stage I.

Dimensionless graphs for various h/b and h/l ratios could be produced using the SEP Method for structural engineers to use in design. However, further analysis for a broader range of values for the thickness h, the width b and the span 2l is required in order to verify whether the dimensionless graphs will remain the same for the same ratios.

One important characteristic of the SEP Method is that it is conservative. The main reason for this conservatism is the neglect of the strain rate sensitivity of the material in

the SEP Method. This means that the yield strength in the SEP Method is smaller than in practice. In the ABAQUS Model, and of course the experiments, strain rate effects are included.

Although conservatism is an advantage for methods of structural analysis, the SEP Method can be too conservative which can lead to concerns over the economy of the SEP solutions. Therefore, the calibration factors discussed previously can be used in order to reduce the conservatism.

Because the calibration factors for the SEP Method, which are always negative reflecting its conservative nature, have a value greater than 20%, a single calibration factor can be proposed for the SEP Method that is 20%. Such a correction would improve the SEP Method as it would remove most of the conservatism in the method and thus render it more economical and also more accurate.

7.9 Summary

The finite element model which was built using ABAQUS has been validated against a number of experiments for beams loaded impulsively and carried out by Symonds and Jones (1972). These beams have been analysed using the ABAQUS Model. The permanent displacements obtained experimentally and predicted by the ABAQUS Model have then been given, compared and discussed. Good agreement has been found between the experimental results and the ABAQUS Model prediction indicating that the ABAQUS Model is accurate.

The ABAQUS Model has then been used, alongside the experiments, as a benchmark against which to test the SEP Method. More cases of beams loaded impulsively, similar to those tested by Symonds and Jones (1972) but with a wider range of variables, have been analysed using the ABAQUS Model and the SEP Method. The permanent displacements predicted by the ABAQUS Model and the SEP Method have been given, compared and discussed for all the cases including those of the experiments. The experimental results have also been used in the comparison. The SEP Method has been shown to be conservative.

The percentage differences between the various results have been detailed and these have provided guidance for proposing the calibration factors to improve the SEP Method.

A design procedure using the SEP Method has been developed. The steps in the SEP Method which include the determination of the fundamental natural period of the beam, checking the nature of the dynamic load whether impulsive or not, choosing the analysis path, then describing the various stages of the response until the determination of the displacement of the beam have been discussed. A flow chart for this design procedure, including the equations used, has been given. Recommendations for the application of the SEP Method in practice have also been presented.

Table 7.1: Comparison of experimental and ABAQUS results

Experiment number	h m	V_0 m/s	$a_{p(Experiment)}$ m	$a_{p(ABAQUS)}$ m	$\frac{a_{p(ABAQUS)}}{a_{p(Experiment)}}$	Mean for each thickness
1	0.0023	35.31	0.00749	0.00770	1.028	1.077
2		47.75	0.00889	0.01065	1.198	
3		64.52	0.01265	0.01453	1.149	
4		67.16	0.01516	0.01513	0.998	
5		72.19	0.01605	0.01626	1.013	
6	0.0028	32.13	0.00640	0.00676	1.056	1.082
7		38.25	0.00729	0.00823	1.129	
8		49.91	0.01052	0.01093	1.039	
9		55.37	0.01105	0.01219	1.103	
10	0.0040	21.54	0.00340	0.00400	1.176	1.013
11		24.31	0.00445	0.00458	1.029	
12		25.07	0.00427	0.00473	1.108	
13		30.30	0.00607	0.00585	0.964	
14		34.57	0.00724	0.00682	0.942	
15		41.61	0.00983	0.00844	0.859	
16	0.0048	21.69	0.00302	0.00379	1.255	1.044
17		27.94	0.00495	0.00522	1.055	
18		30.25	0.00638	0.00566	0.887	
19		35.84	0.00701	0.00685	0.977	
20	0.0060	13.87	0.00142	0.00126	0.887	0.887

Mean 1.043

Standard Deviation 0.105

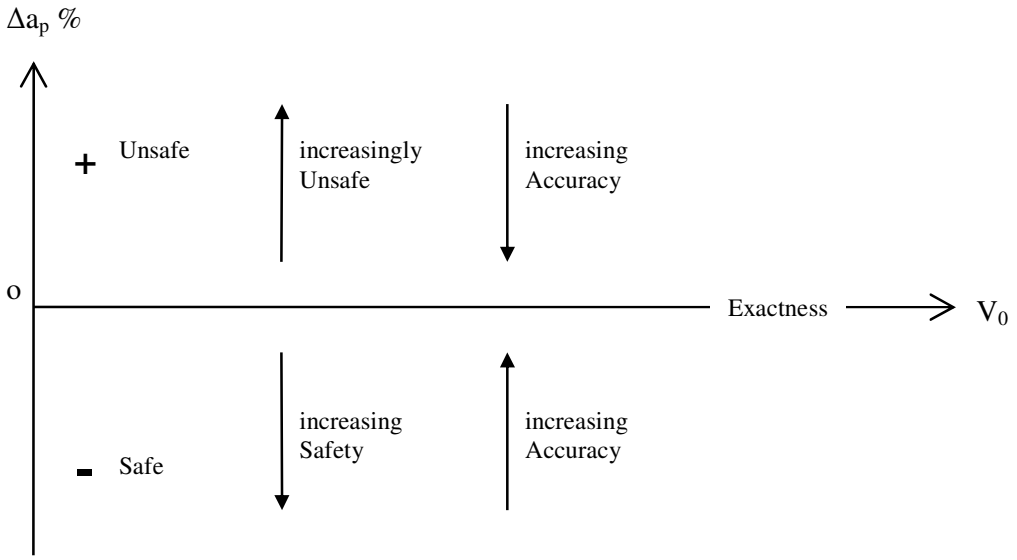

Figure 7.1: Relation between sign and value of Δa_p % and nature and level of both safety and accuracy

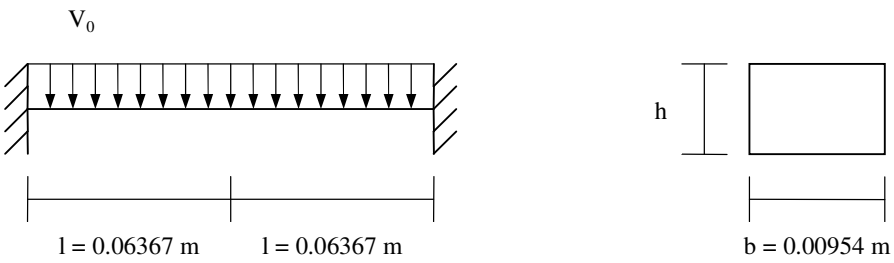

Figure 7.2: (a) Beam and its impulsive load represented by an initial velocity field (b) Cross section of beam

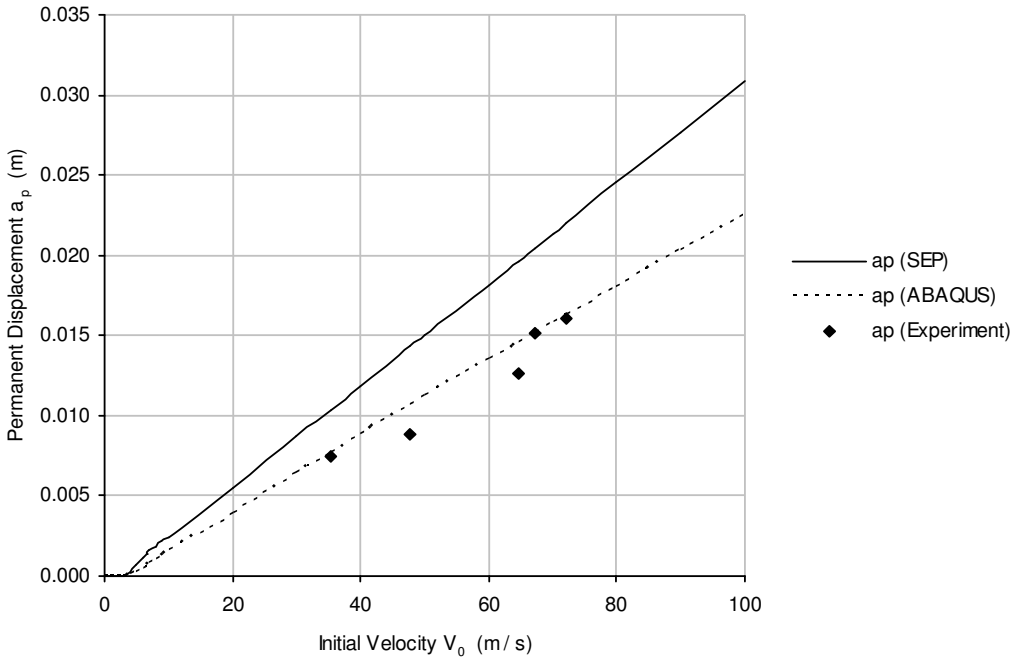

Figure 7.3a: a_p for h=0.0023m, V_0, 0-100m/s

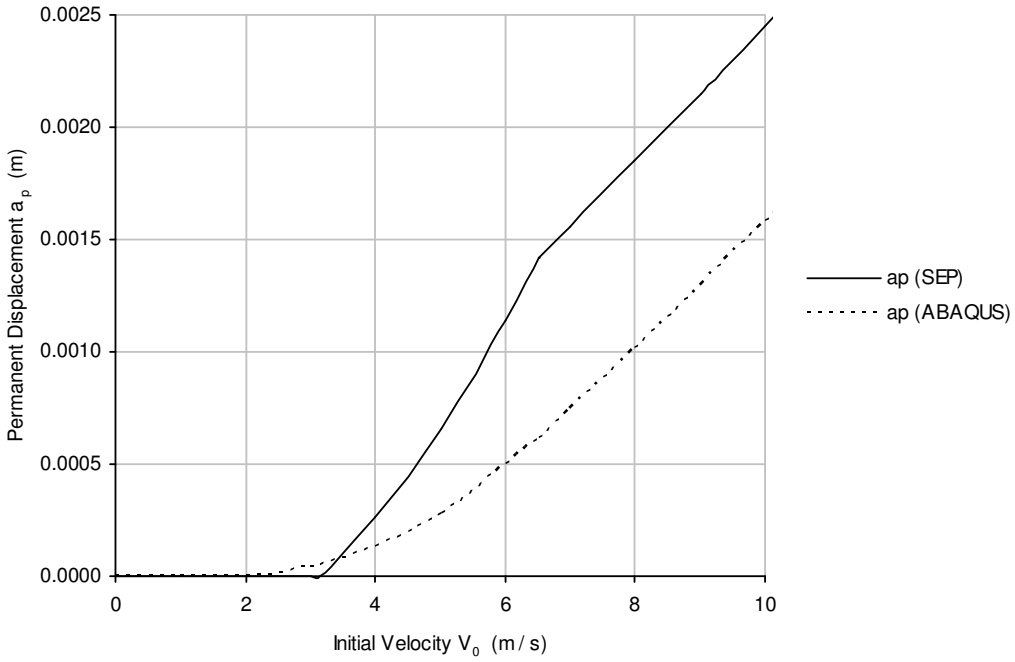

Figure 7.3b: a_p for h=0.0023m, V_0, 0-10m/s

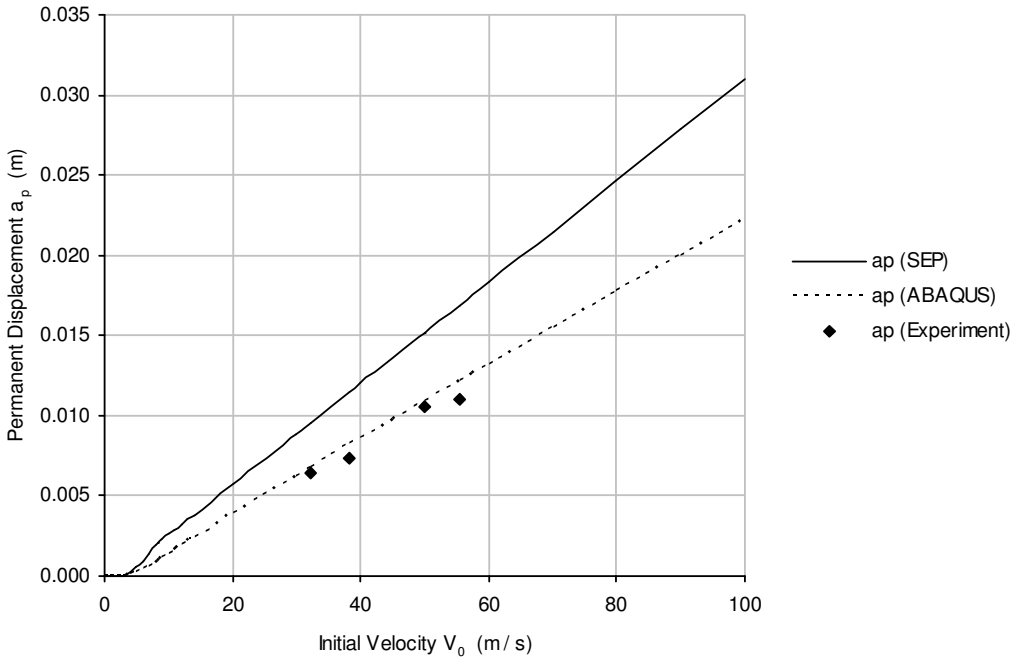

Figure 7.4a: a_p for h=0.0028m, V_0, 0-100m/s

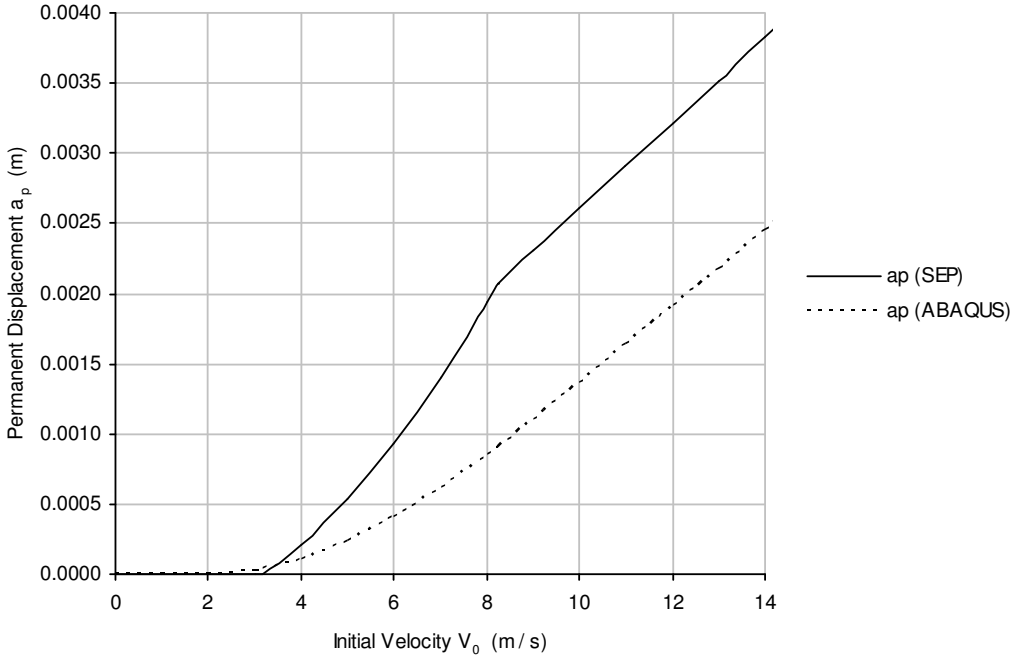

Figure 7.4b: a_p for h=0.0028m, V_0, 0-14m/s

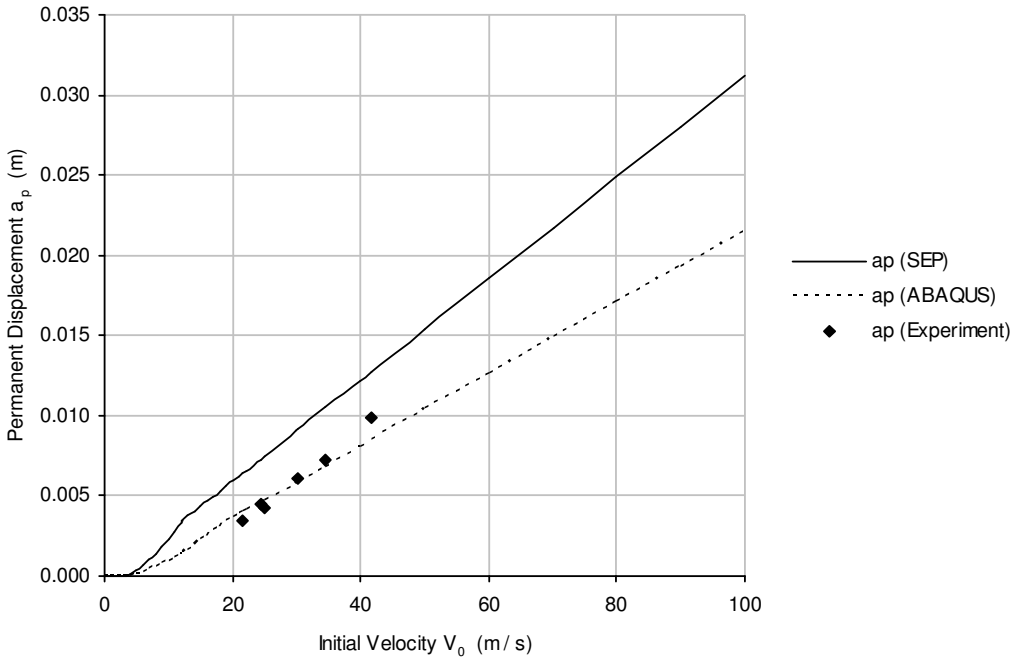

Figure 7.5a: a_p for h=0.0040m, V_0, 0-100m/s

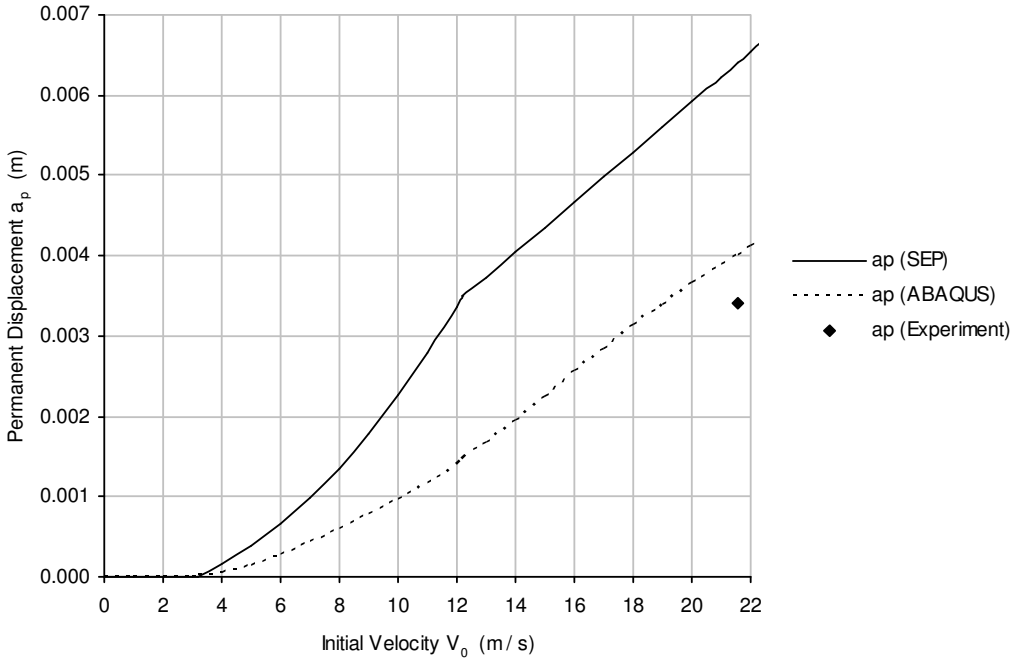

Figure 7.5b: a_p for h=0.0040m, V_0, 0-22m/s

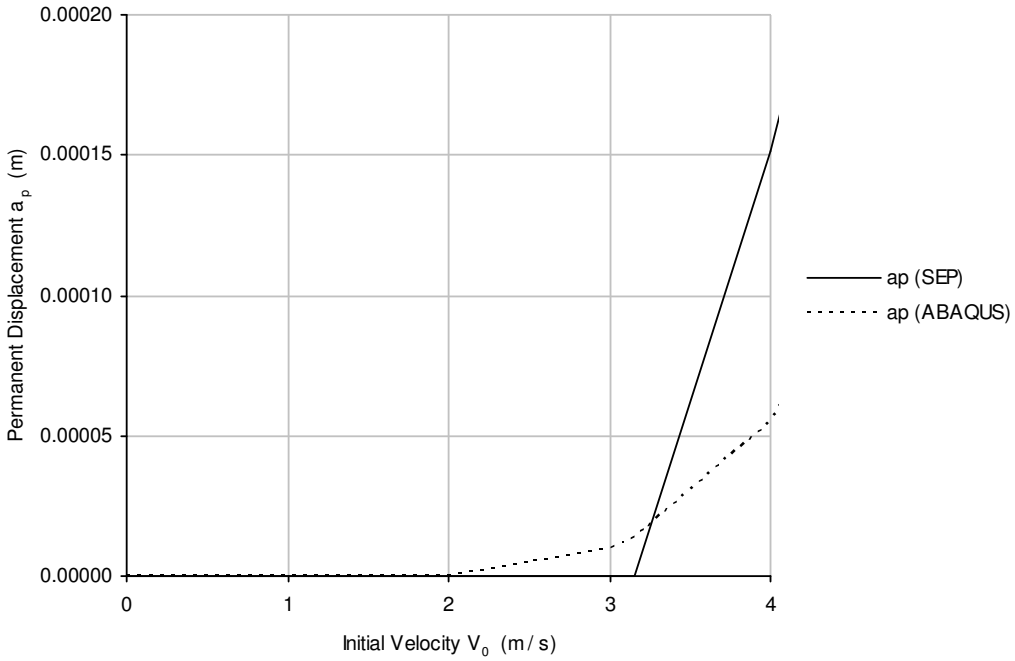

Figure 7.5c: a_p for h=0.0040m, V_0, 0-4m/s

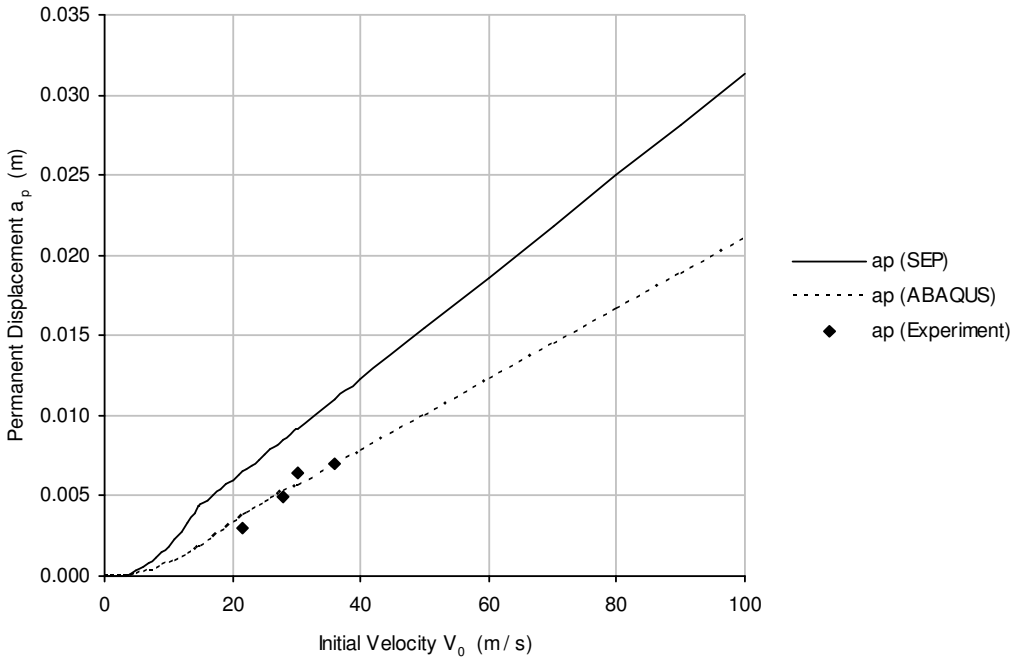

Figure 7.6a: a_p for h=0.0048m, V_0, 0-100m/s

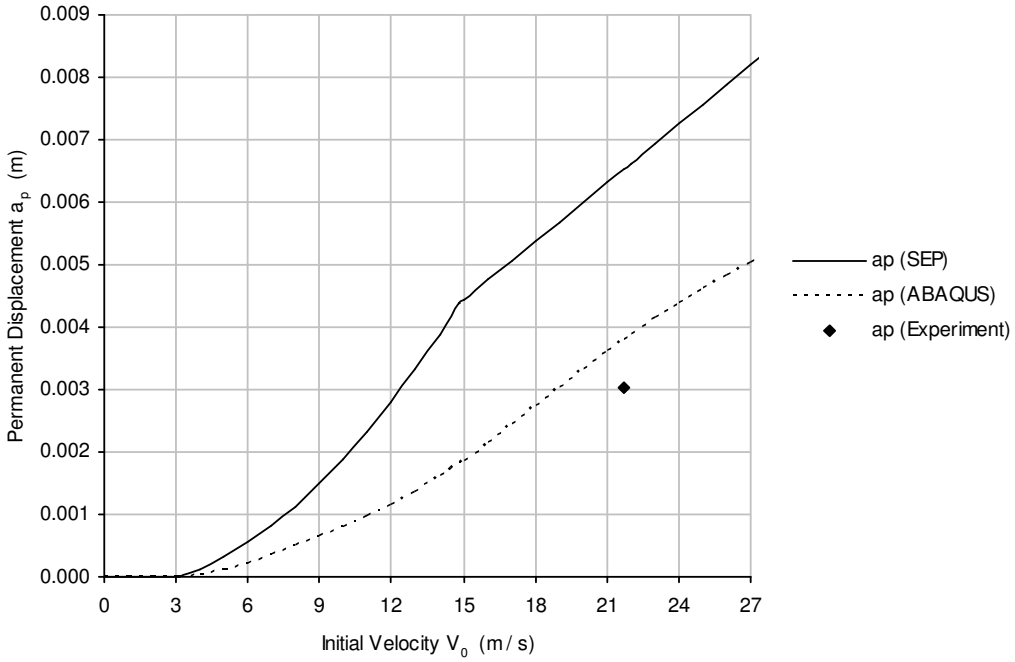

Figure 7.6b: a_p for h=0.0048m, V_0, 0-27m/s

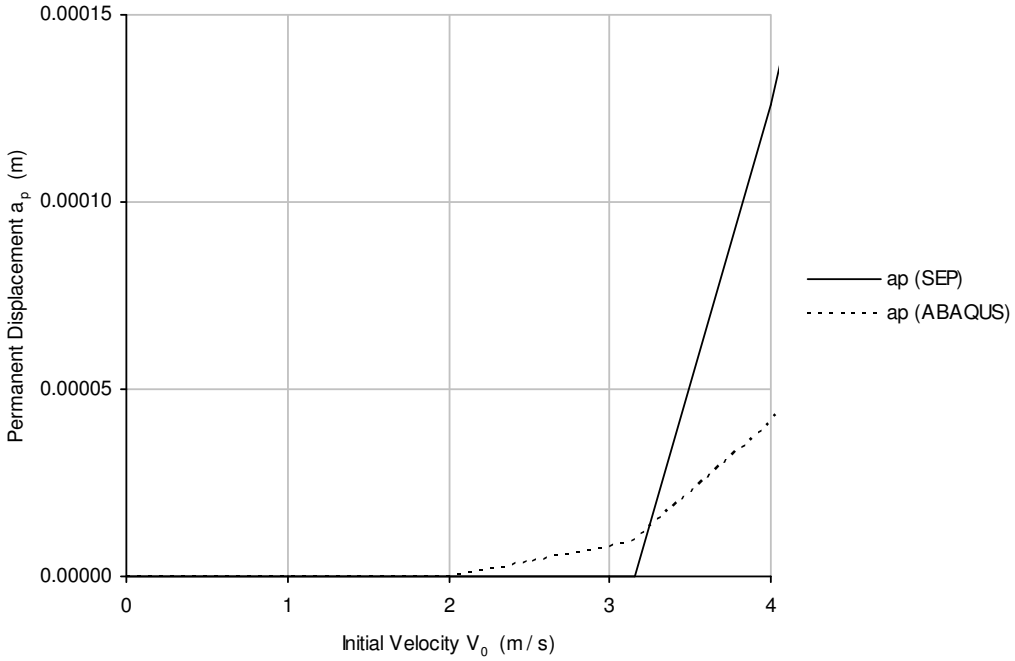

Figure 7.6c: a_p for h=0.0048m, V_0, 0-4m/s

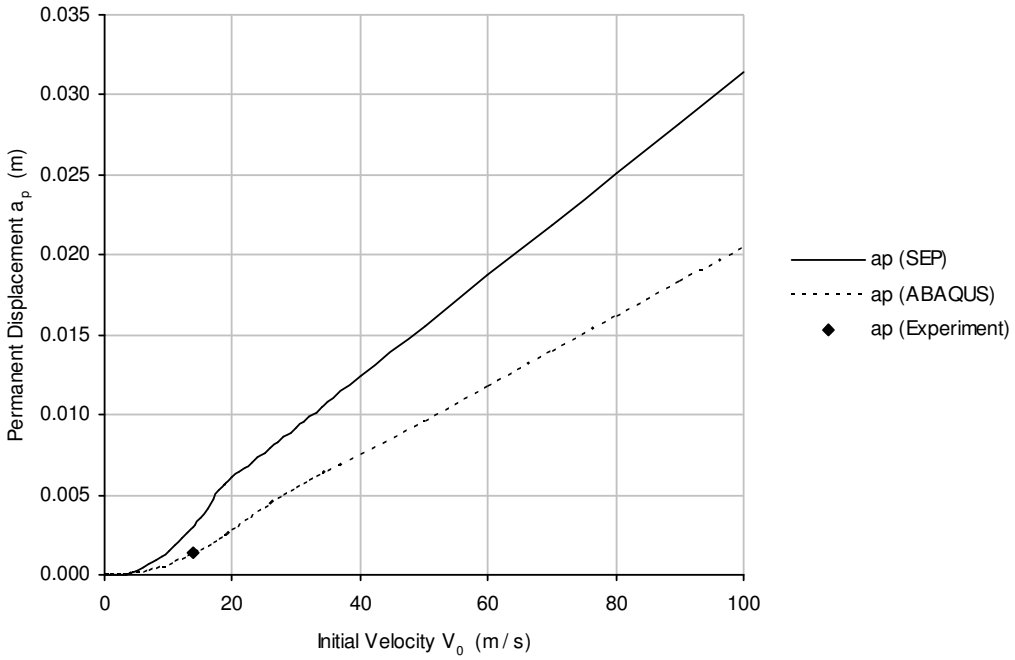

Figure 7.7a: a_p for h=0.0060m, V_0, 0-100m/s

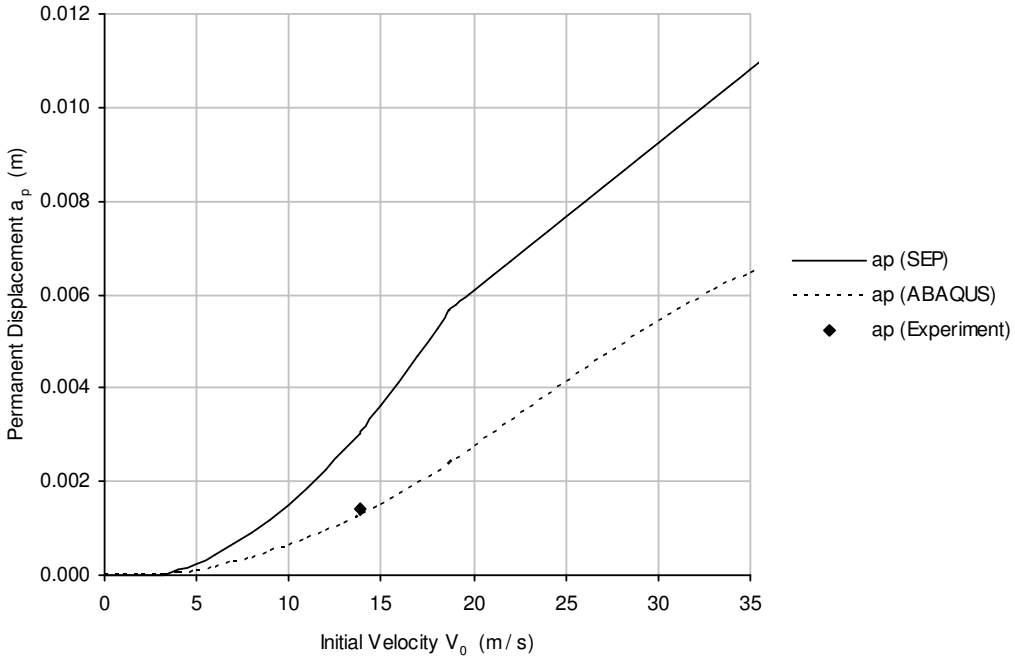

Figure 7.7b: a_p for h=0.0060m, V_0, 0-35m/s

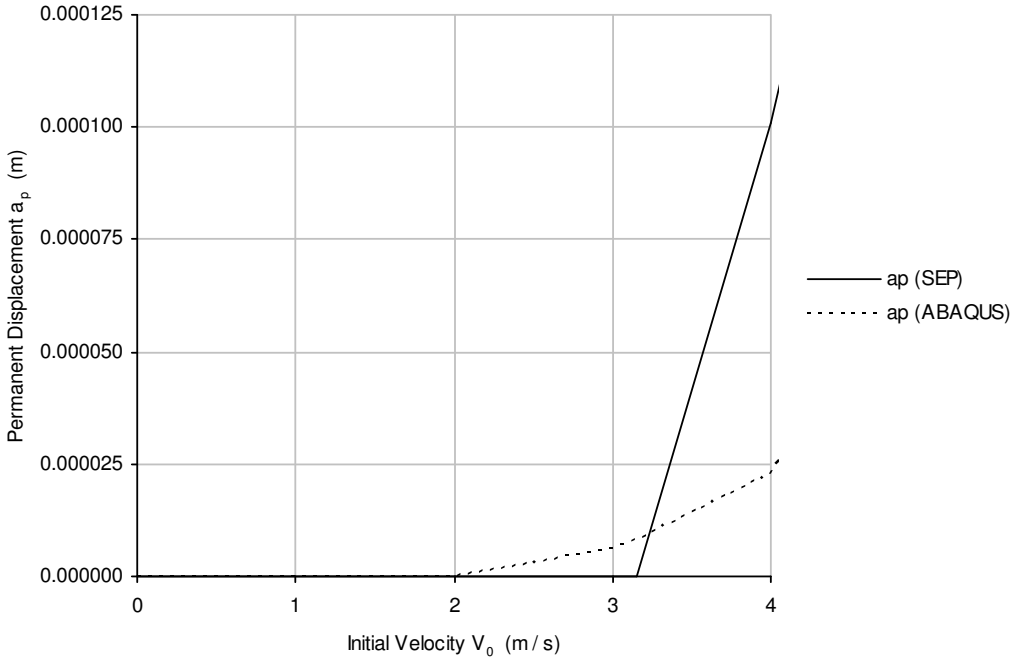

Figure 7.7c: a_p for h=0.0060m, V_0, 0-4m/s

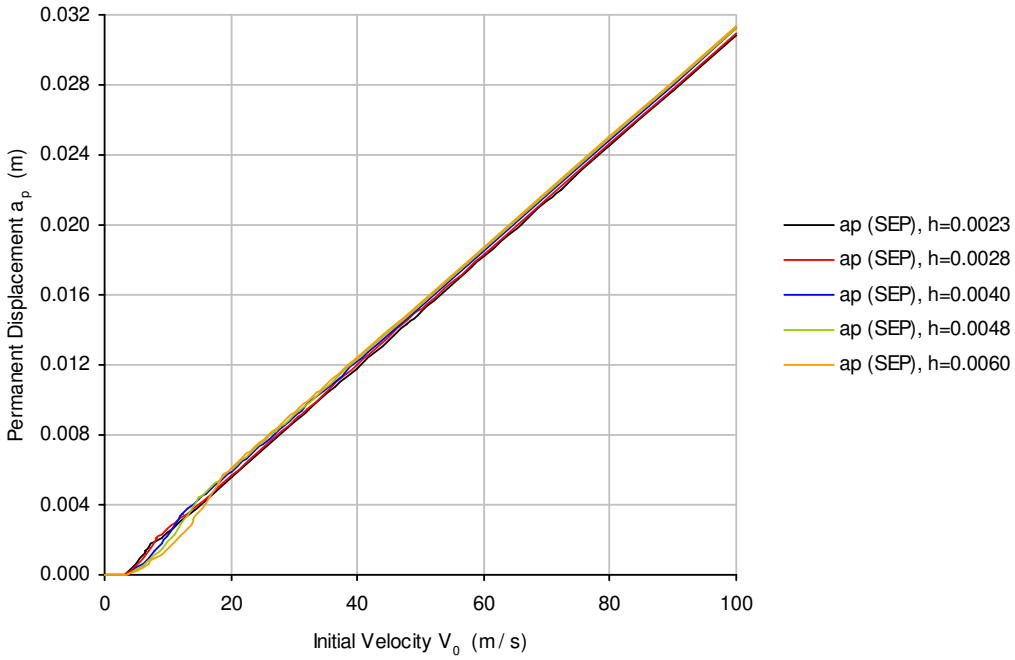

Figure 7.8a: $a_{p(SEP)}$ for different thicknesses h(m), V_0, 0-100m/s

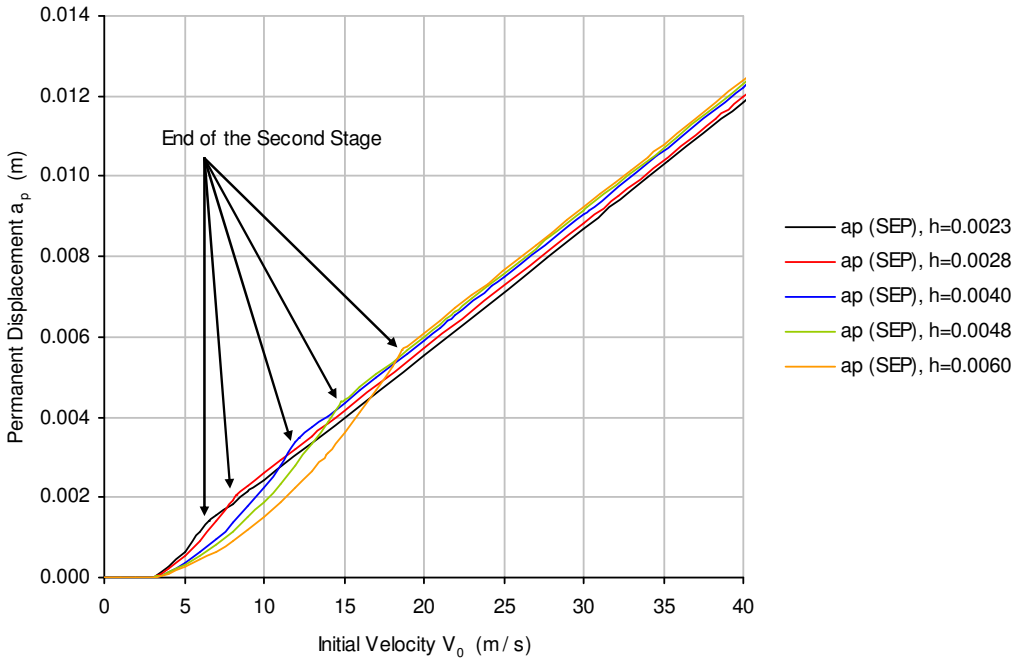

Figure 7.8b: $a_{p(SEP)}$ for different thicknesses h(m), V_0, 0-40m/s

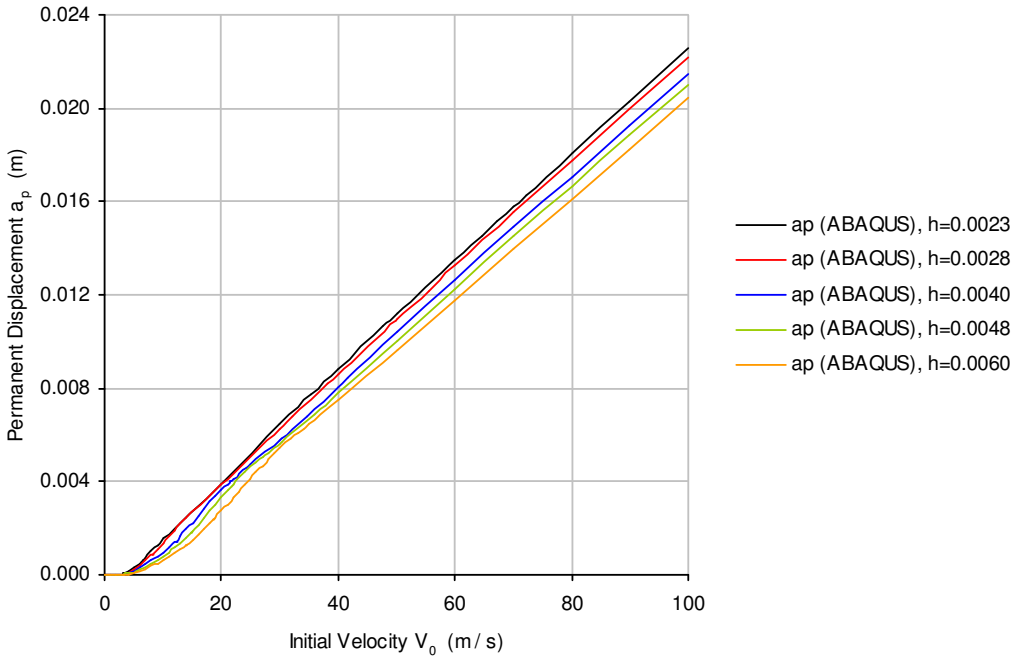

Figure 7.9a: $a_{p(ABAQUS)}$ for different thicknesses h(m), V_0, 0-100m/s

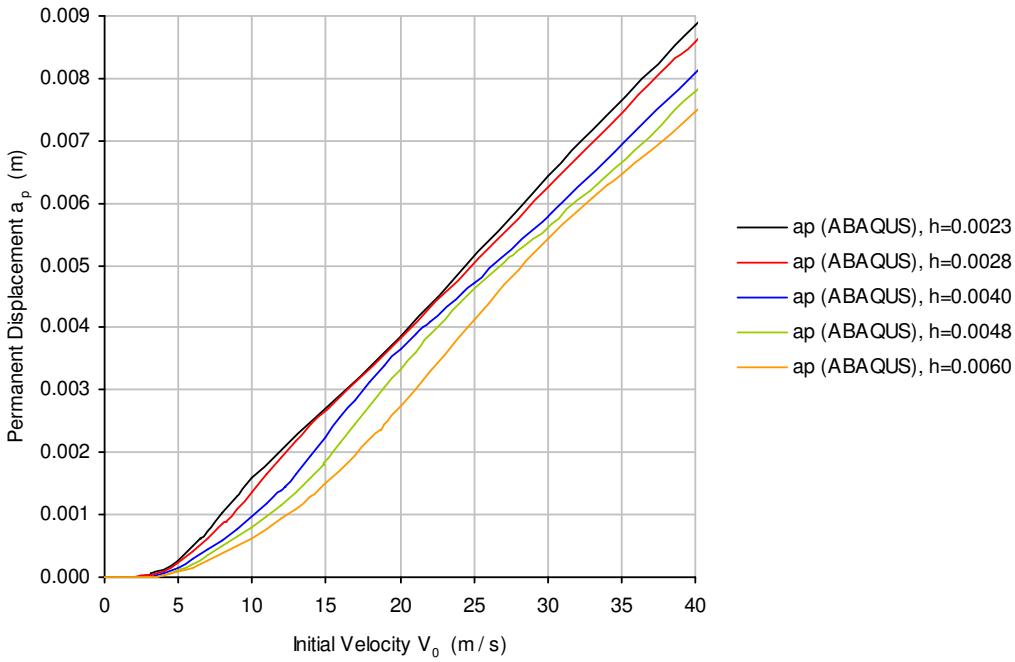

Figure 7.9b: $a_{p(ABAQUS)}$ for different thicknesses h(m), V_0, 0-40m/s

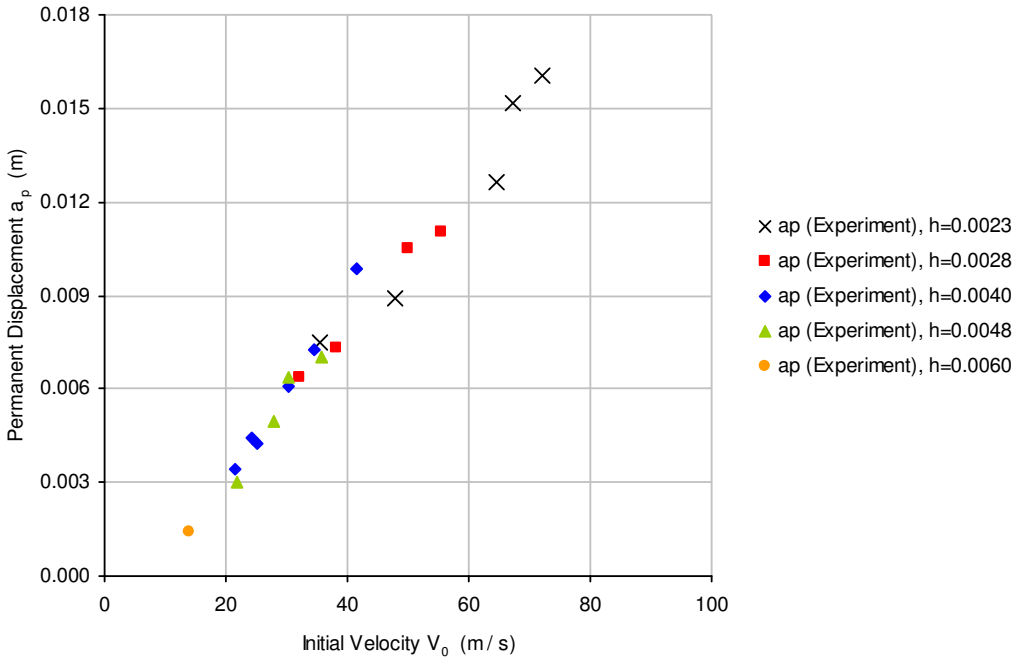

Figure 7.10: $a_{p(Experiment)}$ for different thicknesses h(m)

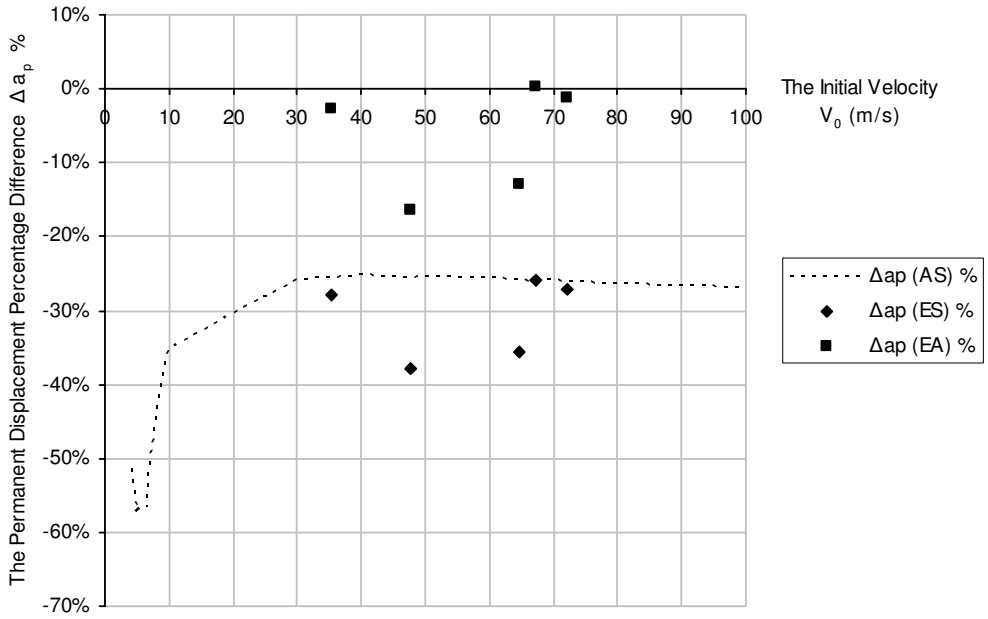

Figure 7.11a: $\Delta a_p\%$ for h=0.0023m, V_0, 0-100m/s

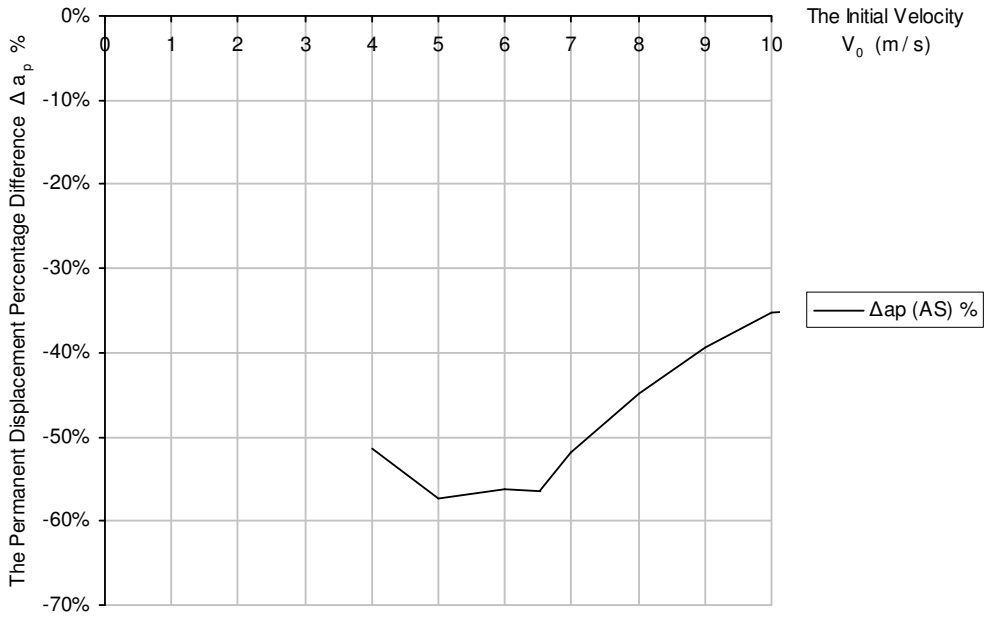

Figure 7.11b: $\Delta a_p\%$ for h=0.0023m, V_0, 0-10m/s

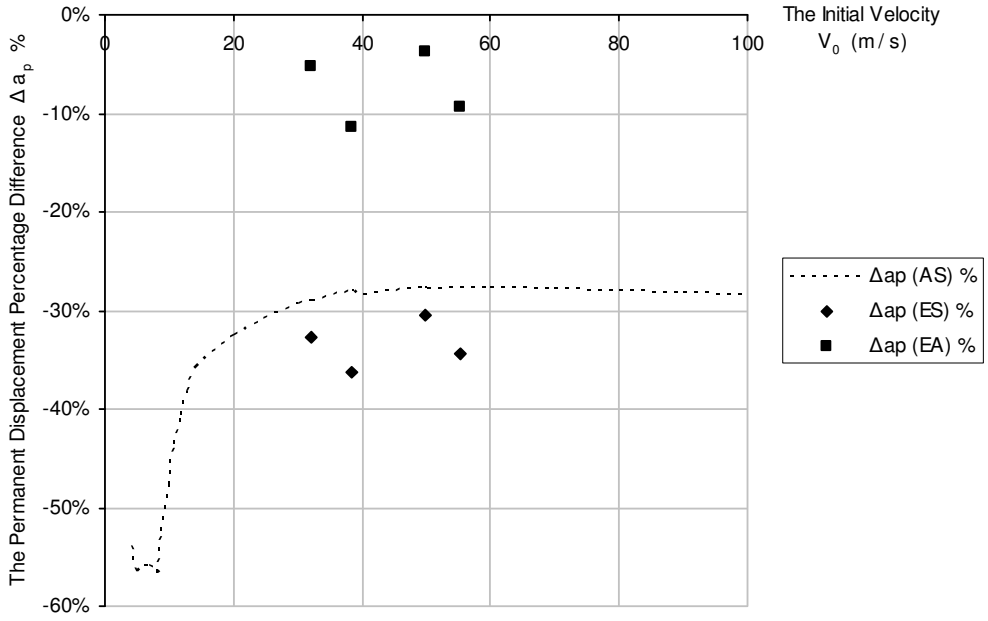

Figure 7.12a: Δa_p% for h=0.0028m, V_0, 0-100m/s

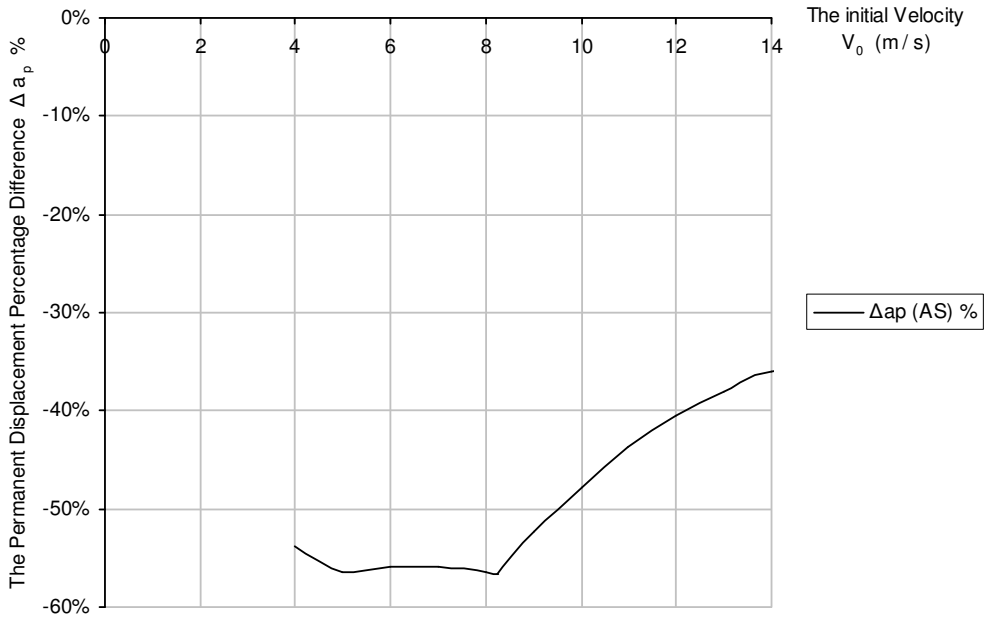

Figure 7.12b: Δa_p% for h=0.0028m, V_0, 0-14m/s

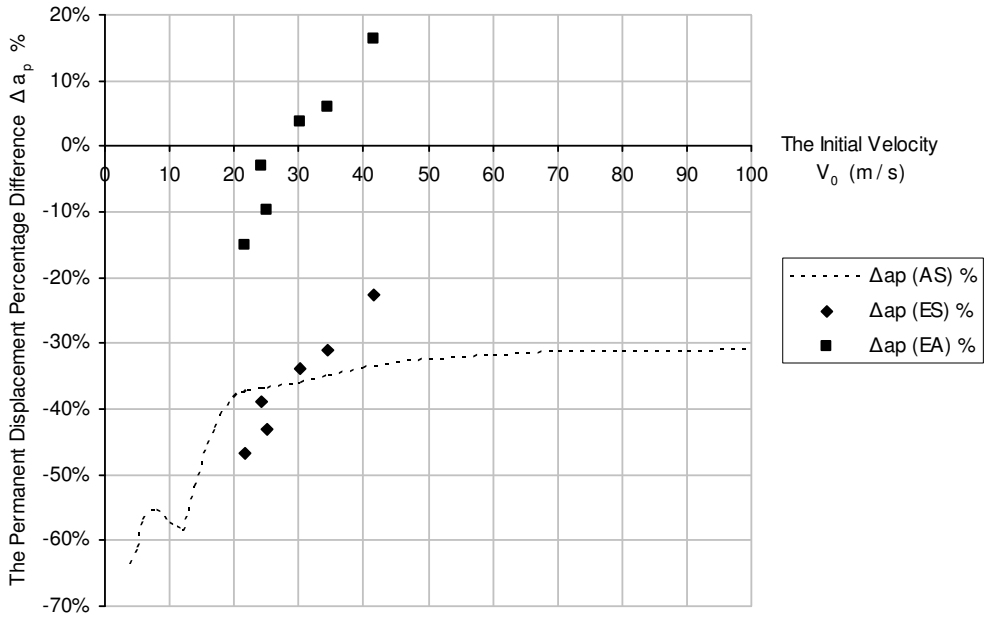

Figure 7.13a: $\Delta a_p\%$ for h=0.0040m, V_0, 0-100m/s

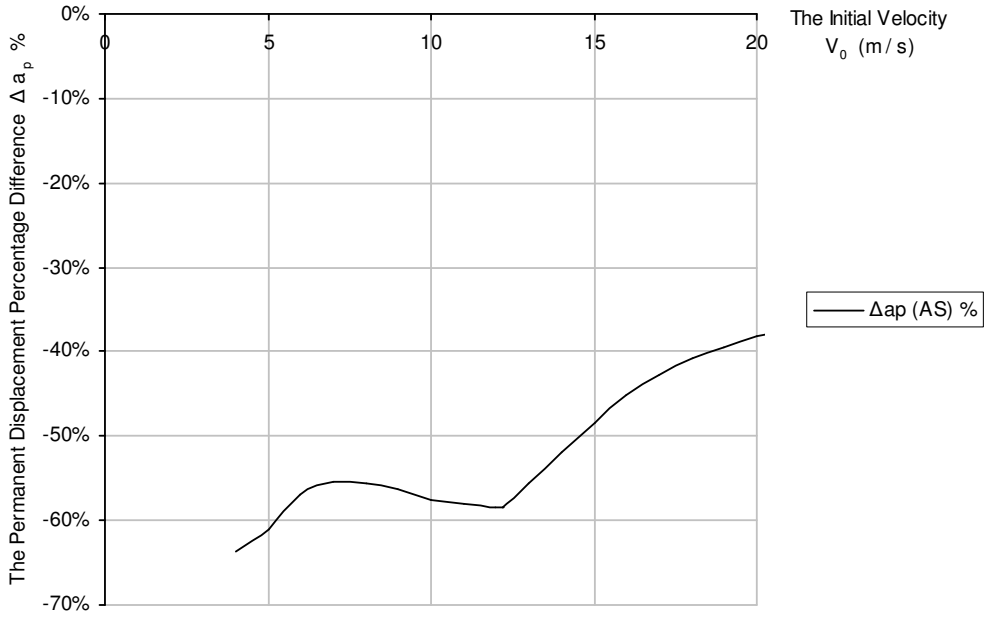

Figure 7.13b: $\Delta a_p\%$ for h=0.0040m, V_0, 0-20m/s

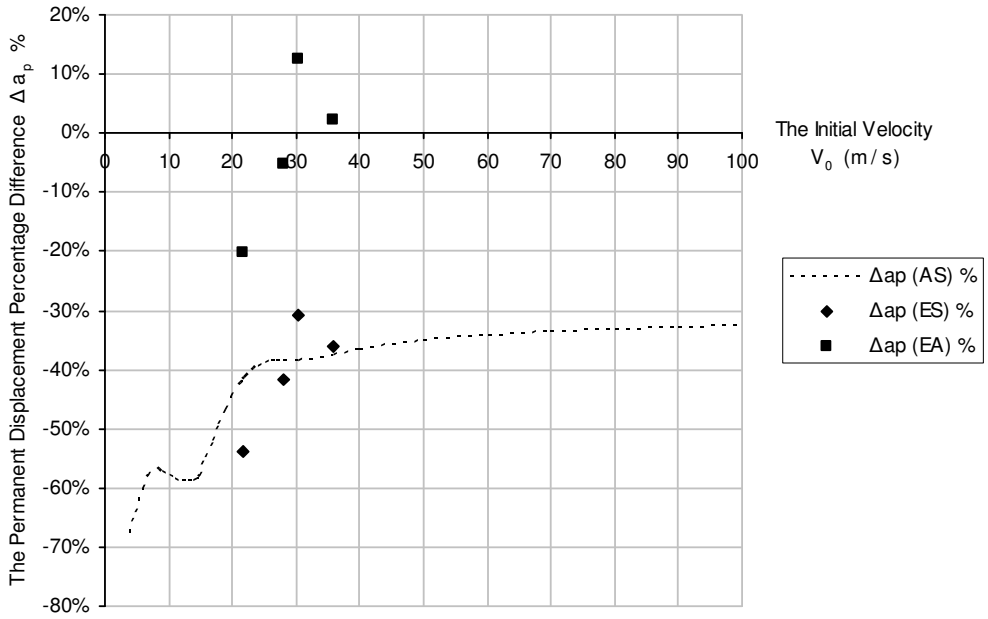

Figure 7.14a: $\Delta a_p\%$ for h=0.0048m, V_0, 0-100m/s

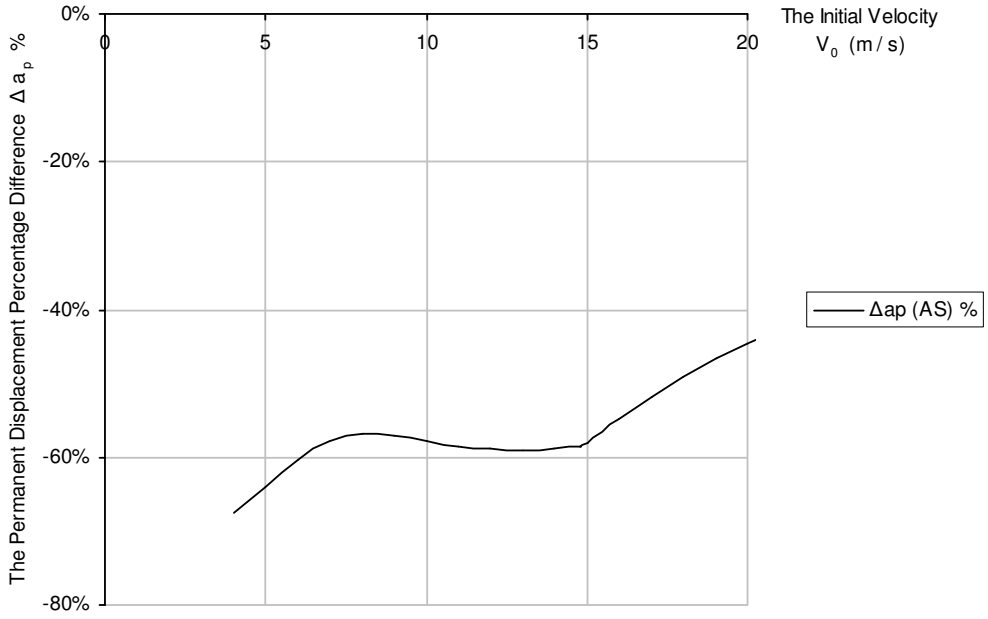

Figure 7.14b: $\Delta a_p\%$ for h=0.0048m, V_0, 0-20m/s

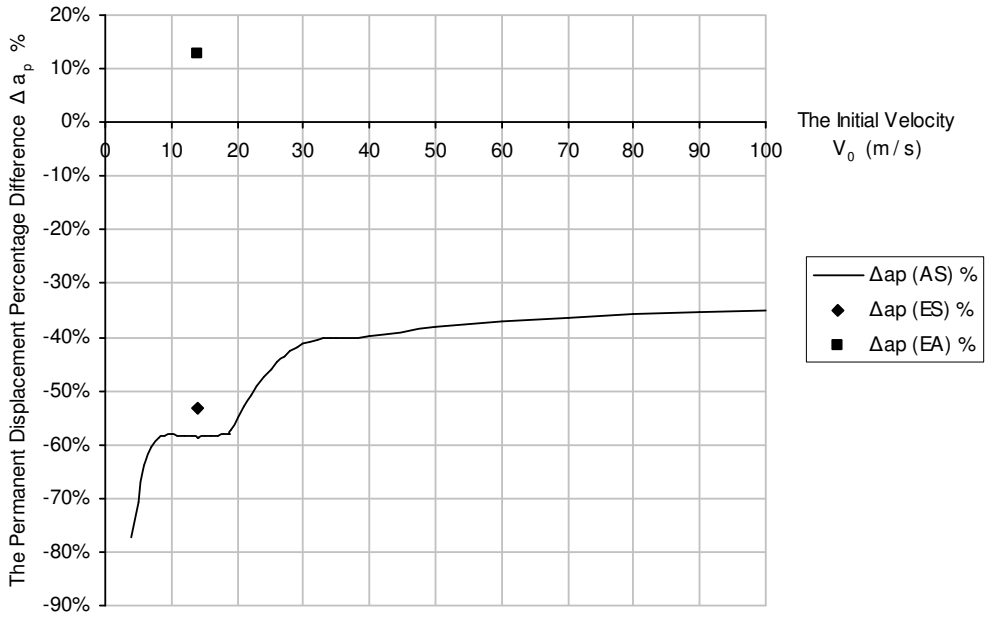

Figure 7.15a: $\Delta a_p\%$ for h=0.0060m, V_0, 0-100m/s

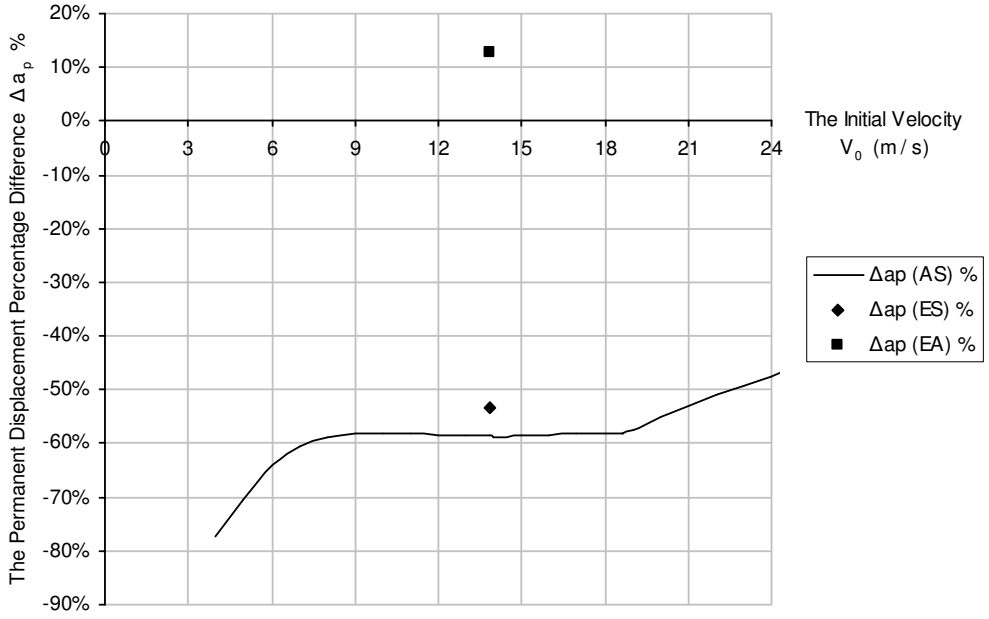

Figure 7.15b: $\Delta a_p\%$ for h=0.0060m, V_0, 0-24m/s

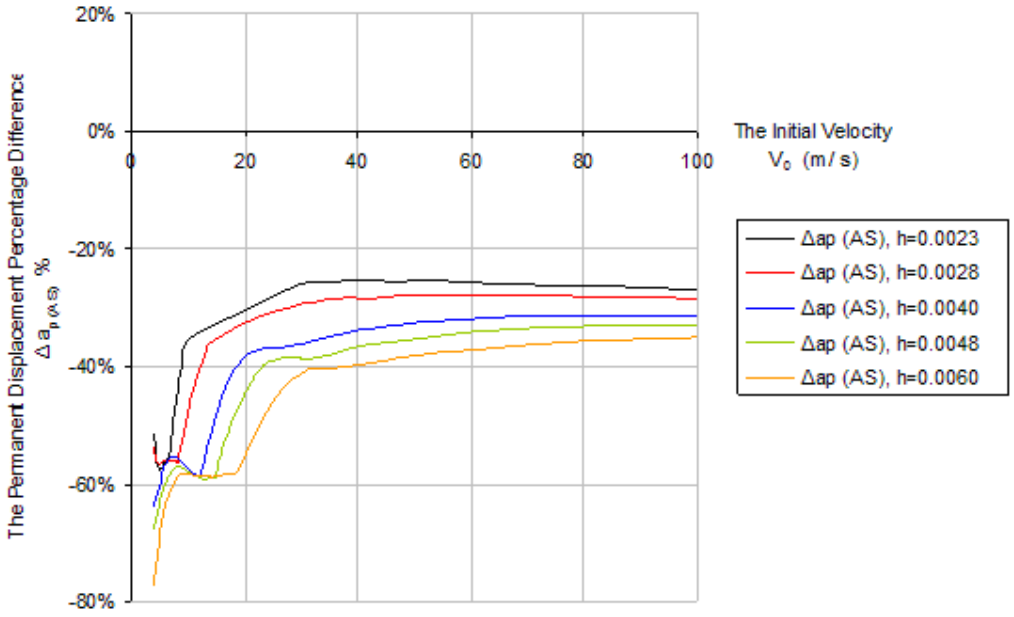

Figure 7.16a: $\Delta a_{p(AS)}$% for different thicknesses h(m), V_0, 0-100m/s

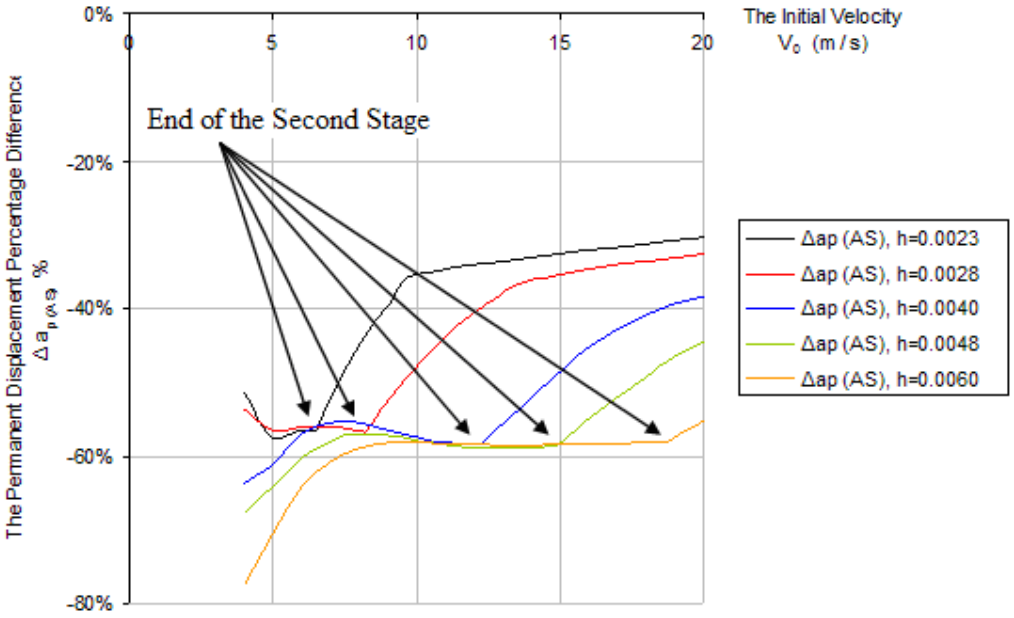

Figure 7.16b: $\Delta a_{p(AS)}$% for different thicknesses h(m), V_0, 0-20m/s

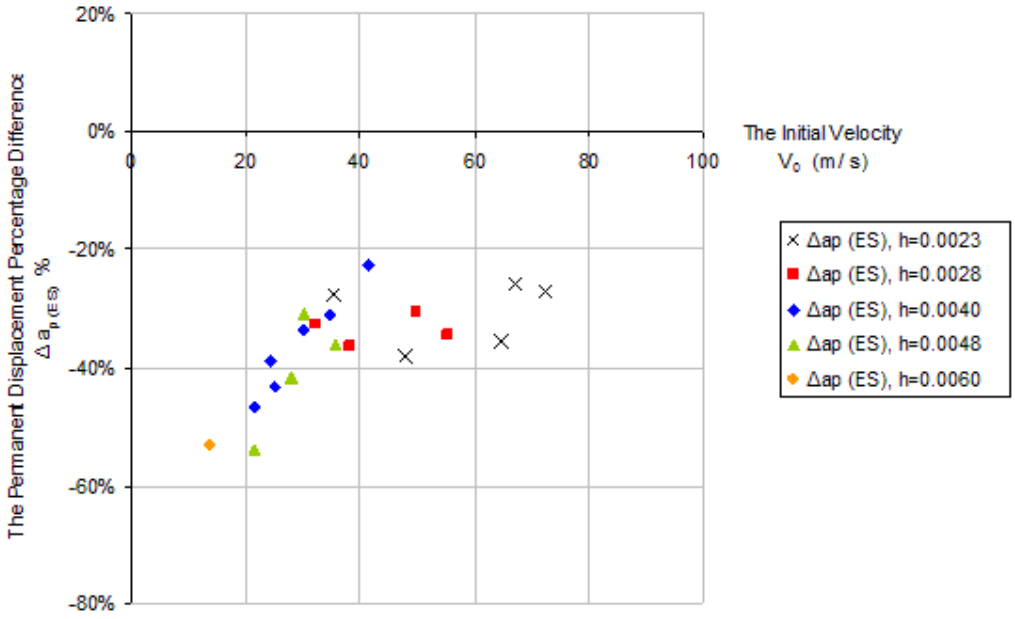

Figure 7.17: $\Delta a_{p(ES)}\%$ for different thicknesses h(m)

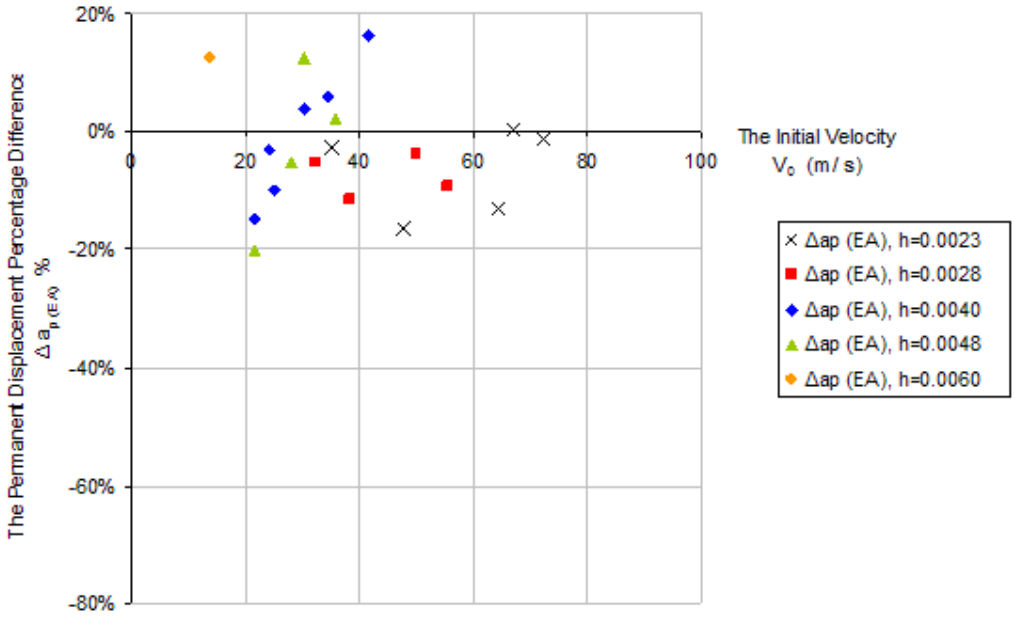

Figure 7.18: $\Delta a_{p(EA)}\%$ between experiments and ABAQUS for different thicknesses h(m)

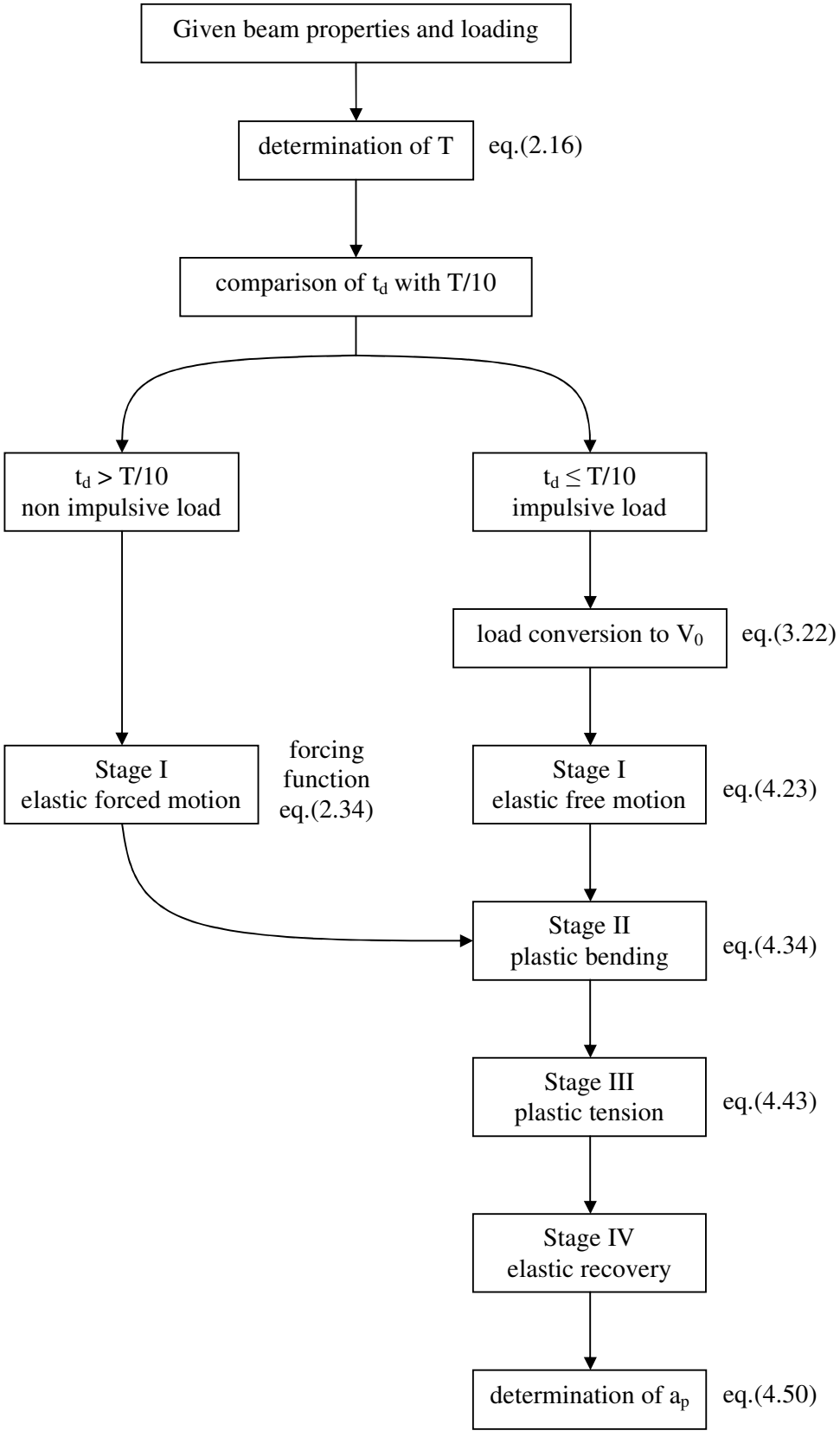

Figure 7.19: A flow chart for the successive procedures of the SEP Method, where the first number within the brackets indicates the chapter in which the equation was given

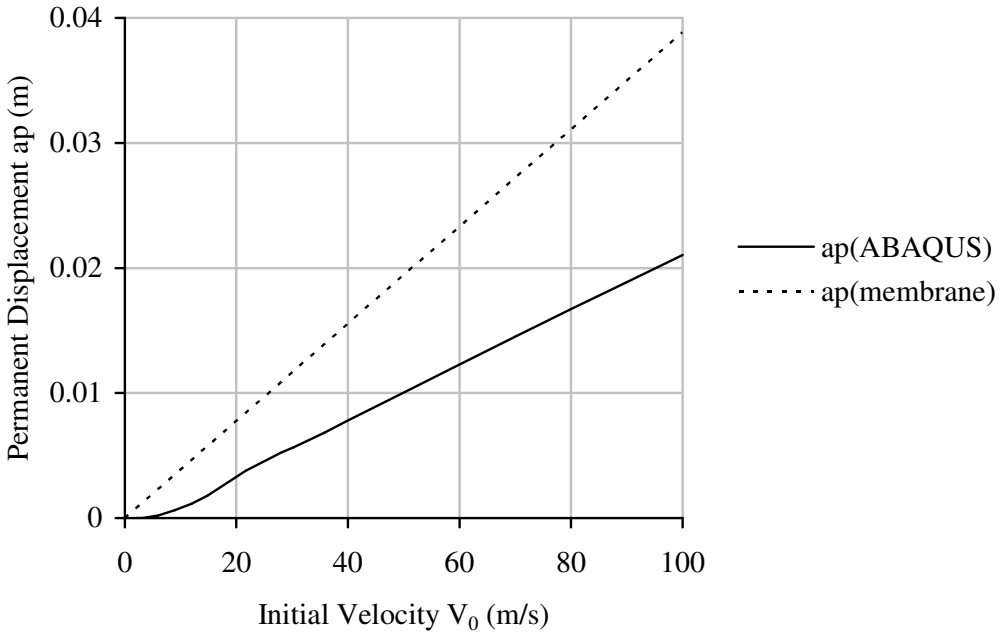

Figure 7.20: A comparison between the ABAQUS Model prediction and the membrane behaviour

Chapter 8 – Conclusions

8.1 The Literature

Various methods for the dynamic analysis of beams have been surveyed in Chapter 2. These methods differ from each other in terms of safety, material economy, cost of analysis and accuracy. Numerous studies have shown that although some analytical methods provide results close to reality, they might be very expensive to run. Also, due to the many assumptions embedded in so called accurate methods, it has been found that these methods often produce solutions which are not exact making the description 'accurate' relative. Simple approximate methods of analysis have been put into use due to their cheap running cost and fast outcomes. However, as approximate methods reduce the confidence in the analysis results, 'accurate' methods remain necessary in many structural situations when comparisons with trusted benchmarks are needed whether in practical design or for research purposes.

8.2 The Theory

Among the various approximate methods of dynamic analysis, the rigid plastic method has been one of the most widely used methods due to its simplicity, accuracy and above all its applicability for a wide range of problems including some very complex ones such as those that also include geometric nonlinearity in addition to material nonlinearity. However, this method ignores the presence of elasticity in the material. Thus, plastic deformations must be present and much larger than the elastic deformations in order for this method to give accurate results, and this means that the energy imparted by the dynamic load should be many times larger than the elastic energy capacity of the beam, otherwise, the rigid plastic method is not applicable. There has been also a need to develop methods that include the effect of elasticity while remaining convenient to use, this has led to the introduction of the elastic-plastic methods, such as the SEP Method presented in Chapter 4 and investigated for this Thesis, which are more accurate and suitable for those situations where elasticity should be taken into account.

The Simplified Elastic Plastic, SEP, Method is an efficient practical tool for analysis which provides solutions in mode form to the beam dynamic problem even when it is necessary to include those effects that are difficult to consider in 'accurate' analytical methods such as nonlinearity, both geometric and material.

8.3 Finite Element Modelling and Time Stepping

The nonlinear dynamic finite element modelling and analysis of the beams in the Thesis were carried out using ABAQUS. The explicit time stepping scheme, which is included in ABAQUS/Explicit Solver, was used due to its computational efficiency for the beams as they were under impulsive loads and thus their responses have a relatively short duration.

8.4 The ABAQUS Model

In the ABAQUS analysis, strain rate sensitivity of the material and geometric nonlinearity were included. The displacements of the beam predicted using the ABAQUS Model and measured from the experiments were very close, and sometimes equal, to each other. That shows the accuracy of the ABAQUS Model and thus it was used as a benchmark against which the SEP Method was compared. The ABAQUS Model can also be used for the design of beams.

Both greater and smaller than one ratios between the displacements from the ABAQUS Model and the experiments were obtained. However, the mean was close to one and the

standard deviation was small. Thus, although the experimental results had some scatter, the ABAQUS Model predicted them fairly accurately.

8.5 The SEP Method

The SEP Method was applied for beams with rectangular cross sections and fully fixed boundaries. According to the prediction of the SEP Method, the response of the beam consists, if the dynamic load is high enough, of four stages which are the elastic stage, the plastic bending stage, the plastic axial tension stage and the elastic recovery stage.

In the SEP Method, strain rate sensitivity of the material was ignored. The displacement of the beam predicted using the SEP Method was greater than that predicted using the ABAQUS Model or that measured from the experiments thus giving the important conclusion that the SEP Method is conservative.

The percentage difference between the displacement from the SEP Method and that from whether the ABAQUS Model or the experiments was negative with a value of at least -20 %. That shows the level of conservatism for the SEP Method.

Studying the variation for the percentage difference between the displacement from the SEP Method and that from the ABAQUS Model showed that as the dynamic load increases, the conservatism of the SEP Method generally decreases and thus the Method becomes more accurate.

The percentage differences can be used as calibration factors for the SEP Method and because they were always negative, reflecting the conservative nature of the SEP Method, and had a value of at least -20 %, a single calibration factor was proposed for

the SEP Method that was -20 %. Such a correction would improve the SEP Method as it would remove most of the conservatism in the method and thus render it more economical and also more accurate.

The level of conservatism in the SEP Method was not much different when the ABAQUS Model was used as the benchmark instead of the experiments.

The ABAQUS Model was found to be more accurate than the SEP Method and that gives the ABAQUS Model an advantage over the SEP Method. However, the SEP Method is cheaper to use.

The SEP Method can be used with confidence in structural design and the ABAQUS Model can be confidently used to give accurate predictions in structural design and additionally for research purposes.

8.6 The Design Procedure

A design procedure using the SEP Method has been developed and is described in the Thesis. The steps in the SEP Method which include the determination of the fundamental natural period of the beam, checking the nature of the dynamic load whether impulsive or not, choosing the analysis path, then describing the various stages of the response until the determination of the displacement of the beam have been discussed. A flow chart for this design procedure, including the equations used, has been given. Recommendations for the application of the SEP Method in practice have also been presented.

8.7 Recommendations for Future Research

The SEP Method has been investigated for beams with rectangular cross sections and fully fixed boundaries. Results from tests carried out on beams with certain dimensions have been used.

Various cases have been analysed using ABAQUS and the SEP Method but no tests have been carried out for them. Among those are the cases when the velocity is high and the thickness is low, and the cases of the highest thickness 0.0060m for which a single test only has been carried out. Also, the SEP Method can be investigated for beams with a wider range of dimensions. Therefore, more tests would be required. However, due to the difficulty and danger of having explosions in laboratories, that work is restricted to the specialised institutions.

Strain rate sensitivity has been ignored in the SEP Method. That can be included in future research to see its influence on the results.

Further research can be carried out for beams with other cross sections and boundary conditions and for other members and more complex structures.

References

ABAQUS, 2008, ABAQUS vr.6.8 User's Manuals, Dassault Systèmes Simulia, Providence, RI, USA

Abhyankar N.S., Hall II E.K. and Hanagud S.V., 1993, *Chaotic vibrations of beams: numerical solution of partial differential equations*, Transactions of the American Society of Mechanical Engineers: Journal of Applied Mechanics, **60**, 167-74

Al-Hassani S.T.S. and Reid S.R., 1992, The Effects of High Strain Rates on Material Properties, Offshore Technology Information Series OTI 92 602, Health and Safety Executive HSE, HMSO, London

Baker W.E., Cox P.A., Westine P.S., Kulesz J.J. and Strehlow R.A., 1983, Explosion Hazards and Evaluation, Series: Fundamental Studies in Engineering 5, Elsevier Scientific Pub. Co., Amsterdam

Bangash M.Y.H., 1993, Impact and Explosion: analysis and design, Blackwell Scientific Publications, Oxford

Bartknecht W., 1981, Explosions: course, prevention, protection, Springer-Verlag, Berlin

Bartknecht W., 1989, Dust Explosions: course, prevention, protection, Springer, Berlin

Benamar R., Bennouna M.M.K. and White R.G., 1991, *The effects of large vibration amplitudes on the mode shapes and natural frequencies of thin elastic structures – part I: simply supported and clamped-clamped beams*, Journal of Sound and Vibration, **149**, 2, 179-95

Biggs J.M., 1964, Introduction to Structural Dynamics, McGraw-Hill, New York

Buchar J., Bilek Z. and Dusek F., 1986, Mechanical Behavior of Metals at Extremely High Strain Rates, Trans Tech Publications, Switzerland

Calis M., Laghrouche O. and Desmulliez M.P.Y., 2007, *The implementation of cosserat theory into haptic sensing technology for large deflection beam model*, ICRM 2007 -

4th International Conference on Responsive Manufacturing, University of Nottingham, Nottingham

Chen Y. and May I.M., 2009, *Reinforced concrete members under drop-weight impacts*, Proceedings of the Institution of Civil Engineers - Structures and Buildings, **162**, 1, 45-56

Clough R.W. and Penzien J., 1993, Dynamics of Structures, McGraw-Hill, New York

Cook R.D., Malkus D.S. and Plesha M.E., 1989, Concepts and Applications of Finite Element Analysis, John Wiley & Sons, New York

Cook R.D., 1995, Finite Element Modelling for Stress Analysis, John Wiley & Sons, New York

Corn S., Bouhaddi N. and Piranda J., 1997, *Transverse vibrations of short beams: finite element models obtained by a condensation method*, Journal of Sound and Vibration, **201**, 353-63

Cowper G.R. and Symonds P.S., 1957, Strain-Hardening and Strain-Rate Effects in the Impact Loading of Cantilever Beams, Technical Report 28, Brown University, Providence

Davies R.M., 1937, *The frequency of transverse vibration of a loaded fixed-free bar – III. the effect of the rotatory inertia of the bar*, Philosophical Magazine, **XXIII**, 563-73

Den Hartog J.P., 1928, *The lowest natural frequency of circular arcs*, Philosophical Magazine, **V**, 400-8

Den Hartog J.P., 1956, Mechanical Vibrations, 4th Edition, McGraw-Hill, New York

Ece M.C., Aydogdu M. and Taskin V., 2007, *Vibration of a variable cross-section beam*, Mechanics Research Communications, **34**, 1, 78-84

Gerstmayr J. and Irschik H., 2003, *Vibrations of the elasto-plastic pendulum*, International Journal of Non-Linear Mechanics, **38**, 1, 111-22

Goldsmith W., 1960, Impact: the theory and physical behaviour of colliding solids, Edward Arnold Publishers, London

Griffiths D.V. and Smith I.M., 1991, Numerical Methods for Engineers, Blackwell Scientific Publications, Oxford

Gupta R.K., Babu G.J., Janardhan G.R. and Rao G.V., 2009, *Relatively simple finite element formulation for the large amplitude free vibrations of uniform beams*, Finite Elements in Analysis and Design, **45**, 10, 624-31

Han R.P.S. and Lu J., 1999, *A space–time finite element method for elasto-plastic shock dynamics*, Journal of Sound and Vibration, **222**, 1, 65-84

Houmat A., 1995, *Vibrations of Timoshenko beams by variable order finite elements*, Journal of Sound and Vibration, **187**, 841-9

Hughes G. and Speirs D.M., 1982, An Investigation of the Beam Impact Problem, Technical Report 546, Cement and Concrete Association, Slough

Irvine H.M., 1986, Structural Dynamics for the Practising Engineer, Allen & Unwin, London

Johnson W., 1972, Impact Strength of Materials, Edward Arnold, London

Jones N. and Gomes de Oliveira J., 1979, *The influence of rotatory inertia and transverse shear on the dynamic plastic behavior of beams*, Transactions of the American Society of Mechanical Engineers: Journal of Applied Mechanics, **46**, 303-10

Jones N., 1989, Structural Impact, Cambridge University Press, Cambridge

Kaneko T., 1975, *On Timoshenko's correction for shear in vibrating beams*, Journal of Physics D: Applied Physics, **8**, 16, 1927-36

Khan A., 2008, Behaviour of Rigid Plastic Structures under Extreme Dynamic Loading, PhD Thesis, Systems and Mechanics Section, Department of Civil Engineering, Imperial College, University of London

Kimberley J., Lambros J., Chasiotis I., Pulskamp J., Polcawich R. and Dubey M., manuscript accepted 2010, *Mechanics of energy transfer and failure of ductile microscale beams subjected to dynamic loading*, Journal of the Mechanics and Physics of Solids, in press

Lalanne C., 2002, Mechanical Vibration and Shock, **2**, mechanical shock, HPS, London

Lepik U. and Just M., 1983, *Automatic calculation for bending of rigid-plastic beams under dynamic loading*, Computer Methods in Applied Mechanics and Engineering, **38**, 19-28

Lepik U., 1994, *Vibrations of elastic-plastic fully clamped beams and flat arches under impulsive loading*, International Journal of Non-Linear Mechanics, **29**, 4, 613-23

Lepik U., 1995, *Elastic–plastic vibrations of a buckled beam*, International Journal of Non-Linear Mechanics, **30**, 2, 129–39

Lewandowski R., 1994, *Non-linear free vibrations of beams by the finite element and continuation methods*, Journal of Sound and Vibration, **170**, 577-93

Lloyd Smith D. and Sahlit C.L., 1991, *Dynamic response of pulse loaded structures as a linear complementarity problem*, Engineering Optimization, **18**, 1, 23-41

Ma G.W., Liu Y.M., Zhao J. and Li Q.M., 2005, *Dynamic asymmetrical instability of elastic-plastic beams*, International Journal of Mechanical Sciences, **47**, 1, 43-62

Macleod I.A., 2005, Modern Structural Analysis: modelling process and guidance, Thomas Telford, London

Major A., 1980, Dynamics in Civil Engineering; analysis and design, **I**, fundamentals in vibration theory and practice including machine foundations, soil dynamics, instrumentation, vibration tolerances, Akademiai Kiado, Budapest

Martin J.B., 1966, *A note on the uniqueness of solutions for dynamically loaded rigid-plastic and rigid-viscoplastic continua*, Journal of Applied Mechanics, **33**, Transactions of the American Society of Mechanical Engineers, **88**, 207-9

Martin J.B. and Symonds P.S., 1966, *Mode approximations for impulsively-loaded rigid-plastic structures*, Proceedings of the American Society of Civil Engineers: Journal of the Engineering Mechanics Division, **92**, EM 5, 43-66

Martin J.B. and Lee L.S.-S., 1968, *Approximate solutions for impulsively loaded elastic-plastic beams*, Transactions of the American Society of Mechanical Engineers: Journal of Applied Mechanics, **35**, 803-9

McEwan M.I., Wright J.R., Cooper J.E. and Leung A.Y.T., 2001, *A combined modal/finite element analysis technique for the dynamic response of a non-linear beam to harmonic excitation*, Journal of Sound and Vibration, **243**, 4, 601-24

Na S. and Librescu L., 2001, *Dynamic response of elastically tailored adaptive cantilevers of nonuniform cross section exposed to blast pressure pulses*, International Journal of Impact Engineering, **25**, 9, 847-67

Newmark N.M., 1959, *A Method of Computation for Structural Dynamics*, Transactions of the American Society of Civil Engineers, **127**, 1406-35

Nonaka T., 1967, *Some interaction effects in a problem of plastic beam dynamics – part 3: experimental study*, Transactions of the American Society of Mechanical Engineers: Journal of Applied Mechanics, **34**, 638-43

Paz M., 1991, Structural Dynamics: theory and computation, Chapman & Hall, New York

Paz M. and Leigh W., 2004, Structural Dynamics: theory and computation, Kluwer Academic Publishers, Massachusetts

Pham D.C., 2000, *Safety and collapse of elastic-plastic beams against dynamic loads*, International Journal of Mechanical Sciences, **42**, 3, 575-92

Rao S.S., 2004, Mechanical Vibrations, 4th Edition, Pearson

Ribeiro P. and Petyt M., 1999, *Non-linear vibration of beams with internal resonance by the hierarchical finite-element method*, Journal of Sound and Vibration, **224**, 4, 591-624

Ribeiro P., 2001, *Hierarchical finite element analyses of geometrically non-linear vibration of beams and plane frames*, Journal of Sound and Vibration, **246**, 225-44

Ribeiro P. and van der Heijden G.H.M., 2009, *Elasto-plastic and geometrically nonlinear vibrations of beams by the p-version finite element method*, Journal of Sound and Vibration, **325**, 1 and 2, 321-37

Seiler J.A., Cotter B.A. and Symonds P.S., 1956, *Impulsive loading of elastic-plastic beams*, Transactions of the American Society of Mechanical Engineers: Journal of Applied Mechanics, **23**, 515-21

Shanley F.R., 1947, *Inelastic column theory*, Journal of the Aeronautical Sciences, **14**, 261-8

Shi Y. and Mei C., 1996, *A finite element time domain modal formulation for large amplitude free vibrations of beams and plates*, Journal of Sound and Vibration, **193**, 453-64

Smith I.M. and Griffiths D.V., 1988, Programming the Finite Element Method, John Wiley & Sons, New York

Strutt J.W., 3rd Baron Rayleigh, 1877, Theory of Sound, **I**, Macmillan and Co., London

Symonds P.S., 1953, *Dynamic load characteristics in plastic bending of beams*, Transactions of the American Society of Mechanical Engineers: Journal of Applied Mechanics, **20**, 475-81

Symonds P.S. and Jones N., 1972, *Impulsive loading of fully clamped beams with finite plastic deflections and strain-rate sensitivity*, International Journal of Mechanical Sciences, **14**, 49-69

Symonds P.S., 1980a, *Elastic, Finite Deflection and Strain Rate Effects in a Mode Approximation Technique for Plastic Deformation of Pulse Loaded Structures*, Journal of Mechanical Engineering Science, **Volume 22**, Number 4, 189-97

Symonds P.S., 1980b, *Finite Elastic and Plastic Deformations of Pulse Loaded Structures by an Extended Mode Technique*, International Journal of Mechanical Sciences, **Volume 22**, 597-605

Symonds P.S. and Yu T.X., 1985, *Counterintuitive behavior in a problem of elastic-plastic beam dynamics*, Transactions of the American Society of Mechanical Engineers: Journal of Applied Mechanics, **52**, 517-22

Thomson W.T., 1966, Vibration Theory and Applications, George Allen & Unwin, London

Thomson W.T., 1993, Theory of Vibration with Applications, 4th Edition, Chapman & Hall, London

Timoshenko S.P., 1921, *On the correction for shear of the differential equation for transverse vibrations of prismatic bars*, Philosophical Magazine, **XLI**, 744-6

Timoshenko S.P., 1922, *On the transverse vibrations of bars of uniform cross-section*, Philosophical Magazine, **XLIII**, 125-31

Timoshenko S.P., 1953, History of Strength of Materials; with a brief account of the history of theory of elasticity and theory of structures, McGraw-Hill Book Company, Inc., New York

Timoshenko S. and Young D.H., 1955, Vibration Problems in Engineering, D. Van Nostrand Company, Princeton, New Jersey

Tinkler R.J., 1986, Mechanical Properties of Metals for High Strain Rate Applications – A Review and Literature Survey, Central Electricity Generating Board, CEGB Report, Technology Planning and Research Division, Berkeley, TPRD/B/0723/N85

Turner M.J., Clough R.W., Martin H.C. and Topp L.J., 1956, *Stiffness and Deflection Analysis of Complex Structures*, Journal of Aerospace Science, **23**, 805-23

Vaziri R., Olson M.D. and Anderson D.L., 1987, *Dynamic response of axially constrained plastic beams to blast loads*, International Journal of Solids and Structures, **23**, 1, 153-74

Vertes G., 1985, Structural Dynamics, Developments in Civil Engineering; **11**, Elsevier, Amsterdam and Akademiai Kiado, Budapest

Warburton G.B., 1964, The Dynamical Behaviour of Structures, Pergamon Press, London

Wearne P., 1999, Collapse: Why Buildings Fall Down, Channel 4 Books, Macmillan Publishers, London

Weaver W.JR. et al., 1990, Vibration Problems in Engineering, John Wiley & Sons, New York

Wilson E.L., Farhoomand I. and Bathe K.J., 1973, *Nonlinear Dynamic Analysis of Complex Structures*, International Journal of Earthquake Engineering and Structural Dynamics, **Volume I**, 241-52

Wood W.L., 1990, Practical Time Stepping Schemes, Clarendon Press, Oxford

Worden K. and Tomlinson G.R., 2001, Nonlinearity in Structural Dynamics: detection, identification and modelling, Institute Of Physics (IOP) Publishing, Bristol and Philadelphia

Wu C. and Hao H., 2003, *Numerical simulation of simultaneous ground shock and airblast pressure on nearby structures from surface detonation*, 5th Asia-Pacific Conference on Shock & Impact Loads on Structures, Changsha, Hunan, China, 379-86

Xu J.-X. and Hasebe N., 1997, *The problem of an elastic–plastic beam dynamics and an incomplete co-dimension two bifurcation*, International Journal of Non-Linear Mechanics, **32**, 1, 127-43

Yagci B., Filiz S., Romero L.L. and Ozdoganlar O.B., 2009, *A spectral-Tchebychev technique for solving linear and nonlinear beam equations*, Journal of Sound and Vibration, **321**, 1-2, 375-404

Yankelevsky D.Z. and Boymel A., 1984, *Dynamic elasto-plastic response of beams – a new model*, International Journal of Impact Engineering, **2**, 4, 285-98

Yankelevsky D.Z. and Karinski Y.S., 2000, *Dynamic elasto-plastic response of symmetrically loaded beams*, Computers and Structures, **76**, 4, 445-59

Zienkiewicz O.C. and Taylor R.L., 1989, The Finite Element Method, 4th Edition, **1**, basic formulation and linear problems, McGraw-Hill, London

Zienkiewicz O.C. and Taylor R.L., 1991, The Finite Element Method, 4th Edition, **2**, solid and fluid mechanics, dynamics and non-linearity, McGraw-Hill, London